OAK RIDGE
NATIONAL LABORATORY
MANAGED BY UT-BATTELLE
FOR THE DEPARTMENT OF ENERGY

C/ORNL99-0568

PHASE II
CRADA ORNL99-0568 REPORT

DEVELOPING TRANSMISSION-LESS INVERTER DRIVE SYSTEMS FOR AXIAL-GAP PERMANENT MAGNET ACCESSORY AND TRACTION MOTORS AND GENERATORS

J. W. McKeever
G. J. Su
G. W. Ott, Jr.
Oak Ridge National Laboratory

Kelly Samons
Visual Computing Services Incorporated

Prepared by the
Oak Ridge National Laboratory
Oak Ridge, Tennessee 37831
managed by
UT-Battelle, LLC
for the
U.S. Department of Energy
Under Contract DE-AC05-00OR22725

C/ORNL99-0568

Engineering Technology Division

Phase II CRADA ORNL 99-0568 Report

DEVELOPING TRANSMISSION-LESS INVERTER DRIVE SYSTEMS FOR AXIAL-GAP PERMANENT MAGNET ACCESSORY AND TRACTION MOTORS AND GENERATORS

J. W. McKeever
G. J. Su
G. W. Ott, Jr.
Oak Ridge National Laboratory

Kelly Samons
Visual Computing Systems

July 2001

Prepared by the
OAK RIDGE NATIONAL LABORATORY
Oak Ridge, Tennessee 37831
managed by
UT-BATTELLE, LLC
for the
U.S. DEPARTMENT OF ENERGY
Under Contract DE-AC05-00OR22725

TABLE OF CONTENTS

TABLE OF CONTENTS

LIST OF FIGURES

LIST OF TABLES

ACRONYMS

ART	Auxiliary Resonant Tank
CARAT	Collaborative Automotive Research for Advanced Technology
CPSR	Constant Power Speed Ratio
CRADA	cooperative research and development agreement
DOE	Department of Energy
DMIC	Dual Mode Inverter Control
DSP	Digital Signal Processor
EMF	Electromotive Force
EMI	Electromagnetic Interference
EERE	Office of Energy Efficiency and Renewable Energy
HEV	Hybrid Electric Vehicle
IGBT	Insulated Gate Bipolar Transistors
LMTC	Lynx Motion Technology Corporation
MOSFET	Metal Oxide Semiconductor Field Effect Transistors
OAAT	Office of Advanced Automotive Technologies
OEM	Original Engineering Manufacturers
ORNL	Oak Ridge National Laboratory
OTT	Office of Transportation Technologies
PCU	Power Control Unit
PEEMRC	Power Electronic and Electric Machinery Research Center
PM	Permanent Magnet
PNGV	Partnership for a New Generation of Vehicles
PWM	Pulse-Width Modulated
RSI	Resonant Snubber Inverter
SEMA	Segmented Electromagnetic Array
SPM	Surface Mounted Permanent Magnets
STTR	Small Business Technology Transfer
UQM	Unique Mobility, Inc.
UTK	The University of Tennessee-Knoxville
VCS	Visual Computing Systems, Inc.
ZCS	Zero Current Switching
ZVS	Zero Voltage Switching

ABSTRACT

Researchers of the Oak Ridge National Laboratory's (ORNLs) Power Electronics and Electric Machine Research Center (PEEMRC) collaborated with Visual Computing Systems (VCS) to develop an electric axial-gap permanent magnet (PM) motor controlled by a self-sensing inverter for driving vehicle accessories such as power steering, air conditioning, and brakes. VCS designed an 8 kW motor based on their Segmented Electromagnetic Array (SEMA) technology. ORNL designed a 10 kW inverter to fit within the volume of a housing, which had been integrated with the motor. This modular design was pursued so that multiple modules could be used for higher power applications. ORNL built the first inverter under the cooperative research and development agreement (CRADA) ORNL 98-0514 and drove a refurbished Delta motor with no load during the Merit Review at ORNL on Monday, May 17, 1999. Inverter circuitry and instructions for assembling the inverters were sent to VCS. A report was prepared and delivered during the Future Car Congress in April 2000, at Arlington, Virginia.

Collaboration continued under CRADA ORNL 99-0568 as VCS designed and built a SEMA motor with a dual coil platter to be the traction motor for an electric truck. VCS and ORNL assembled two 45 kW inverters. Each inverter drove one coil, which was designed to deliver 15 kW continuous power and 45 kW peak power for 90 s. The vehicle was road tested as part of the Future Truck Competition. A report was prepared and delivered during the PCIM in October 2000, at Boston, Massachusetts.

BACKGROUND

During 1996 and 1997 VCS, the Participant, and Lockheed Martin Energy Research Corporation (Now UT-Battelle), the Contractor, collaborated in Phase I of a Small Business Technology Transfer (STTR) under the Department of Energy (DOE) grant DE-FG02-96ER86052 to construct and demonstrate a motor/alternator capable of operation at 6000 rpm using SEMA components, which had been developed by the Participant. The original goal was to demonstrate an advanced, low-cost motor/alternator drive system suitable for flywheel energy storage applications. Results from this collaboration indicated reasonable motor performance and the Participants' research indicated that it was cost effective, which encouraged further development of this technology.

The results were submitted with a Phase II proposal to focus on further design development and optimization, manufacturing development, and prototype construction, testing, and evaluation of an axial gap motor/alternator capable of meeting required cost and performance goals. Since the emphasis on flywheel energy storage had diminished the system whose cost and performance goals were to be targeted was not specified. The section about commercial application of this research highlighted high-speed motor alternator concepts for a typical passenger car, with systems that could be scaled up for commercial trucks and military vehicles and down for utility vehicles. The Phase II STTR grant was awarded to VCS in mid-1997.

During the interval between the grant award and preparation of the CRADA's statement of work, which began in March of 1998, VCS conducted market research to identify and match customers and products. The impetus was the intent of the Phase II STTR collaboration, which is to

provide a basis for future salable motor products. Their potential customers included a car company and a manufacturer of pumps for the military, who have indicated a common need. VCS's commercialization arm, Lynx Motion Technology Corporation (LMTC), was birthed to adapt basic VCS designs into products that match specific customers.

Although the new electric vehicle direction for this Phase II research deviates from the original flywheel objectives, the commercial potential of the resulting technology will be greater. The DOE contract administrator approved the change in scope.

CRADA ORNL 98-0514, was submitted to VCS for review and consideration on May 18, 1998. On June 23, 1998, fully executed copies of the CRADA were sent to VCS for their signature. On August 20, 1998, ORNL received the check from VCS, who had to get it from DOE's Chicago Office.

The CRADA August 20, 1999 expiration date slipped by before a request for extension was issued with $50,000 left at ORNL. Consequently, a second CRADA had to be written. Timing was perfect for the new CRADA because in October 1999 the Participant entered into an agreement with the University of Tennessee–Knoxville (UTK) to participate in DOE's Future Truck Competition. In this competition universities convert a donated Chevy Suburban to a hybrid electric vehicle (HEV) to improve fuel efficiency and reduce emissions without impairing its stock performance. The Participant agreed to provide a 30 kW continuous and 90 kW peak power traction motor that would be configured in parallel with a small direct injection turbo-diesel engine. The second CRADA, ORNL 99-0568, was written so that the Contractor could assist the Participant in modifying the self-sensing accessory power control unit (PCU) to drive the variable speed SEMA-based traction motor with funding that remained for ORNL's Phase II collaboration with VCS. The CRADA was sent to VCS for review and consideration on December 13, 1999. VCS executed it on January 12, 2000 and work began.

An internal letter report was submitted to fulfill the CRADA requirements for ORNL 98-0514. It reviewed the status of the tasks in 98-0514 and included a paper presented at the Future Car 2000 Conference. This final report includes information for both ORNL 98-0514 and ORNL 99-0568 and includes the early paper and a paper on the traction motor drive presented at the PCIM in November 2000.

STATEMENT OF OBJECTIVES

The threefold purpose of these CRADAs was: 1) to provide and demonstrate a self-sensing inverter that can drive a 8 kW SEMA motor; 2) to collaborate with VCS during development of a traction drive system; and 3) to provide a platform for VCS and ORNL to continue collaboration. ORNL and VCS anticipate that there will be future collaborative research opportunities to apply ORNL inverter technology to VCS SEMA-based motors.

BENEFITS TO THE FUNDING DOE OFFICES'S MISSION

DOE's funding office for this STTR is the Office of Energy Efficiency and Renewable Energy (EERE). The Office of Advanced Automotive Technologies (OAAT) has provided oversight for the research. OAAT is under the Office of Transportation Technologies (OTT) within EERE.

One of the OAAT's highest priorities is to improve fuel economy of light vehicles such as the HEV. As a member of the Partnership for a New Generation of Vehicles (PNGV) it has established the goal of developing technologies that will enable midsize passenger vehicles to achieve 80 mpg by 2004 without sacrificing safety, performance, and affordability. It seeks to develop and validate advanced technologies that might not be independently researched by industry due to substantial risk. When Ford, General Motors, and Daimler-Chrysler issue requests for proposals to original engineering manufacturers (OEMs) to supply them with auxiliary and traction motors, the advanced technologies must be developed and validated or they will not even be considered.

This STTR research is to develop inverters for HEV auxiliary systems such as hydraulic pumps and for traction drives. The induction motor, being the most mature, is the industry's first choice. This funding supports research on the SEMA axial-gap PM motor, which is an advanced technology electric motor quite different from the induction motor that might not be considered by the OEMs that supply car manufacturers as a candidate. In fact it is even different from most PM motors because the SEMA stator is not wound over iron teeth. Consequently, it has low inductance, high energy density, and torque proportional to current far beyond that of stators wound over iron teeth, which are limited because the iron in the teeth saturates.

Research from this effort will benefit the electric and HEVs by making validated advanced technology available to the OEMs as they supply the components to the car manufacturers. Furthermore, this same technology may also be applied to power tools, mining machines, construction vehicles, trucking vehicles, military vehicles, electric scooters, mobile robots, electric wheel chairs, electric locomotive, elevator drives, and general traction drives.

TECHNICAL DISCUSSION OF WORK

What follows is a summary of the work completed for the tasks in both CRADAs of this Phase II collaboration.

Work Completed during CRADA ORNL 98-0514

The primary objective of this first part of the Phase II work was to design, build, and test a low-cost, self-sensing 15 kW inverter/controller that would drive a SEMA-based accessory 10 kW PM motor. This single-speed motor operates accessory systems such as the hydraulic pump for a vehicle’s power steering and brakes.

Phase II collaboration activities for CRADA 98-0514 were:

- Task 1 - management and coordination;
- Task 2 - establishing motor/alternator and inverter specifications;

- Task 3 - design of the self-sensing inverter;
- Task 4 - fabrication of a working prototype;
- Task 5 - characterization of the SEMA-based Delta motor driven by the prototype inverter; and
- Task 6 - preparation of the CRADA report.

From the beginning of the CRADA until October 17, 1998, ORNL studied and addressed issues whose resolution would indicate subsequent research direction. Should soft switching be used in the inverter? What semiconductor devices should be used in the inverter? VCS was considering metal oxide semiconductor field effect transistors (MOSFETs) and insulated gate bipolar transistors (IGBTs). Can field weakening be applied through control of the inverter? Dual Mode Inverter Control (DMIC) technology was just being invented. Can a self-sensing control be used to drive the accessory motor? The results of this study were faxed to VCS on October 17, 1998 and are included in Appendix A of this CRADA report.

VCS and LMTC visited ORNL on December 1–2, 1998 and the team prepared a detailed MicroSoft Project plan. The first task was to agree on what the inverter had to do to drive the VCS motor. ORNL signed off the Task 2 inverter specifications in a document entitled "STTR Power Inverter Requirements" on December 13, 1998. A second document signed off at the same time was entitled "ORNL PCU Electronics Development Program Management Plan."

Jerry Mitchell, who coordinated the MicroSoft Project representation of the Phase II inverter development of the CRADA, requested cost information for the inverter components. The following summary was sent to VCS on December 9, 1998.

Table 1. Component costs of ORNL inverter/controller

Item	Cost, $
Gate Driver Board	
$163 setup + $51.95 /board x 5 boards	$423
Signal Conditioning Board	
$170 setup + 114.11/board x 5 boards	$740
Components to Populate Both Boards	
$335/(gate driver and signal conditioning board) x 5	$1,675
Heat Sink	
($272 base system + $14.02 fan + $82.74 finger guard) x 3	$1,107
DSP Board	
$1495 x 5 TMS320C24X Evaluation Board (including power supply)	$4,485
$995 x 2 Debugger	$1,990
Total	$10,420

The deliverable for Task 1 was changed from a spreadsheet methodology for estimating production inverter/controller costs to documents with text and pictures explaining how to assemble the gate drive and the inverter. That document was sent to VCS on June 8, 1999 and is included in Appendix C entitled "Assembly Instructions for the VCS STTR Inverter Components."

The Task 3 design and simulation of the self-sensing inverter was completed by the end of December 1998 and design of the prototype began immediately. A functional block diagram of the VCS STTR Motor Controller is included in Appendix B. Position may be sensed either by back emf in the inactive phase or by an encoder mounted on the shaft.

The Task 4 fabrication of the first inverter proceeded on an accelerated schedule to be ready to test the first Delta motor in April so that the PCU would be ready in early May. Photos at different stages of the build are shown in Figs. 1–4. Figure 5 shows the CRADA team, Gui-Jia Su, Curt Ayers, and George Ott from ORNL and Keith Seymour from VCS during the first test of the inverter.

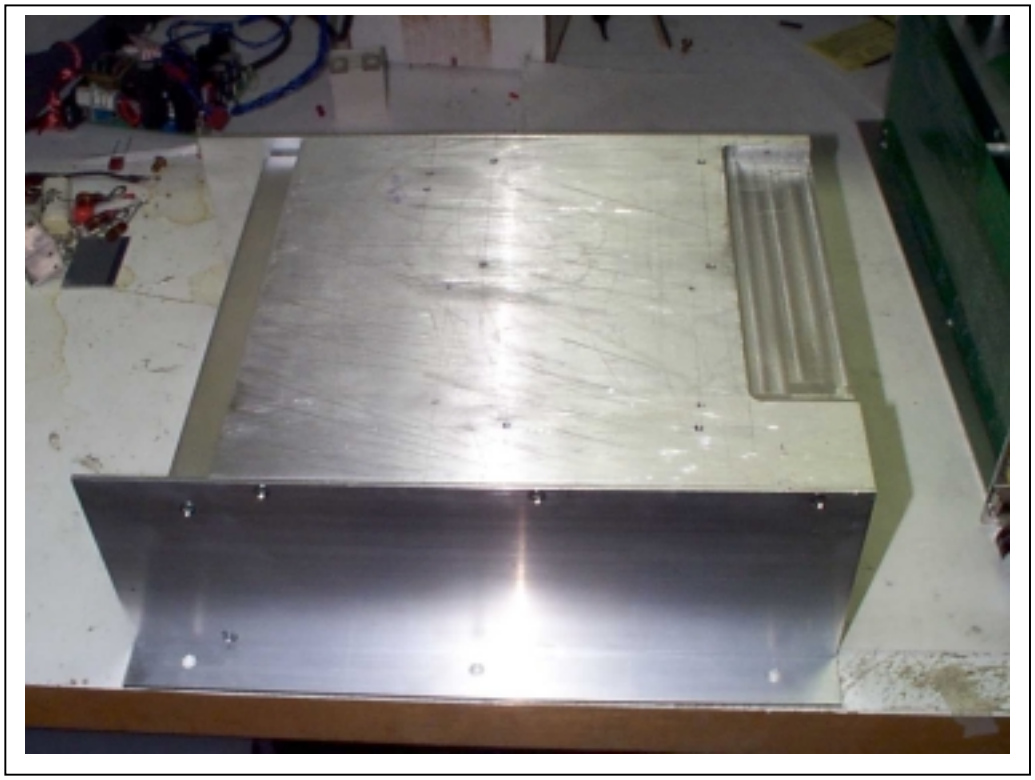

Fig. 1. Heat sink.

A detailed test plan was prepared for the Task 5 characterization of the Delta accessory motor driven by the self-sensing inverter. This test plan included in Appendix D is entitled, "ORNL Test Plan for STTR Motor and Power Inverter." The VCS SEMA based Delta motor released a magnet during operation by VCS. After its repair it was de-rated and the test plan was modified accordingly with limits and strikethroughs specified by VCS. The limits are inserted in bold print in Appendix D.

Fig. 2. IGBT, board, and capacitor layout.

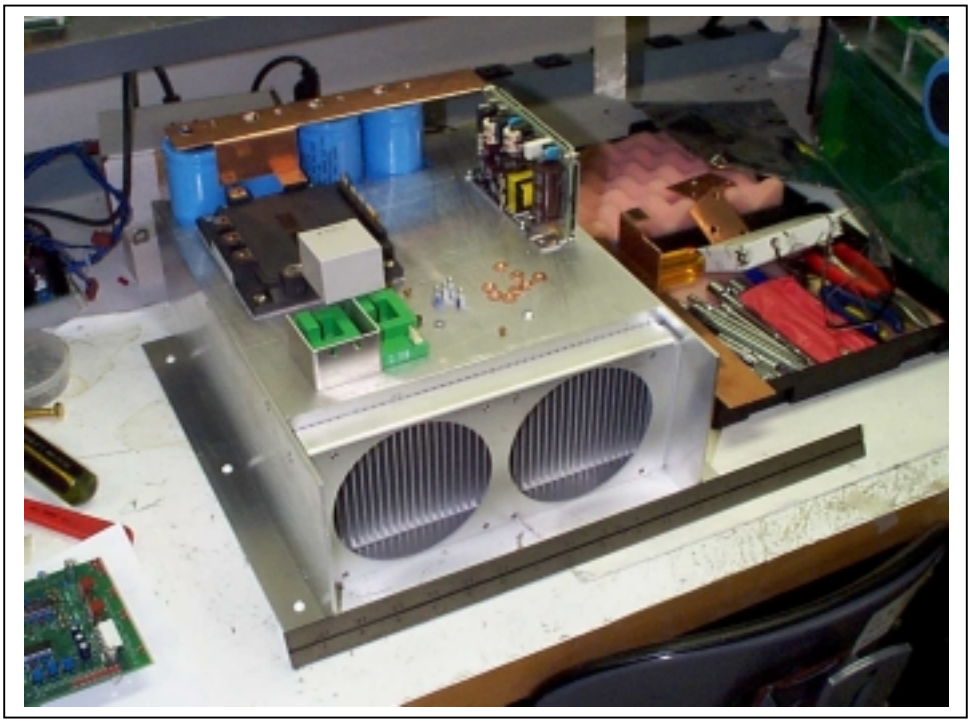

Fig. 3. Copper bus bar attached.

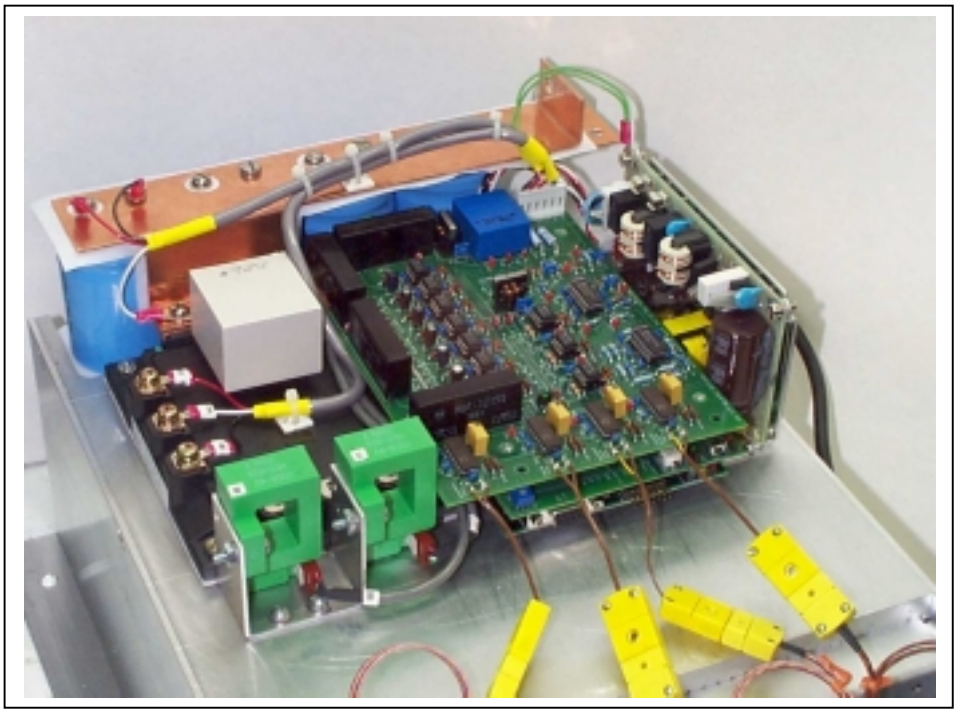

Fig. 4. Assembled inverter ready to test.

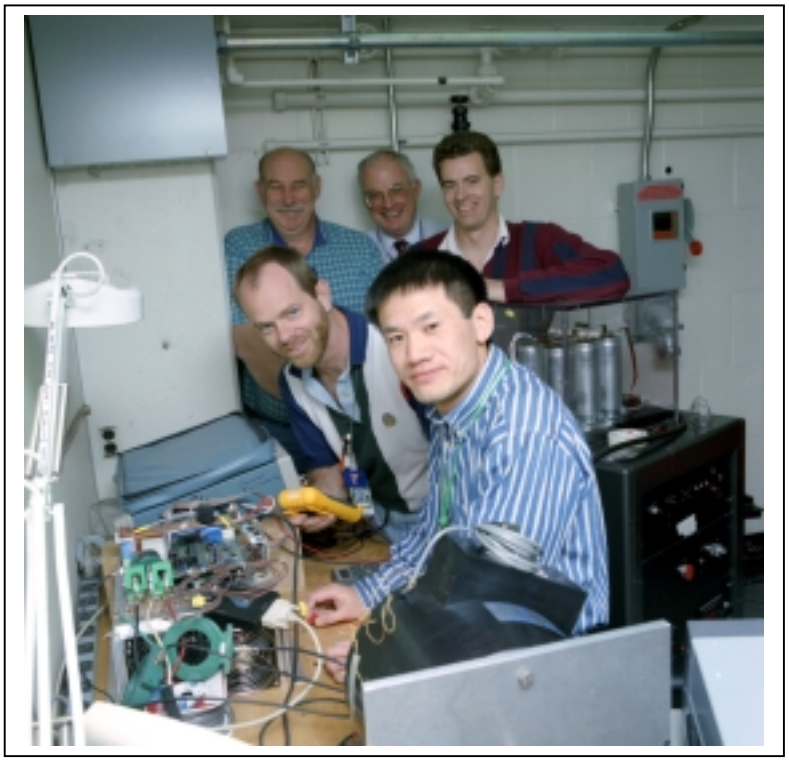

Fig. 5. CRADA team during first test of inverter.

The ORNL inverter was tested in the laboratory by driving a UQM (formerly Unique Mobility, Inc.) radial gap PM motor with not load prior to the demonstration with the Delta motor. Before the demonstration test the inverter drove the de-rated Delta motor at 1480 RPM with a 40 in-lbf load for a several minute test during which the temperature climbed to 41°C.

During the test demonstration at ORNL's Advanced Propulsion Lab on May 17, 1999, the motor was driven for an hour with a load of 20 in.-lbf. The temperature climbed slowly and steadily to 51°C during the demonstration. The test was stopped when the temperature reached 56°C because the thermocouple meter's battery discharged. Observers at the demonstration included Milo Friesen and Miguel Lagunas from LMTC, Roy Kessinger from VCS, three representatives from the Chattanooga Area Regional Transit Authority, and three from Advanced Vehicle Systems.

The motor and inverter were moved to PEEMRC, where the demonstration continued during the evening tour, which was a part of DOE's 1999 Merit Review in Oak Ridge. The test results are in Appendix E entitled "Testing and Demonstration of the Delta Motor."

Emphasis on other pressing collaboration and availability of only a derated motor prevented further inverter testing.

The deliverable of Task 6, which is a report, was fulfilled by a draft summary. Included with the summary was a copy of the paper describing the accessory inverter designed by ORNL. The paper entitled, "Development of a Sensor-less Speed Control Inverter for an Automotive Accessory Permanent Magnet Motor," was delivered as part of the Future Car Congress 2000 at Arlington, Virginia in April 2000. A copy of the paper is included in Appendix F.

Work Completed during CRADA ORNL 99-0568

The objective of this second part of the Phase II work was to have two 15 kW bi-directional inverters to drive a dual-coil 30 kW SEMA based axial-gap PM traction motor in the Future Truck Competition. The inverters were based on ORNL's modified design of the inverter used to drive the accessory SEMA motor in the first part of this Phase II work. VCS built a SEMA motor with dual coil windings in the coil platter.

Phase II collaboration activities for CRADA 98-0514 were:

- Task 1 – Project Management;
- Task 2 – Modify Accessory PCU Circuitry for Variable Speed Operation;
- Task 3 – Modify Accessory PCU Software for Regenerative Operation with Torque Control and Assist Participant's Preparation of Synchronized Stacked Modules;
- Task 4 – Verification Testing of Traction CPU at UTK;
- Task 5 – Develop a Plan for Operating SEMA based Motors and Generators above Base Speed;
- Task 6 - Documentation.

Task 1 covered the program development and project oversight tasks for the final year of the CRADA.

Task 2 was accomplished efficiently because the original design of the PCU for driving the accessory SEMA motor provided for use of an encoder to sense position. The deliverable was a circuit modification that allowed the accessory motor PCU to determine shaft position from Hall Probe signals. A functional block diagram of the SEMA Traction Motor controller, which uses Hall Effect Probes, is included in Appendix G.

Task 3 continued through the spring and summer as ORNL collaborated with VCS during their build of the dual-coil SEMA motor. VCS and ORNL assembled two 45 kW inverters. Each inverter drove one coil, which was designed to deliver 15 kW continuous power and 45 kW peak power for 90 s. The vehicle was road tested as part of the Future Truck Competition. A report entitled "Design of a PM Brushless Motor Drive for Hybrid Electrical Vehicle Application" was prepared and delivered during the PCIM in October 2000, at Boston, Massachusetts. It is included in Appendix H.

During Task 4, ORNL collaborated with VCS and UTK as they tested their motor in a converted Suburban truck.

ORNL communicated the new DMIC technology for driving a SEMA motor, which has low inductance, above base speed. The Task 5 plan for applying this technology to a SEMA motor is to respond to a solicitation by DOE's EERE for a cooperative program with states for R&D and demonstration. The demonstration will be a prototype vehicle with increased performance and fuel economy over its conventional counterparts.

The deliverable of Task 6 is this report.

COMMERCIALIZATION POSSIBILITIES

Two types of technology were developed in this CRADA. The first technology was a 5 kW SEMA auxiliary motor driven by a self-sensing inverter. The second technology was a 30 kW SEMA traction motor whose stator contained two 15 kW SEMA coils parallel connected to two of the same inverters with a shaft encoder replacing the self-sensing circuitry. Both technologies were demonstrated to low power levels during this CRADA.

The commercialization of the SEMA auxiliary motor is good. Ford has indicated an interest in using them. The commercialization of the SEMA traction motor is low, but will increase if it can be demonstrated that heat may be removed from the coil platter, that the traction motor may be driven at a constant power speed ratio (CPSR) of 4, and that the current ripple is not unacceptable. Future collaboration with ORNL is anticipated during which some of these problems will be addressed.

PLANS FOR FUTURE COLLABORATION

ORNL and VCS anticipate that there will be future collaborative research opportunities to apply ORNL inverter technology to VCS SEMA-based motors. One of the traction motor requirements of the car companies is that they deliver constant torque up to some speed, called the base speed, and constant horsepower from base speed to 5 times base speed. This ratio is called CPSR. CPSRs above 3 give the vehicle a familiar feel. A motor with CPSR above 4 can achieve better acceleration for lower rated power. A vehicle with CPSR above 5 will probably spin its wheels often. ORNL has patented and demonstrated inverter drive technology that can drive low inductance motors above a CPSR of 6. VCS and ORNL will seek collaborative funding to apply this technology to drive low inductance SEMA motors at a CPSR of 4. Task 1.5 of the second CRADA was to develop a plan to accomplish this. This plan was formulated at a Workshop held at the National Transportation Research Center on March 19 and 29, 2001.

VCS has responded to an EERE state solicitation through the State Energy Policy Division of the Indiana Chamber of Commerce with a three-year proposal. The objective of the proposal is to develop and test a high-efficiency direct-drive HEV drive train based on the high performance SEMA electric motor technology and the ORNL advanced DMIC.

CONCLUSIONS

Related to CRADA ORNL 98-0514

1. A digital signal processor (DSP) and intelligent IGBT module implementation of a position and speed self-sensing control based on indirect back electromotive force (EMF) detection for an automotive accessory PM motor drive greatly reduced the number of components and facilitated a compact inverter package.
2. An analysis of the influence of low inductance on current ripple was used to design a fast current control loop so the inverter could accommodate the low inductance characteristic of SEMA PM motors.
3. The self-sensing control was coupled with the position error correction to extend control to lower speeds by eliminating position detection errors, which are large at low speeds.
4. Torque ripple was reduced and motor efficiency was improved by keeping the motor current waveform in phase with the back EMF waveform.

Related to CRADA ORNL 99-0568

5. The modular approach can reduce development time and cost of designing both inverter and PM motor for traction (adjustable speed) drives at scalable power ratings.
6. The modular approach increases the level of fault tolerance.
7. Two pulse-width modulation (PWM) motoring strategies examined. For the first strategy, the upper three switches of the inverter phase legs toggle the PWM to regulate current, while the appropriate bottom switch remains closed for 120 electrical degrees corresponding to the negative segment of the back EMF waveform. For the second strategy, each of the six switches toggles PWM during only its first 60 electrical degrees but remains closed during

its second 60 electrical degrees. The second strategy induces smaller disturbances in the conducting phase current during each switching state and thus produces a better current waveform.

8. Altering the second PWM motoring strategy so that each switch implements PWM during its second 60 electrical degrees has an adverse effect on the waveform.
9. Two PWM regeneration strategies were examined. For the first strategy, the lower three switches toggle PWM to regulate current during the 120 electrical degrees corresponding to the positive segment of the back EMF waveform. For the second strategy, the same three lower switches toggle PWM for 180 electrical degrees producing an overlap of 60 degrees between successive fundamental cycles. The second strategy again induces smaller disturbances in the conducting phase current during commutation instants and thus produces a better current waveform.
10. Although the first regenerative PWM strategy produces less switching noise since only one switch toggles PWM at a time, it will generate larger di/dt noise due to the sharp change in the current waveform at commutation instants.
11. Experimental results have demonstrated successful operation of a modular SEMA motor having two three-phase stator coils each driven by its own inverter. The inverter design was similar to that designed by ORNL for the accessory motor. Three Hall Effect probes replaced the self-sensing circuitry and devices capable of delivering 45 kW replaced the devices that delivered 10 kW. The inverter's printed circuit board also has an interface for an encoder that may be used instead of Hall Effect probes.

INTERNAL DISTRIBUTION

1. D. J. Adams
2. C. W. Ayers
3. J. M. Bailey
4. C. L. Coomer
5. E. C. Fox
6. J. S. Hsu
7. G. W. Ott
8. F. Z. Peng
9. R. M. Schilling
10. M. B. Scudiere
11. G. J. Su
12. L. M. Tolbert
13. C. P. White
14. K. M. Wilson, Technology Transfer and Economic Development
15. R. E. Ziegler
16. Laboratory Records – RC

17–18. Laboratory Records for submission to OSTI (2)

EXTERNAL DISTRIBUTION

19. P. A. Carpenter, Department of Energy, Oak Ridge Operations Office, P.O. Box 2008, Oak Ridge, Tennessee 37831-6269
20. D. B. Hamilton, DOE/OAAT, 1000 Independence Avenue, FORS, EE-32, Rm. 5G-023, Washington, D.C. 20585
21. R. Kessinger, Visual Computing Services Corporation, 9540 Highway 150, Greenville, Indiana 47124
22. R. S. Kirk, DOE/OAAT, 1000 Independence Avenue, FORS, EE-32, Rm. 5G-046, Washington, D.C. 20585
23. R. A. Kost, DOE/OAAT, 1000 Independence Avenue, FORS, EE-32, Rm. 5G-045, Washington, D.C. 20585
24. J. A. Merritt, DOE/OAAT, 1000 Independence Avenue, FORS, EE-32, Rm. 5G-064, Washington, D.C. 20585
25. P. Overholt, DOE/OPWT, 1000 Independence Avenue, FORS, EE-11, Rm. 5H-065, Washington, D.C. 20585
26. K. Samons, Visual Computing Services Corporation, 9540 Highway 150, Greenville, Indiana 47124
27. R. A. Sutula, DOE/OAAT, 1000 Independence Avenue, FORS, EE-32, Rm. 5G-046, Washington, D.C. 20585
28. W. Van Dyke, DOE-HQ, Office of Disposition Technologies, 19901 Germantown Road, GTN, Rm. B-433, NE-40, Germantown, Maryland 20874-1290

APPENDIX A

To: **Kelly Salmons at Visual Computing Systems**
From: **John W. McKeever**
Date: **November 18, 1998**

Preliminary Studies for the VCS SEMA Motor Inverter Drive

Introduction

Preferred and potential approaches for designing a drive inverter for an 8 kW, 4000 RPM electric motor, which employs Visual Computing System's (VCS's) Segmented Electromagnetic Array (SEMA) technology, are addressed in this summary. The electric motor is a patented axial-gap permanent magnet electric motor, which will be used to operate automobile accessories. The inverter to drive the accessory motor is being developed as part of a Small Business Technology Transfer (STTR) grant for collaboration between VCS and the Oak Ridge National Laboratory (ORNL). VCS is concurrently developing a 32 kW traction motor under a Collaborative Automotive Research for Advanced Technology (CARAT) grant and hopes to leverage ORNL's collaboration to develop a modular inverter. If each module provides 8 kW then one module can drive the accessory motors and four modules can be connected under one controller to drive the traction motor.

The original schedule is to complete testing of the STTR accessory motor drive inverter by April 6, 1999. Since "working tested" electronics for the CARAT are needed a week before this date and since testing the single-module STTR inverter must be an early step in development of the multiple-module inverter, the schedule must be significantly compressed. The earliest time that the accessory motor will be available is late February. Thus early March should be scheduled to drive the accessory motor with the single-module inverter at ORNL. This will allow some additional time for modules to be built and connected to drive the traction motor.

Subjects that will be discussed include: 1) soft- versus hard-switching in the inverter circuitry; 2) the power electronic switch that should be used in the inverter; 3) the use of field weakening to match the permanent magnet (PM) motor's performance above design speed with an electric vehicle's constant horsepower requirement; 4) selection of a self-sensing controller for the STTR inverter capable of delivering 8 kW; 5) modular design of the inverter to deliver 32 kW or more; and 6) schedule considerations.

Hard-Switching versus Soft-Switching Inverters – Dr. Fang Peng

ORNL has developed soft-switching technology in the past four years with the resonant snubber inverter (RSI) and the auxiliary resonant tank (ART) inverter. Soft-switching attempts to control operation of the power semiconductors so that they switch only when the voltage across the switch or the current through the switch is zero. Zero voltage switching (ZVS) is most common because zero current switching (ZCS) is more difficult to control. Both RSI and ART are ZVS devices. RSI technology is readily applied to single-phase systems, while the ART inverter technology is readily applied to three-phase devices.

Dr. Peng and Don Adams have completed efficiency analyses which indicate that there is not sufficient gain at power levels above 10 kVA to warrant the additional cost of soft-switching. Figure A.1 shows that hard switching is marginally better than ART soft-switching over 4/5 of the output range. The model used for the analysis is a pulse width modulated inverter switched at 10 kHz with space vector control driving an induction motor at a constant control ratio of voltage to frequency.

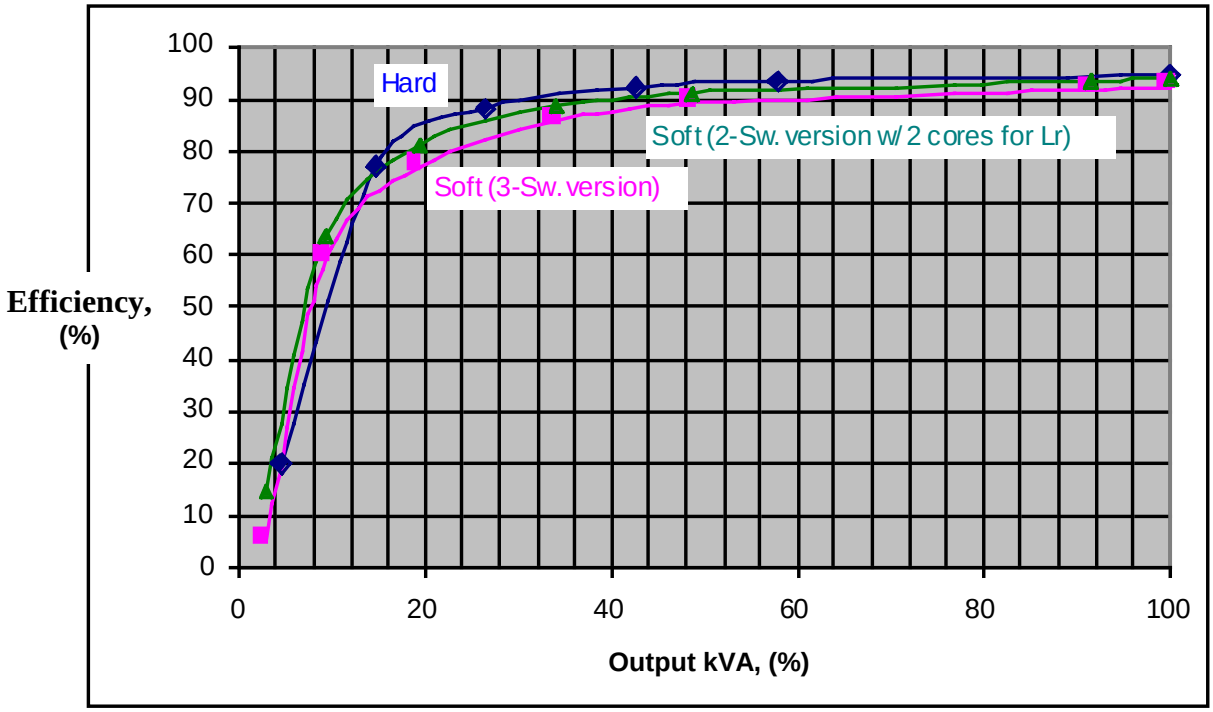

Fig. A.1. Comparison of hard-switched inverter efficiency with a soft-switched (ART) inverter efficiency at a 10 kVA level.

The energy loss that dominates at low kVA levels is caused by the stray inductance, L_s, which stores energy that must be dissipated each time the IGBT module is switched off. The magnitude of this energy is $0.5 x L_s x I_{off}^2$, which is the first term in the expression for E_{off} shown in Fig. A.2. L_s is the sum of the circuit's external stray inductance, L_{es}, and the IGBT module's internal stray inductance, L_{is}. When a hard-switched inverter is turned off the voltage, v(t), rises linearly from 0 toV_{DC} and the current, i(t), falls linearly from I_{off} to 0. Integrating the product of v(t) and i(t) over dt from 0 to t_f produces the second term of the expression for E_{off} Fig. A.2. Soft-switching greatly reduces this second term by switching when v(t) is very low. For hard-switched inverters, the second term is a small fraction of the first term when the kVA level falls between 10 and 100. From Fig. A.1 it is apparent that other losses in the additional circuitry of the soft-switched circuit, even though slight, cause it's efficiency to fall below that of the hard-switched inverter. Because of the low inductance of the SEMA motors it is best to precisely

control the switching, which is best controlled with hard-switching. In the region below 100 kVA a decision to use soft-switching would be based on a requirement for lower electromagnetic interference (EMI) or reduced line interference.

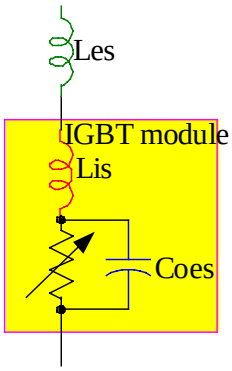

Turn-off Loss: $E_{off} = \frac{1}{2} L_S I_{off}^2 + \frac{1}{6} V_{DC} I_{off} t_f$

where Ls=Les+Lis, t_f is the fall time.

- **For Example:**
  - **600V600A FUJI IGBT**
  - **Lis=75nH, tf=0.2us**
  - **V_{DC}=300V, Les=25nH**

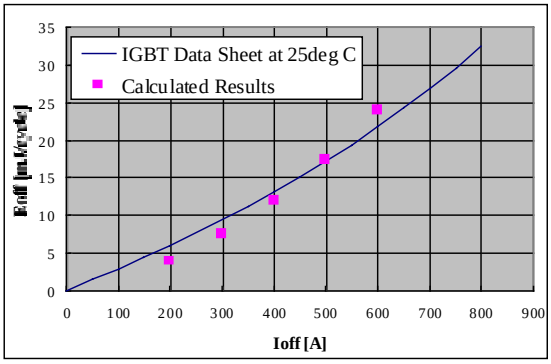

Fig. A.2. Simplified device model at switching.

The conclusions of this study are: 1) true ZVS is not possible because of internal stray inductance; 2) reduction of the turn-off loss of a single device is limited by the external stray inductance; and 3) when multi-device modules are used to minimize external stray inductance the natural increase in internal stray inductance can severely limit reduction of turn-off loss. New packaging/integration techniques to minimize internal stray inductance are needed to make the most of zero voltage switching.

Although traction motors with high kVA levels above 100 can expect improved efficiency, ORNL recommends that the Phase II drive development focus on hard-switching for both the STTR accessory motor. Since the kVA level of the CARAT traction motor is 40, ORNL recommends that it too be driven by a hard-switched inverter.

Devices to use for the Phase II Drive – Dr. Fang Peng and Dr. Gui-Jia Su

The device with which to design the inverter depends mainly upon the voltage and current required by the motor being driven. The STTR accessory motor specification for the rms line voltage is 227 V for which the zero-to-peak value is 321 V. Fifty volts should be added for control purposes with an additional 150 V added as a reliability and safety margin. Consequently, the power semiconductor should be able to withstand 521 V. The specification for rms line current is 21.4 A. The design margin as a factor of 2 so that the power semiconductor should be able to withstand 42.8 A.

The two power semiconductor candidates are MOSFETs and IGBTs. The main advantage of MOSFETs is that they can switch at 100 kHz, while IGBTs are limited to about 20 kHz. MOSFETs also have about half the voltage drop of IGBTs during operation. In the past, MOSFETs have had lower voltage and current ratings, but recent advances in MOSFET technology have increased these values. MOSFET APT5010B2VR sold by Advanced Power Technology is rated for 500 V and 47 A and has a diode forward voltage of 1.3 V at rated current. A dual IGBT H-series module sold by Powerex is rated for 600 V and 50 A and has a diode forward voltage of 2.8 V at rated current. A six IGBT H-series module is also available from Powerex at the same rating.

Availability of the modules with six IGBTs mounted makes the IGBT the favored candidate for the inverter to drive the STTR accessory motor. The great benefit is the small volume, which allows increased power density. Additional advantages are the built in protection and convenient gate connections. If the MOSFETs were used it would be necessary to design and configure six as well as their protection. ORNL recommends that the six IGBT modules be used to design the Phase II inverter.

Relation Between Current Ripple and Inverter Switching – Dr. Gui-Jia Su

It may be desirable to design inverters that can drive motors at higher rotational speeds. The information above mentions that IGBTs can switch at 20- to 25 kHz, while MOSFETs can switch at 60- to 100 kHz. Can IGBTs be used to design an inverter that will drive a brushless dc motor at speeds as high as 20,000 rpm for a motor with 12 poles? The corresponding electrical frequency is 2000 Hz, which has a period of 0.5 ms. For an IGBT operating at 20 kHz the period is 0.05 ms, which provides 10 switching cycles to fashion each electrical cycle delivered to the motor. The determining factor is whether the torque ripple that results is acceptable.

From the dc link voltage and the motor's inductance and back emf neglecting the stator coil resistance, the current ripple may be derived as a function of the motor's rotational frequency and the inverter's switching frequency. Figure A.3 shows the equivalent circuit. Ignoring the state coil resistance, R, the stator current peak-to-peak ripple at steady state for continuous conduction mode can be approximated by the equation,

$$I_{ripple(P-P)} \approx \frac{1}{L f_{SW}} \left(1 - \frac{K_{emf}\Omega}{V_{DC}}\right) K_{emf}\Omega, \qquad (1)$$

where

- L is the motor inductance of the two conducting phases;
- f_{SW} is the switching frequency of the inverter;
- V_{DC} is the inverter d.c. link voltage;
- K_{emf} is the ratio of line-to-line back emf to motor speed; and
- Ω is the motor speed.

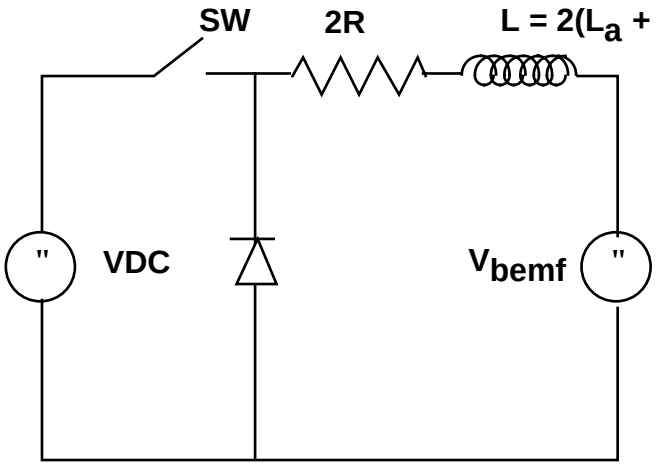

Fig. A.3. Equivalent circuit for an inverter driving two phases of a brushless dc motor.

The equation for current ripple has a maximum when the back emf is half the dc link voltage. At this point the maximum current ripple is

$$I_{ripple,\,max} = \frac{V_{DC}}{4 L_{total} f_{SW}}. \tag{2}$$

For a phase inductance, L_a=45 μH, with corresponding mutual inductance, M=22.5 μH, so that L_{total}=135 μH , a switching frequency, f_{SW}=20 kHz, a line-to-line peak voltage of 300 V at rated speed of 4000 rpm so that K_{emf}=0.075 V/rpm, and a dc link voltage, V_{DC}=350 V, the maximum current ripple is 32.4 amps. The torque ripple is, in turn, directly proportional to the motor's current ripple and is readily calculated once the torque constant is known.

Car manufacturers specify that torque ripple from 1 to 15 Hz must be controlled because it excites mechanical resonant frequencies in the driveline. A torque ripple of 15 Hz corresponds to a vehicle speed of about 0.625 mph (~1 ft/s for a motor with 8 poles and a gear ratio of 4). Separate PNGV EE tech team specifications quantify this control. Torque ripple should increase linearly from 0 to 5% of peak torque as a function of command torque up to 10% of peak torque. Above 10% of peak torque, the ripple should not exceed 5% peak value.

Background Discussion of d-axis and q-axis

Reference frame transformations have been developed to handle the time varying inductance variations in a salient pole generator under transient conditions. A typical salient pole synchronous machine is shown in Fig. A.4. We note that the magnetic reluctance along the centerline of the pole (direct axis) is much smaller than the reluctance perpendicular to this centerline (quadrature axes). We also see the stator axes labeled centerline of phase a, b, and c.

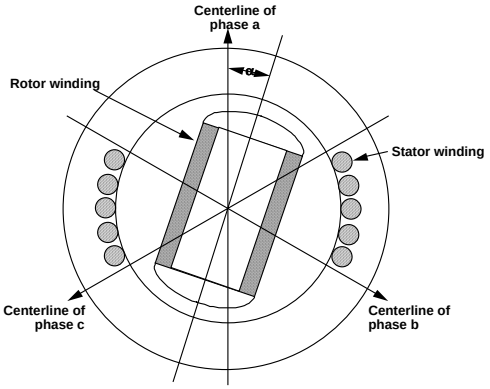

Fig. A.4. Synchronous three-phase motor with salient poles.

The important equation for the generator case in which current flows out of each phase leg is,

$$\underline{V^{T}} = -\underline{R} - \frac{d}{dt}\left(\underline{L}i\right). \tag{3}$$

Elgerd [1] develops a matrix form for the inductances of the stator axes as a function of the rotor position, α, as

$$\underline{L} = \begin{vmatrix} aa & ab & ac & ar \\ ba & bb & bc & br \\ ca & cb & cc & ar \\ ra & rb & rc & rr \end{vmatrix} = \begin{bmatrix} L_1 + L_2\cos 2\alpha & -L_3 + L_2\cos\left(2\alpha - \frac{2\pi}{3}\right) & -L_3 + L_2\cos\left(2\alpha + \frac{2\pi}{3}\right) & L_5\cos\alpha \\ -L_3 + L_2\cos\left(2\alpha - \frac{2\pi}{3}\right) & L_1 + L_2\cos\left(2\alpha + \frac{2\pi}{3}\right) & -L_3 + L_2\cos & L_5\cos\left(\alpha - \frac{2\pi}{3}\right) \\ -L_3 + L_2\cos\left(2\alpha + \frac{2\pi}{3}\right) & -L_3 + L_2\cos 2\alpha & L_1 + L_2\cos\left(2\alpha - \frac{2\pi}{3}\right) & L_5\cos\left(\alpha + \frac{2\pi}{3}\right) \\ L_5\cos\alpha & L_5\cos\left(\alpha - \frac{2\pi}{3}\right) & L_5\cos\left(\alpha + \frac{2\pi}{3}\right) & L_4 \end{bmatrix} . \tag{4}$$

This corresponds to equation Eq. (4.13) in his book. Note that this is a 4 x 4 matrix because the rotor voltage, v_r, is included as a variable. The vector voltage is,

$$\underline{v}^{T} = \left[v_a\, v_b\, v_c\, v_r\right], \tag{5}$$

where v_a, v_b, and v_c are the standard per phase voltages and
v_r is the rotor voltage.

The generator equivalent circuit is shown in Fig. A.5.

The important equation is Eq. [4.15]. Note this is written for the generator case. The remainder of Section 4.3.2 illustrates the complicated nature of the characterizing differential equations. At best they are "time-varying" and with varying load they can be non-linear.

We now note the two axes, stator and rotor (direct and quadrature). The trick here is to make a transformation between these two axes. We define a set of currents centered in the rotor axis as

$$\underline{I}_B^T = \left[i_d, i_q, i_o\right] \text{ (Eq. 4.28 in Elgerd)}, \tag{6}$$

I_o is termed the zero sequence current and is taken from the theory of "symmetrical components." For balanced operations, this current is zero and is added to make the transformation unique.

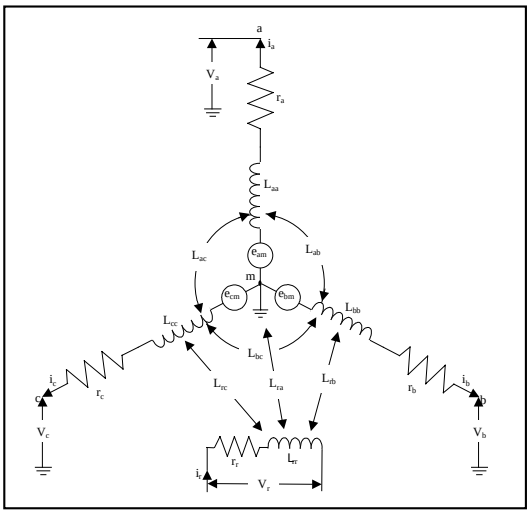

Fig. A.5. Generator equivalent circuit.

We must remember that Elgerd received his education in Sweden and his is the continental view of priorities. Thus, he refers to the "Blondel" [1] transformations,

$$\underline{I}_B = B\underline{I}_s, \tag{7}$$

where

$$\underline{I}_B^T = \left[i_d\, i_q\, i_o\right],$$

and

$$\underline{I}_s^T = \left[i_a\, i_b\, i_c\right].$$

In the U.S., we refer to Parks transformation and Krause [2] or Bose [3] use the notation

$$\underline{I}_{qdo} = K\underline{I}_{abc}. \tag{8}$$

Saadat [4] uses the notation

$$\underline{I}_{odq} = P\underline{I}_{abc}. \tag{9}$$

We note

$$\underline{I}^{T}_{qdo} = \left[i_q, i_d, i_o\right],$$

and

$$I_{odq} = \left[i_o, i_d, i_q\right].$$

We now show these axes transformations

$$B = \frac{2}{3}\begin{bmatrix} \cos\alpha & \cos\left(\alpha - \frac{2\pi}{3}\right) & \cos\left(\alpha + \frac{2\pi}{3}\right) \\ -\sin\alpha & -\sin\left(\alpha - \frac{2\pi}{3}\right) & -\sin\left(\alpha + \frac{2\pi}{3}\right) \\ 0.5 & 0.5 & 0.5 \end{bmatrix}, \tag{10}$$

$$K = \frac{2}{3}\begin{bmatrix} \cos\theta & \cos\left(\theta - \frac{2\pi}{3}\right) & \cos\left(\theta + \frac{2\pi}{3}\right) \\ \sin\theta & \sin\left(\theta - \frac{2\pi}{3}\right) & \sin\left(\theta + \frac{2\pi}{3}\right) \\ 0.5 & 0.5 & 0.5 \end{bmatrix},$$

$$P = \sqrt{\frac{2}{3}}\begin{bmatrix} 1/\sqrt{2} & 1/\sqrt{2} & 1/\sqrt{2} \\ \cos\theta & \cos\left(\theta - 2\pi/3\right) & \cos\left(\theta + 2\pi/3\right) \\ \sin\theta & \sin\left(\theta - \frac{2\pi}{3}\right) & \sin\left(\theta + \frac{2\pi}{3}\right) \end{bmatrix}.$$

B, K, and P are orthogonal, i.e. the 3 x 3 matrix

$$P^{-1} = P^{T} \qquad [P^{-1}]^{T} = P^{TT} = P. \tag{11}$$

The power equation becomes

$$p = \underline{I}_B^T \left(B^{-1}\right)^T B^{-1} \underline{V}_B, \tag{12}$$

$$\left(B^{-1}\right)^T B^{-1} = \begin{vmatrix} 3/2 & 0 & 0 \\ 0 & 3/2 & 0 \\ 0 & 0 & 3 \end{vmatrix},$$

and

$$p = \frac{3}{2}\left(v_d i_d + v_q e_q + 2 v_0 i_0\right). \tag{13}$$

Remembering that Elgerd is writing equations for a generator, we express his Eq. (4.36) as Eqs. (12, 13). (We are not interested in v_r and v_0).

$$\frac{d_{i_d}}{dt} = \frac{1}{L_d}\left[v_d - i_d r_s + \omega_e L_q i_q\right], \tag{14}$$

and

$$\frac{d_{i_d}}{dt} = \frac{1}{L_d}\left[v_q - r_s i_q - \left(L_d i_d + L_5 i_r\right)\omega_e\right]. \tag{15}$$

In our motor, the rotor consists of a magnet. Thus the back emf generated by the magnets is

$$E_r = \omega_e L_5 I_r, \tag{16}$$

where

ω_e = the operating frequency in rad/s,

and

$$\omega_e = \frac{P}{2}\,\omega_{\text{mechanical}},$$

where

P = no. of poles.

Krause [3] derives the torque (T_e) equation as

$$T_e = \frac{3P}{4}\left[\left(L_d - L_q\right)i_d i_q + \frac{E_f}{\omega_e} i_q\right], \tag{17}$$

since

$$\frac{E_f}{\omega_e} = \psi_{mag} \text{ (flux linkages due to magnet),}$$

$$T = \frac{3P}{4}\left[\psi_{mag} i_q + \left(L_d - L_q\right)i_d i_q\right]. \tag{18}$$

Thus, we have new axes fixed in the rotor and rotating with a speed ω_e rad/sec. We refer to the axes components as the direct axes (I_d) and quadrature axes (I_q). One helpful relationship is that sinusoidal quantities in the (a,b,c) axes become dc quantities in the rotating axes (d,q). The equivalent circuit becomes

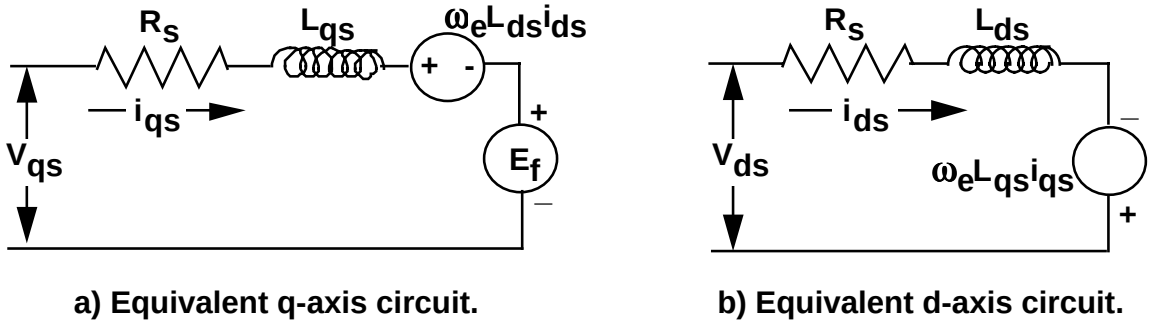

a) Equivalent q-axis circuit. **b) Equivalent d-axis circuit.**

Fig. A.6. Equivalent circuit for dq axis analysis.

We note

1) E_f is a linear function of speed,
2) L_q, L_d are given by Elgerd's Eq. (4.37), and
3) The mechanical torque is

$$\frac{d\omega_{mech}}{dt} = \frac{1}{J}\left[T_e - T_L - B\omega_{mech}\right],$$

where

T_L = Load torque,
B = viscous friction coefficient,

Field Weakening – J. Milton Bailey

Some of Dr. Bailey's work is included to explain field weakening. The alternate approach referred to on page A-13 is part of some work performed for DOE in FY1998. A disclosure is being prepared and as soon as that is complete, we will discuss it with you under the protection of a non-disclosure agreement. It applies to low inductance motors just like yours and is a nice piece of creative technical work.

The appropriate equations used to develop the dynamic characteristics of these motors are

$$\frac{di_{qs}}{dt} = \frac{1}{L_{qs}}\left(V_{qs} - R_s i_{qs} - \omega_e L_{ds} i_{ds} - E_f\right)$$

$$\frac{di_{ds}}{dt} = \frac{1}{L_{qs}}\left(V_{ds} - R_s i_{qs} - \omega_e L_{ds} i_{ds}\right) \qquad (19)$$

$$\frac{d\varpi_r}{dt} = \left(T_e - T_L\right)/J$$

$$T_e = \frac{3p}{4}\left[\left(L_{ds} - L_{qs}\right) i_{ds} i_{qs} + \frac{E_f}{\omega_e} i_{qs}\right]$$

where

R_s = stator resistance,
L_{qs}= q-axis inductance,
L_{ds} = d-axis inductance,
E_f = back emf due to magnetic flux
ω_e = operating frequency,
V_{qs} = q-axis voltage component,
V_{ds} = d-axis voltage component,
i_{qs} = q-axis current component,
i_{ds} = d-axis current component,
ω_r = rotor angular frequency,
T_e = generated torque,
T_L = generated torque,
J = inertia, and
p = pole number.

The torque equation takes on different forms depending on the L_{ds} and L_{qs} relationships that are shown in Table A.1.

Table A.1. Torque equations

MOTOR	PARAMETERS	TORQUE
SPM	$L_{ds} = L_{qs}$	$T_e = \frac{3P}{4}\frac{E_f i_{qs}}{\omega_e}$
IPM	$L_{ds} \neq L_{qs}$	$T_e = \frac{3P}{4}\left[\left(1_{ds} - 1_{qs}\right)i_{ds}i_{qs} + \frac{E_f i_q}{\omega_e}\right]$
Synchronous Reluctance	$E_f = 0$	$T_e = \frac{3P}{4}\left[\left(1_{ds} - 1_{qs}\right)i_{ds}i_{qs}\right]$

Once the system is in the field-weakening mode, care must be taken to ensure stator currents stay within limits. These limits are a function of system parameters and the inverter voltage limit. To illustrate, return to the dynamic model of Eq. (18) and make the following assumptions

a) The system is in the steady state where all derivatives are zero, and
b) The resistances are negligible.

Equation (18) now becomes

$$v_d = \omega_e L_q i_q^{*} \tag{20}$$

$$v_q = \omega_e L_d L_d + E_f \tag{21}$$

subject to the limitations

$$v_d = \omega_e L_q i_q^{*} \tag{22}$$

and

$$v_q = \omega_e L_d L_d + E_f \tag{23}$$

where

I_r = rated current value in amperes, and
V_r – rated voltage value in volts.

[*] We have dropped the subscript "s" on the currents, voltages, and inductances.

Combining Eqs. (19–22)

$$(\omega_e L_q i_q)^2 + (\omega_e L_q i_q + E_f)^2 = v_r^2$$

Defining

$$\frac{E_f}{\omega_e} = \lambda_{mag} = \text{ flux linkages due to the magnet.} \tag{24}$$

Equation (23) becomes

$$\left(\frac{V_r}{\omega_e}\right)^2 = \left(\frac{i_q}{1/L_q}\right)^2 + \left(\lambda_{mag} + \frac{i_d}{1/L_d}\right)^2 \tag{25}$$

In the I_q, I_d plane, Eq. (25) is an ellipse centered at $-\lambda_{mg}$. With V_r fixed, the ellipse shrinks inversely with ω_e. Thus, one has a voltage-limit ellipse and a current-limit circle. We note that for the surface mounted permanent magnets (SPMs), L_q and L_d are equal.

In the field-weakening regime, the problem facing the designer is that of choosing the right current pair (i_q, i_d) so as to maximize the constant power as well as the CPSR and stay within the current-limit circle and the voltage-limit ellipse.

ALTERNATE APPROACH

While this approach is quite suitable for developing field-weakening schemes, it does not emphasize the role that the motor inductance must play in these schemes. In most of the papers surveyed, much attention is given to developing a per unit basis for Eqs. (18–25) which can obscure the details of the motor inductance. For this reason, we (ORNL) have taken another approach to field weakening which emphasizes the effect of motor inductance, power output, and current demand. At this stage of the program, we are considering the SPM configuration.

Selection of Sensorless Control – Dr. Gui-Jia Su

ORNL recommends use of the sensorless (or self-sensing) inverter for the Phase I SEMA motor.

REFERENCES

1) O. I. Elgerd, *Electric Energy Systems Theory : An Introduction*, Chapter 4 and Appendix, McGraw Hill Book Company, 1971.
2) P. C. Krause, *Analysis of Electric Machinery*, Chapter 5, McGraw Hill Book Company, 1986.
3) B. K. Bose, *Power Electronics and AC Drives*, Chapter 2, Printice-Hall, 1986.
4) H. Saadat, *Power Systems Analysis*, Chapter 8, WCB McGraw-Hill, 1999.

Appendix B

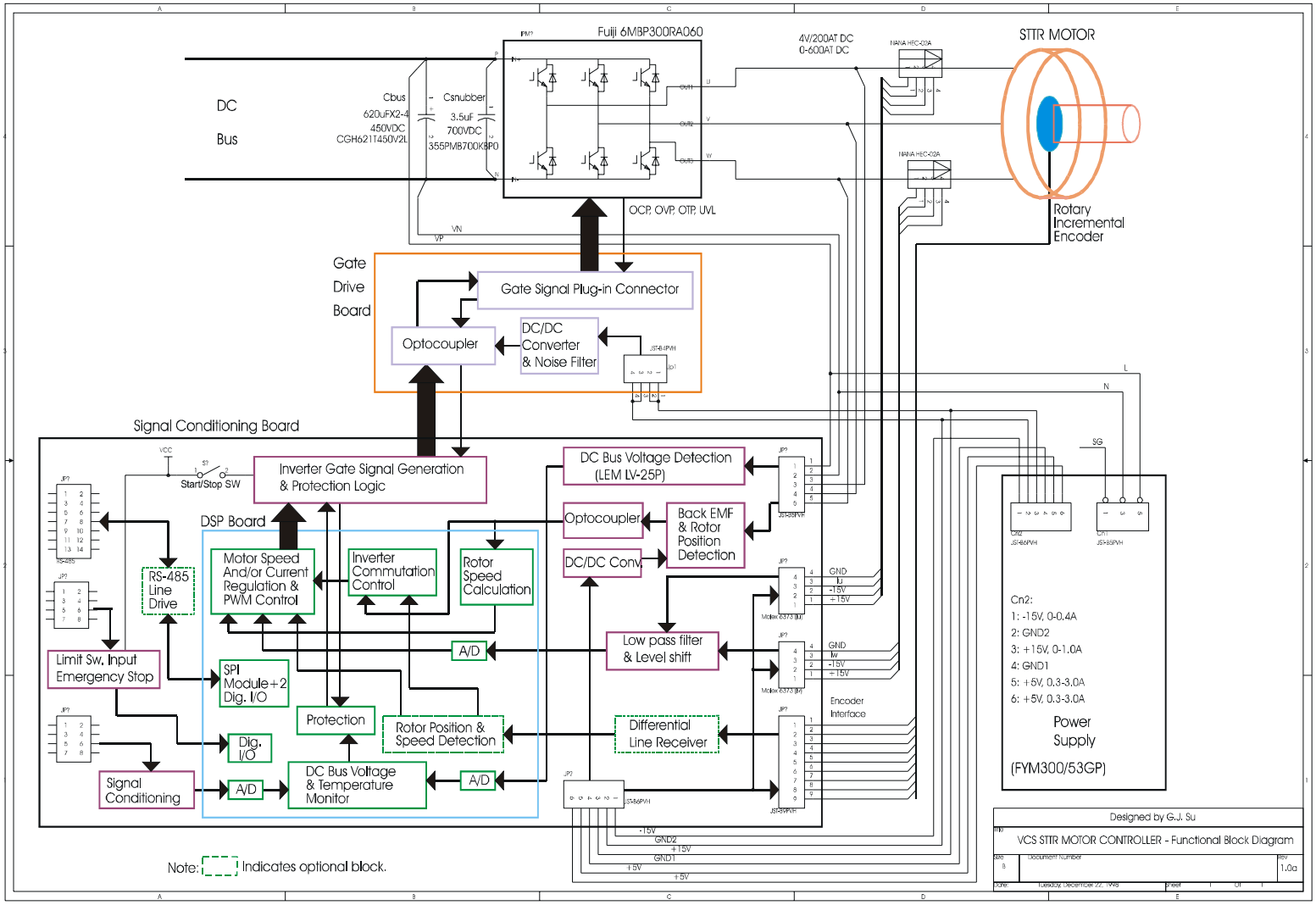

Fig. B.1. Block diagram of SEMA motor controller using back EMF or encoder.

Appendix C

Assembly Instructions for the VCS STTR Inverter Components

Appendix C.1

Signal Conditioning Board

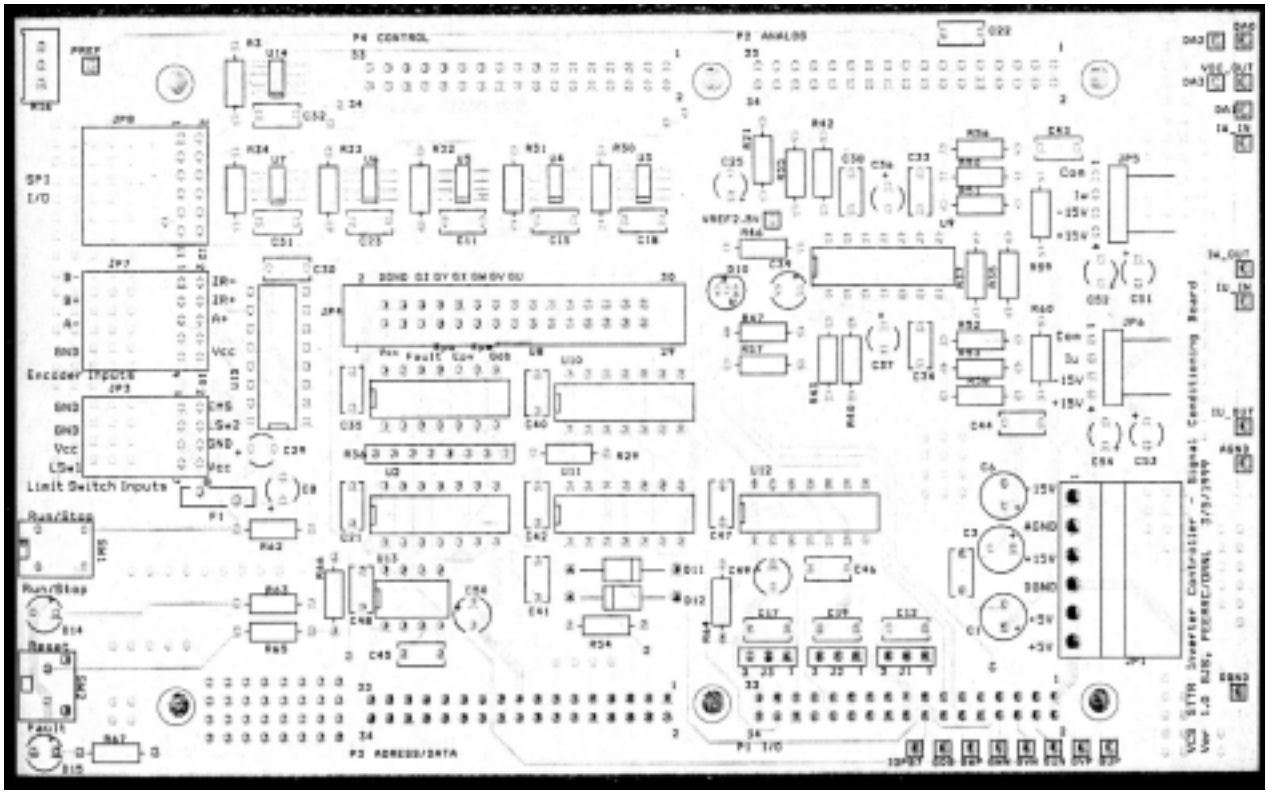

Appendix C.2

Parts List for Signal Conditioning Board

Bill of Materials March 16, 1999 Revised: March 4, 1999 Revision: 1.0

Item	Quantity	Reference	Part
1	1	C1	Al 100 μF, 16 V
2	2	C6,C3	Al 47 μF, 25 V
3	2	C29,C8	Tan 1 μF, 16 V
4	17	C11,C15,C18,C21,C22,C23, C30,C31,C32,C33,C34,C35, C40,C42,C45,C47,C48	0.1 μF, 50 V
5	4	C12,C17,C19,C46	100 πF, 50 V
6	7	C25,C36,C37,C51,C52,C53,C54	Tan 1.5 μF, 25 V
7	1	C38	1 μF
8	1	C39	Tan 10 μF, 16 V
9	1	C41	1 nF
10	2	C44,C43	0.01 μF, 50 V
11	2	C49,C50	Tan 2.2 μF, 10 V
12	1	D10	Vref LT1004ILP-2.5
13	2	D12,D11	Schottky Diode 1N5617
14	1	D14	Green LED 5370T5LC
15	1	D15	Red LED 5370T1LC
16	1	F1	Resettable PTC 60R010
17	1	JP1	JST-B6PVH (Right angle)
~~18~~	~~1~~	~~JP2~~	~~Jumper~~
19	1	JP3	Amp 103164-2 Right angle 4x2
20	1	JP4	Samtec TSS-115-02-G-D Header 15x2
21	1	JP5	Molex 6373 (Iw) Right angle
22	1	JP6	Molex 6373 (Iu) Right angle
23	1	JP7	Amp 103164-3 Right angle 5x2
24	1	JP8	Amp 103164-4 Right angle 6x2
25	3	J1,J2,J3	3-pin jumper with contact
26	1	P1	P1 I/O
27	1	P2	P2 Analog
28	1	P3	P3 Address/Data
29	1	P4	P4 Control
30	6	R3,R30,R31,R32,R33,R34	130 Ω, 1/4 W
31	1	R16	310 kΩ side adjust potentiometer
32	1	R21	20 kΩ, 1/4 W
33	1	R29	10 kΩ, 1/4 W
34a	8	R37,R43,R51,R52,R55,R56, R57,R58	47 kΩ, 1/4 W
~~34b~~	~~4~~	~~R35,R40,R50,R53~~	~~Do not load these 4 resistors~~

Item	Quantity	Reference	Part
35	1	R36	20 kΩ Resistor SIP 8
36	1	R42	200 Ω, 1%
37	1	R46	22 Ω, 1/4 W, 5%
38	1	R47	100 kΩ, 1/4 W, 5%
39	3	R54,R64,R66	4.7 kΩ, 1/4 W, 5%
40	4	R59,R60,R62,R65	33 kΩ, 1/4 W, 5%
41	2	R67,R63	560 Ω
42	1	SW1	GS02MCKE SPST Slide switch, Run/Stop
43	1	SW2	TL1105WF160 SPST Push button switch, Rest
44	1	PC Test point 1	DGND
45	1	PC Test point 2	AGND
46	1	PC Test point 10	Pref
47	1	PC Test point 14	Iu_OUT
48	1	PC Test point 15	Vdc_OUT
49	1	PC Test point 16	DA2
50	1	PC Test point 17	Iw_OUT
51	1	PC Test point 18	DA3
52	1	PC Test point 19	DA1
53	1	PC Test point 20	DA0
54	1	PC Test point 24	Gup
55	1	PC Test point 25	Gun
56	1	PC Test point 26	Gvn
57	1	PC Test point 27	Gvp
58	1	PC Test point 28	Gwn
59	1	PC Test point 29	Gwp
60	1	PC Test point 30	IOPB7
61	1	PC Test point 31	Gdb
62	1	PC Test point 32	Vref 2.5 V
63	1	PC Test point 33	Iw_IN
64	1	PC Test point 34	Iu_IN
65	1	U2	MM74HC14N
66	6	U3,U4,U5,U6,U7,U14	DS485N
67	2	U8,U10	MC74HC03AN
68	1	U9	LM124AJ
69	1	U11	MM74HC74AN
70	1	U12	MM74HC08N
71	1	U13	TLC7705QP
72	1	U15	DS34C86TN

Appendix C.3

Sensing and Gate Drive Board

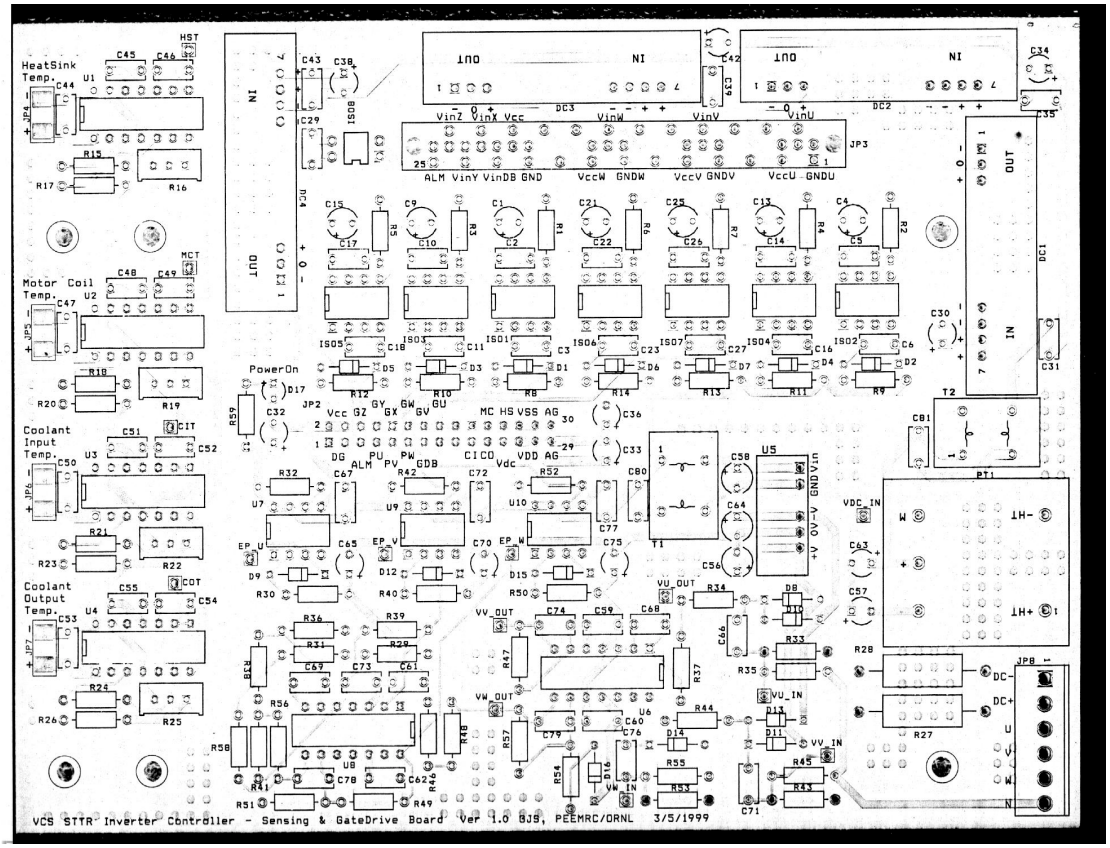

Appendix C.4

Parts List for Sensing and Gate Drive Board

Fuiji IGBT-IPM 7MBP300RA060 Gate Drive Revised: March 8, 1999 Revision: 1.0
Bill of Materials March 16, 1999

Item	Quantity	Reference	Part	
1	7	C1,C4,C9,C13,C15,C21,C25	Al	10 μF, 35 V
2a	18	C2,C5,C10,C14,C17,C22, C26,C31,C35,C39,C43,C59, C60,C61,C62,C67,C72,C77		0.1 μF, 50 V
2b	8	Additional bypass caps for the four thermocouple interfaces	Connect between pins 11 to 13 and 7 to ground of U1, U2, U3, and U4	
3a	12	C3,C6,C11,C16,C18,C23, C27,C29,C44,C47,C50,C53		100 pF, 50V
3b	3	C69,C73,C78		3500 pF, 50 V
4	6	C30,C33,C34,C36,C38,C42	Tan.	4.7 μF, 25 V
5	1	C32	Tan.	4.7 μF, 6.3 V
6	4	C45,C48,C51,C55		0.01 μF
7	4	C46,C49,C52,C54		300 pF (standard)
8	2	C65,C56	Tan.	4.7 μF, 16 V
9	5	C57,C63,C65,C70,C75	Tan.	1 μF, 35 V
10	1	C58	Tan.	10 μF, 6.3 V
11	3	C66,C71,C76		0.33 μF
12	3	C68,C74,C79		0.022 μF
13	2	C81,C80		1 μF
14	4	DC1,DC2,DC3,DC4	DC-DC Converter (HDF1215S)	
15	16	D1,D2,D3,D4,D5,D6,D7,D8, D9,D19,D11,D12,D13,D14, D15,D16	Small signal diode (low leakage) (1N4148)	
16	1	D17	Green LED 5370T5LC	
17	7	ISO1,ISO2,ISO3,ISO4,ISO5, ISO6,ISO7	HCPL-4504	
18	1	ISO8	TLP-621 (or NTE3098)	
19	1	JP2	Header 15x2 Samtec BCS-115-L-D-TE	
20	1	JP3	Samtec BCS25PE	
~~21~~	~~4~~	~~JP4,JP5,JP6,JP7~~	~~Header 2 not used~~	
22	1	JP8	JST-B6PVH	
23	1	PT1	LEM LV 25-P	
24	7	R1,R2,R3,R4,R5,R6,R7	20 kΩ, 1/4 W, 5%	
25	7	R8,R9,R10,R11,R12,R13,R14	270 Ω, 1/4 W, 5%	
26	4	R15,R18,R21,R24	8.2 MΩ, 1/4 W, 5% (standard)	
27	4	R16,R19,R22,R25	Potentiometer, 100 kΩ	

Item	Quantity	Reference	Part
28	4	R17,R20,R23,R26	15 MΩ, 1/4 W, 5%
29	2	R28,R27	22 kΩ, 2 W
30	6	R29,R37,R39,R47,R49,R57	1 MΩ, 1/4 W, 1%
31	3	R30,R40,R50	3 kΩ, 1/4 W, 5%
32	3	R31,R41,R51	3.01 kΩ, 1/4 W, 1% (standard)
33	3	R32,R42,R52	2 kΩ, 1/4 W, 5%
34	3	R33,R43,R53	100 kΩ, 1 W, 1%
35	3	R34,R44,R54	150 kΩ, 1/4 W, 1%
36	3	R35,R45,R55	1.82 kΩ, 1/4 W, 1% (standard)
37	3	R36,R46,R56	47.5 kΩ, 1/4 W, 1%
38	3	R38,R48,R58	12.1 kΩ, 1/4 W, 1%
39	1	R59	560 Ω
40	1	TP1	Vdc_IN
41	1	TP2	Ep_u
42	1	TP3	VU_OUT
43	1	TP4	VU_IN
44	1	TP5	Ep_v
45	1	TP6	VV_OUT
46	1	TP7	VV_IN
47	1	TP8	Ep_w
48	1	TP9	VW_OUT
49	1	TP10	VW_IN
50	1	TP11	HST
51	1	TP12	MCT
52	1	TP13	CIT
53	1	TP14	COT
54	2	T2,T1	CommMode (SU9V-05020)
55	4	U1,U2,U3,U4	AD595AQ (thermocouple reader)
56	1	U5	DC/DC Converter, NMH0509S
57	1	U6	LM124AJ
58	3	U7,U9,U10	HCPL-261N
59	1	U8	LM139J

Appendix C.5

Assembly Instructions for the Sensing and Gate Drive Board

(ORNL Power Control Unit Designed for the VCS Accessory SEMA Motor. Refer to Appendix C.4 for definition of parts.)

Sequential assembly instructions will be given for each board. Pictures will reinforce location of the components which are also clearly labeled on each board. Variations from the normal assembly because of silkscreen errors or circuit modifications will be noted in bold print.

Generic Instructions
Soldering temperature should be between 750 and 800^{o} F.
Remove appropriate components from the packages for each step.
Each component is labeled from top to bottom and from left to right on each figure.

First Board
VCS STTR Inverter Controller - Sensing and Gate Drive Board

1. Insert appropriate ICs (black, 17) with pin 1 in the square pad and solder. Board locations are labeled ISO1 through ISO7 and U1 through U10. See Fig. 1. Refer to parts list in C.4 for details.

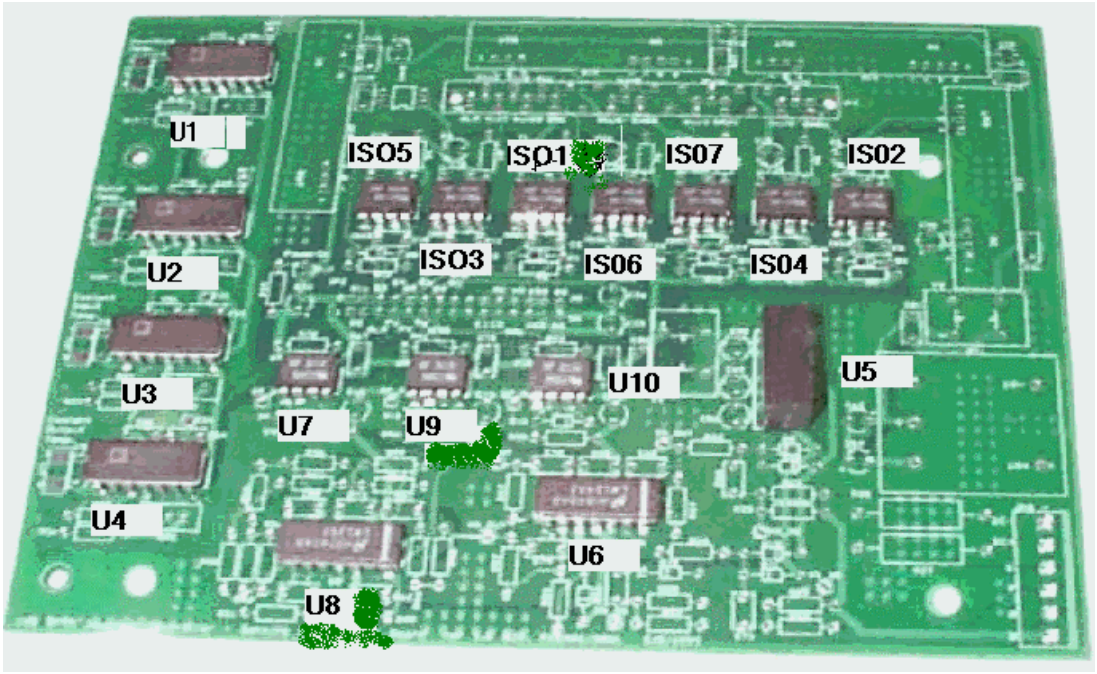

Figure 1

2. See Fig. 2 for steps 2 and 3. Insert voltage sensor LV25-P (blue, 1) and solder. Board location is labeled PT1.

3. Insert four dc-dc converters HDF1215S (black located on the top of the board), solder and clip lead wires. Board locations are labeled DC1 through DC4.

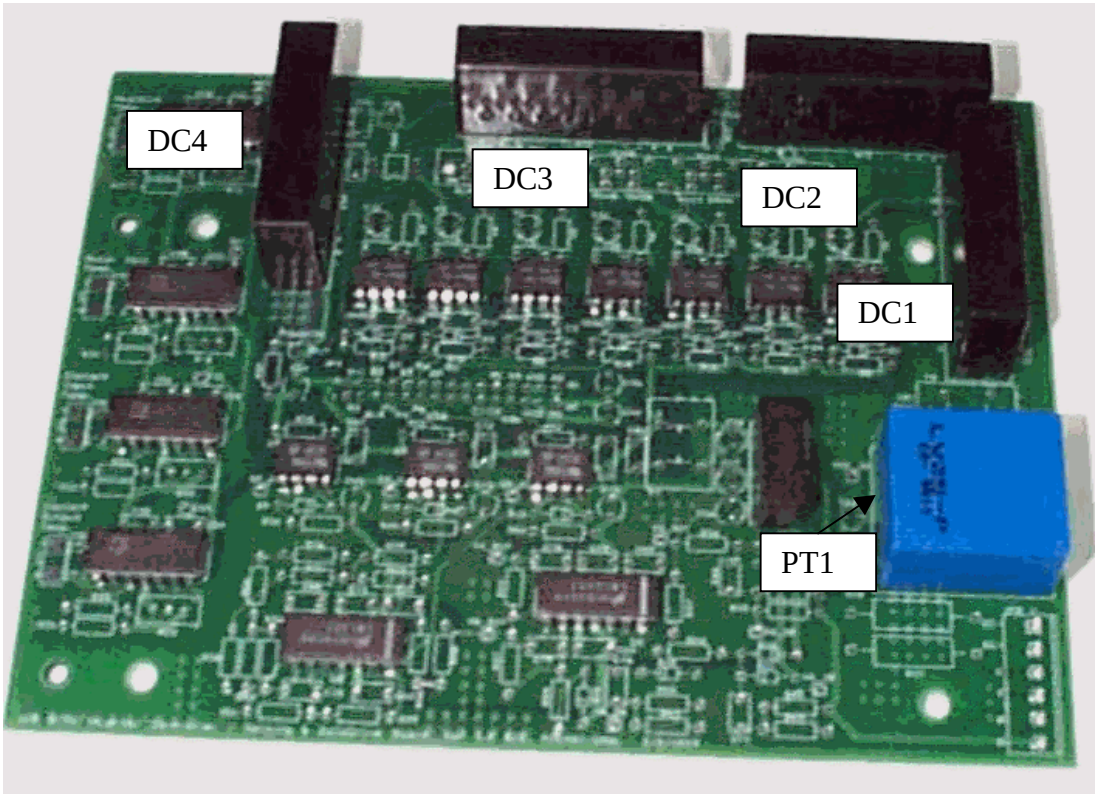

Figure 2

4. See Fig. 3 for steps 4 through 8. Insert ISO8 and solder.
5. Insert common mode chokes T1 and T2. Solder and clip lead wires.
6. Insert test points T1 through T14 and solder.
7. Insert connector (white) JP8 and solder.
8. Insert resistors R27 and R28 and solder.
9. See Fig. 4 for steps 9 and 10. Insert IGBT connector JP3 in backside.
10. Insert signal conditioning board connector JP2 in backside and solder.
11. See Fig. 5 for steps 11 through 17. **Insert diodes D1 through D16 with polarity opposite to that shown on silkscreen.** Insert Light Emitted Diodes D17 (green) as polarity is indicated on silkscreen. Insert 4 blue 100K Ω potentiometer R16, R19, R22, and R25.
12. See Fig. 5 for steps 11 through 17. **Insert diodes D1 through D16 with polarity opposite to that shown on silkscreen.** Insert Light Emitted Diodes D17 (green) as polarity is indicated on silkscreen. Insert 4 blue 100K Ω potentiometer R16, R19, R22, and R25.
13. Resistors R1-R7 should be inserted. The resistors have a value of 20KΩ, 1/4 Watt.
14. Insert R8 thru R14 (270Ω, 1/4 Watt).
15. Insert resistors: R15, R18, R21, and R24 (8.2 MegΩ, 1/4 Watt). Also insert R17, R20, R23, and R26 (15 MegΩ, 1/4 Watt).

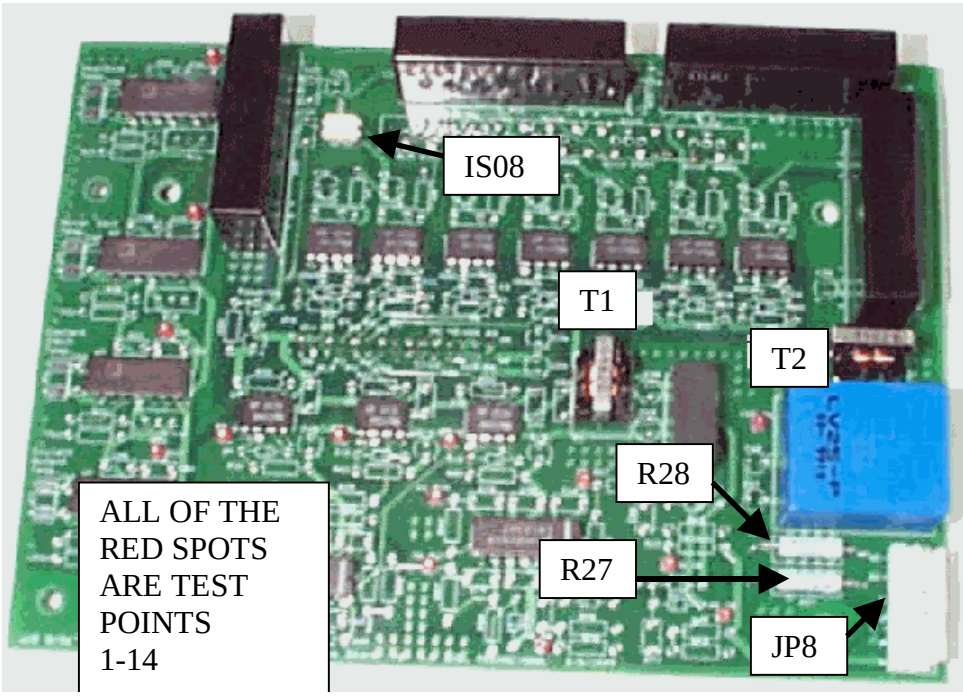

Figure 3

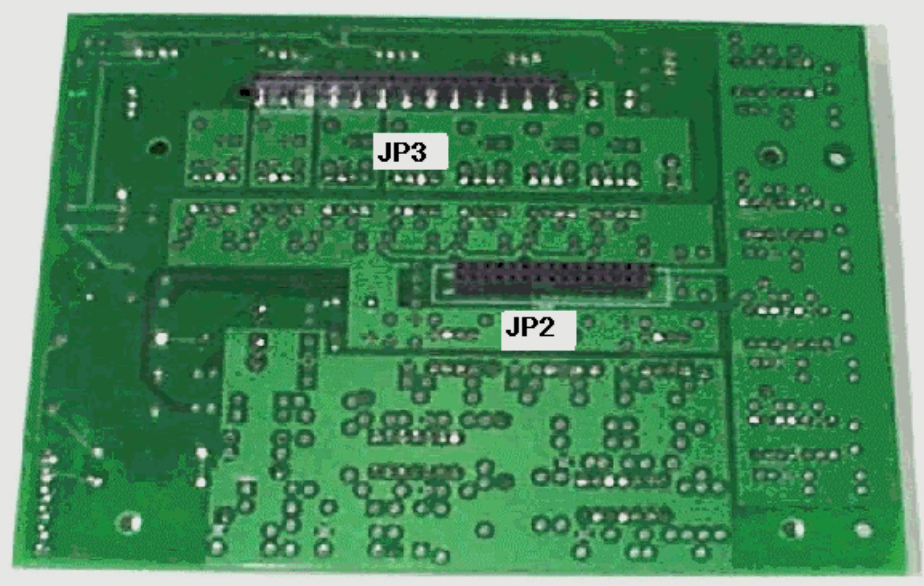

Figure 4

16. Insert R29, R37, R39, R47, R49, and R57 (1MegΩ, 1/4 Watt). Also, insert R30, R40, and R50 (3KΩ, 1/4 Watt).

17. Insert R31, R41, and R51 (3.01KΩ, 1/4 Watt). In addition, insert R32, R42, and R52 (2KΩ, 1/4 Watt).
18. Also insert R34, R44, and R54 (150 KΩ, 1/4 Watt). Insert R33, R43, and R53 (100KΩ, 1 Watt). See figure 5 for steps 11 through 17.

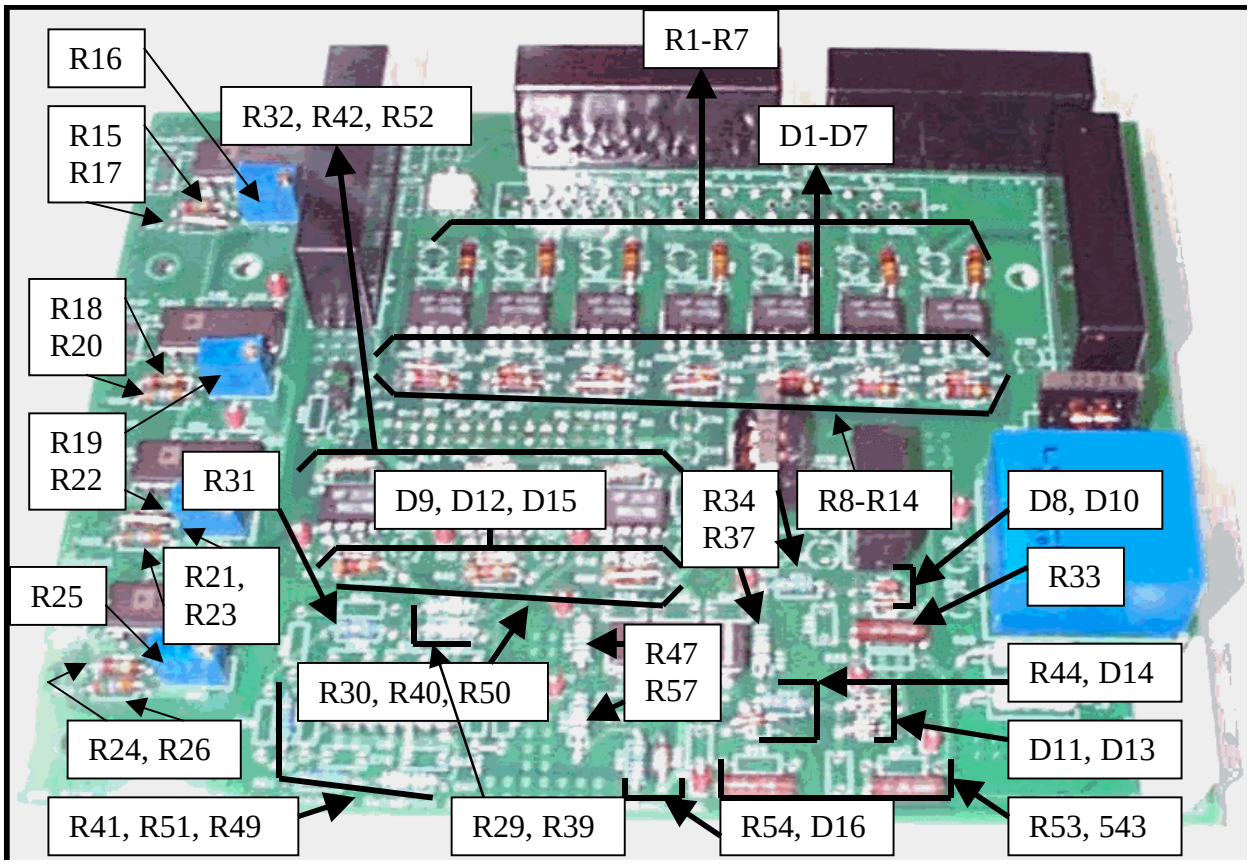

Figure 5

19. See Fig. 6 for step 18. Insert R35, R45, and R55 (1.82KΩ, 1/4 Watt). Insert R36, R46, and R56 (47.5 KΩ, 1/4 Watt). Also, insert R38, R48, and R58 (12.1KΩ, 1/4 Watt). Insert the last resistor R59 (560Ω, 1/4 Watt).
20. See Fig. 7 for step 19. Insert seven black canister capacitors C1, C4, C9, C13, C15, C21, and C25 (10 uF, 35 Volts).
21. See Fig. 9 for step 21. Insert 8 thermocouple amplifier bypass capacitors on the backside of the board (0.1uF, 50 Volts).
22. See Fig. 10 for steps 22 through 24. Finally insert C58 (10uF, 6.3 wV). Next insert C32 (4.7uF, 6.3V). Insert C30, C33, C34, C36, C38, and C42 (4.7uF, 25 V). Insert C57, C63, C65, C70 and C75 (1uF, 35 V). Insert C56 and C64 (4.7uF, 16V) **Polarity of C64 is wrong on the PC board; therefore, place the capacitor in the board in the opposite direction**. Insert C80 and C81 (1uF, 50V).

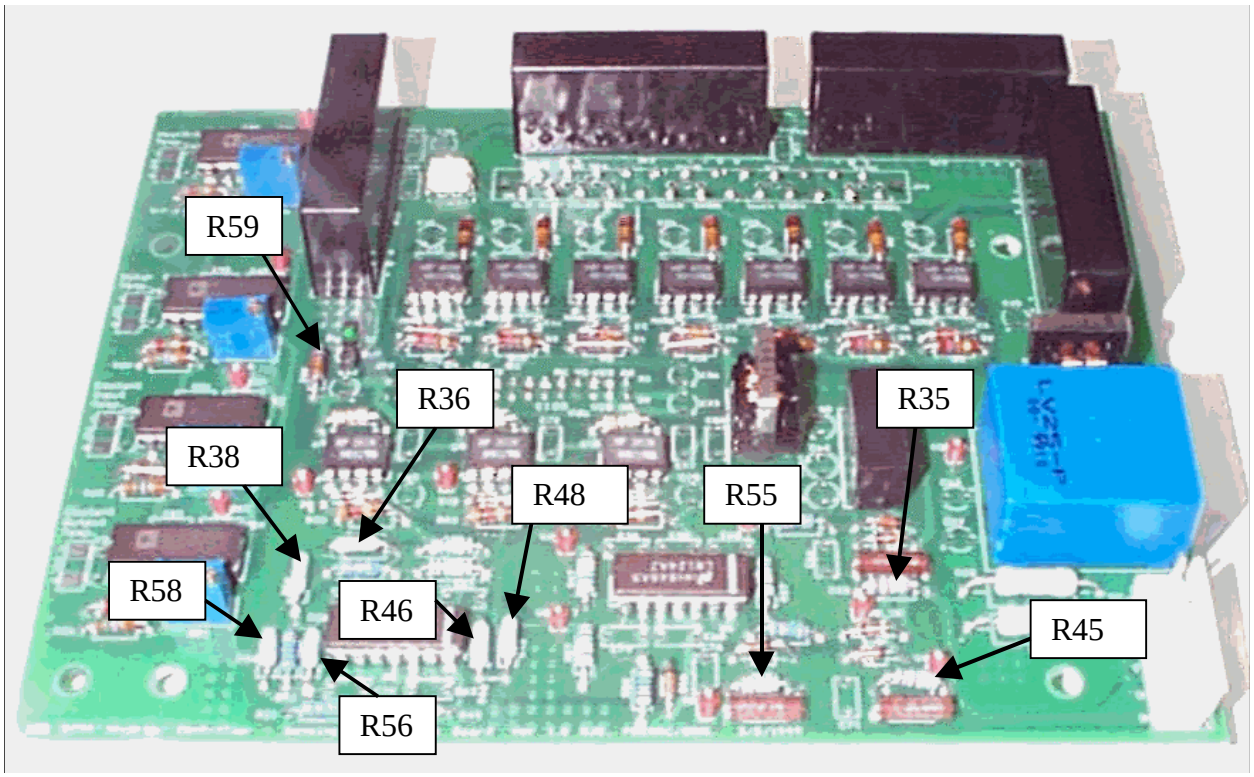

Figure 6

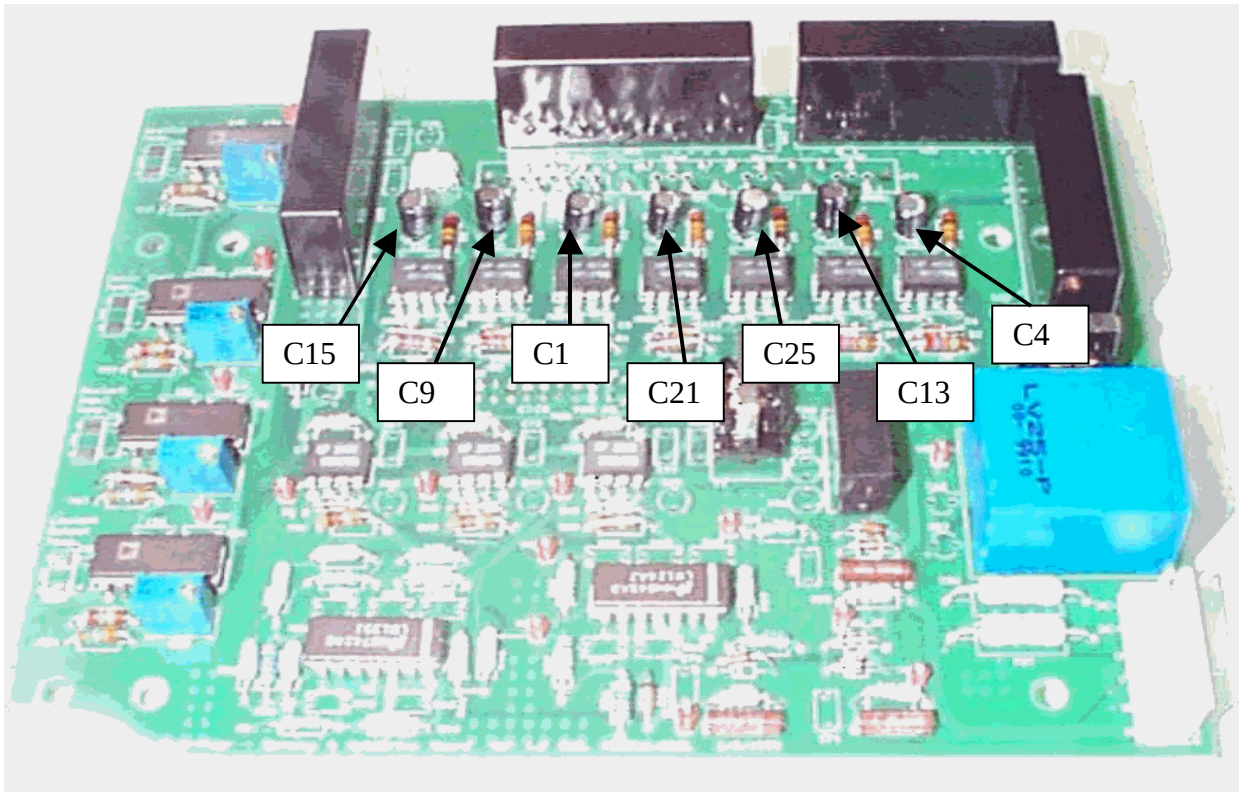

Figure 7

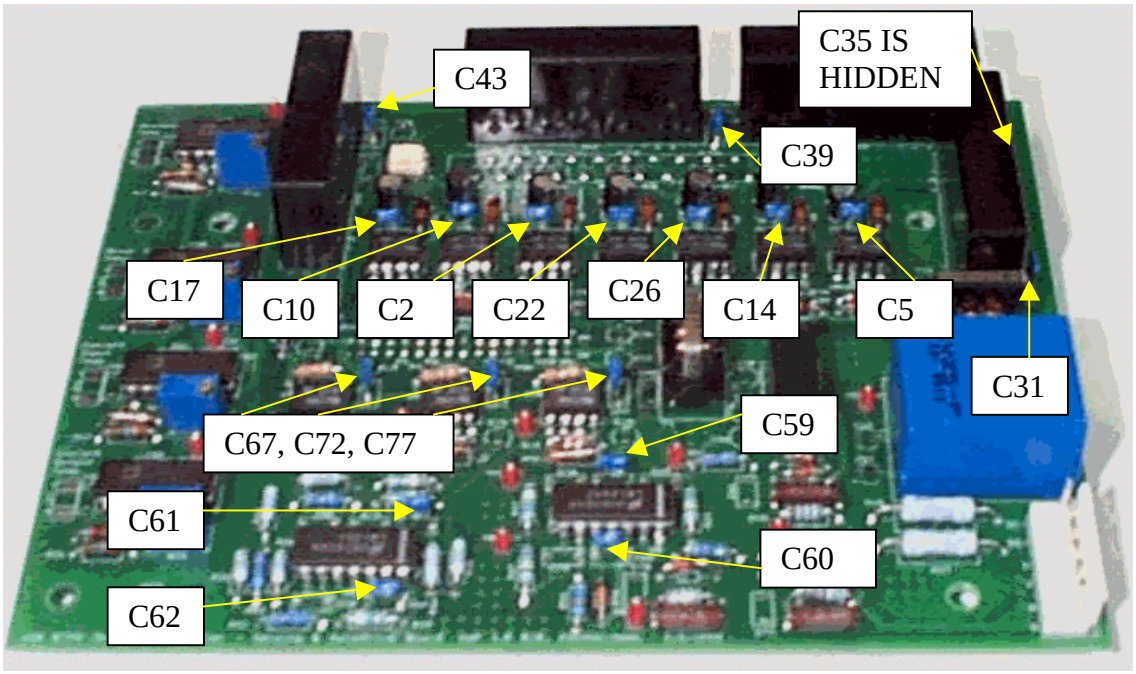

Figure 8

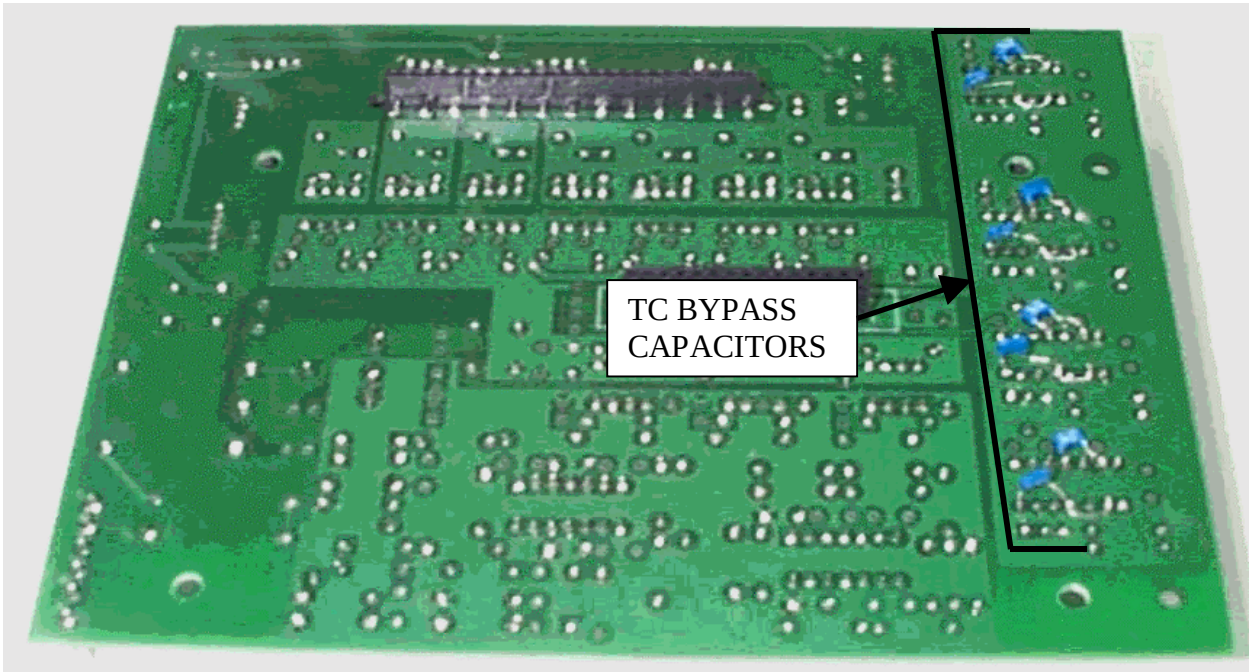

Figure 9

23. Insert C68, C74, and C79 (0.022uF, 50 V). Insert C66, C71, and C76 (0.33uF, 50 V). Insert C46, C49, C52, and C54 (330pF, 50 V). Insert C45, C48, C51 and C55 (0.01uF, 50 V).
24. Insert C3, C6, C11, C16, C18, C23, C27, C29, C44, C47, C50, and C53 (100pF, 50V). Insert C69, C73 and C78 (3300 pF, 50V).

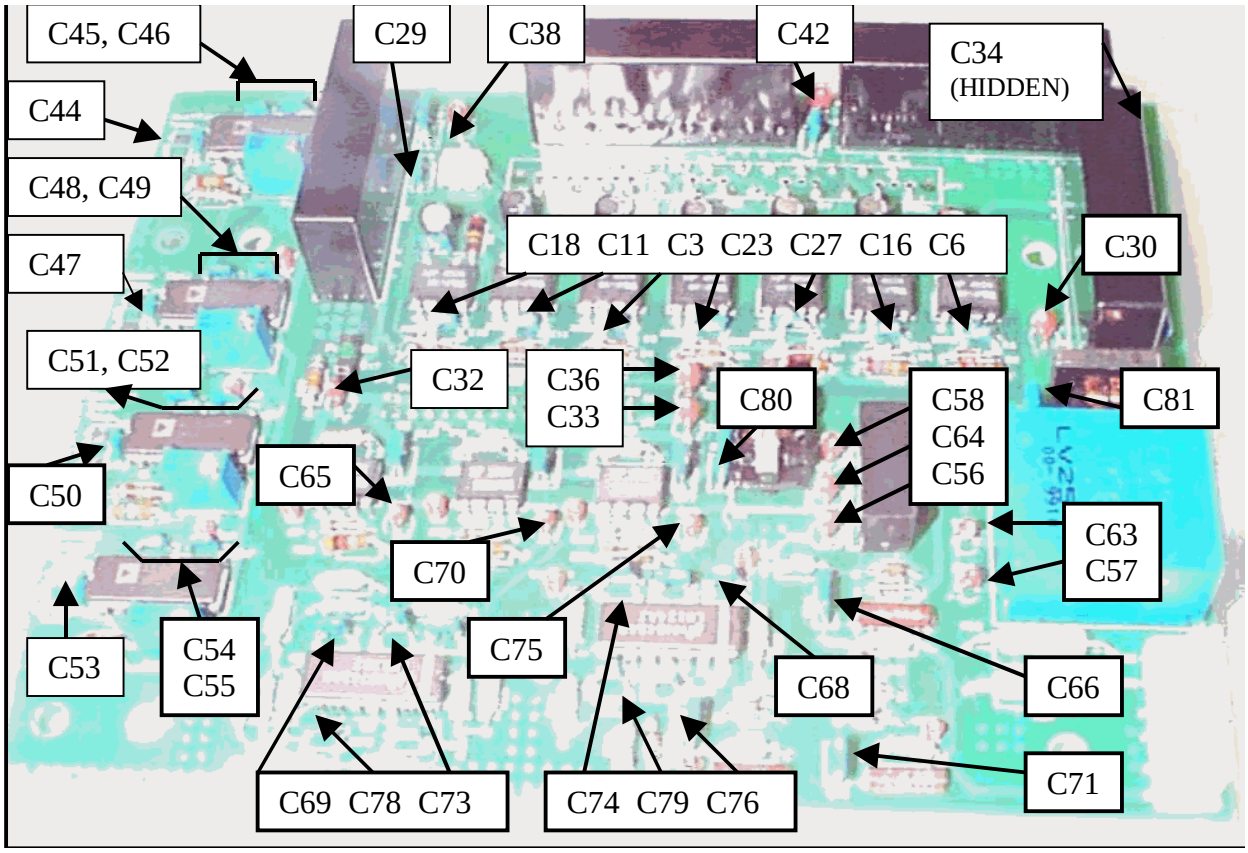

Figure 10.

Appendix C.6

Assembly Instructions for the Signal Conditioning Board

(ORNL Power Control Unit Designed for the VCS Accessory SEMA Motor. Refer to Appendix C.2 for definition of parts.)

1. See Fig. 11 for steps 1 through 3. Insert U2, U3, U4, U5, U6, U7, and U14.

2. Insert U8, U10, U9, U11, U12, U13, and U15.

3. Also insert D15 (Red LED 5370T1LC). Insert D14 (Green LED 5370T5LC). Insert F1 (PTC 60R010). Insert SW2 (TL1105WF160). Insert SW1 (GSO2MCKE). Insert D10 (LT1004CLP-2.5).

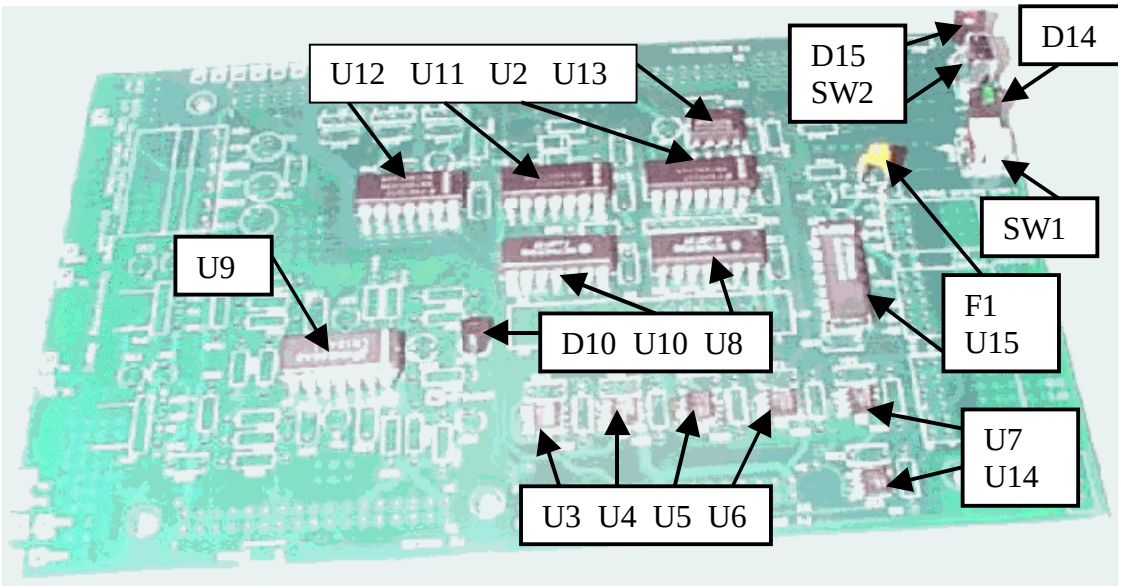

Figure 11

4. See Fig. 12 for step 4. Insert D12 and D11 (1N5817). Insert test points VREF2.5V, DA0-DA3, VDC_OUT, DAI, IW_IN, IW_OUT, IU_IN, IU_OUT, AGND, DGND, GUP, GVP, GUN, GVN, GWN, GWP, GDB, and IOPB7.

5. See Fig. 13 for steps 5 through 7. Insert JP5 and JP6 (4 Pin Right Angle Molex 6373. Insert JP1 (JST B6PVH Right angle).

6. Insert JP8 (103164-4 Amp). Also insert JP7 (103164-3 Amp).

7. Insert JP3 (103164-2).

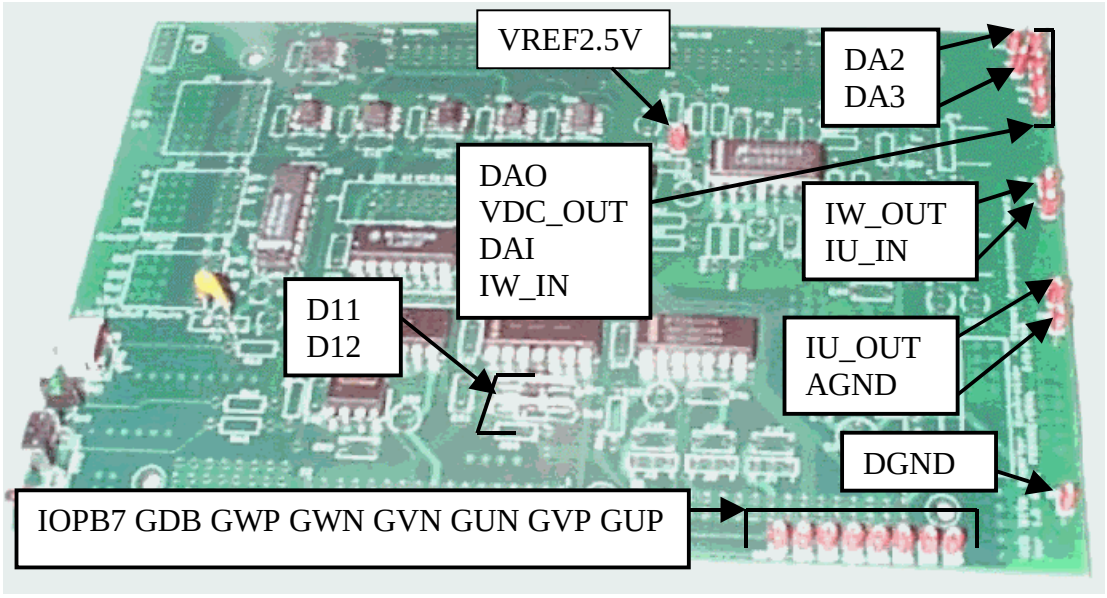

Figure 12

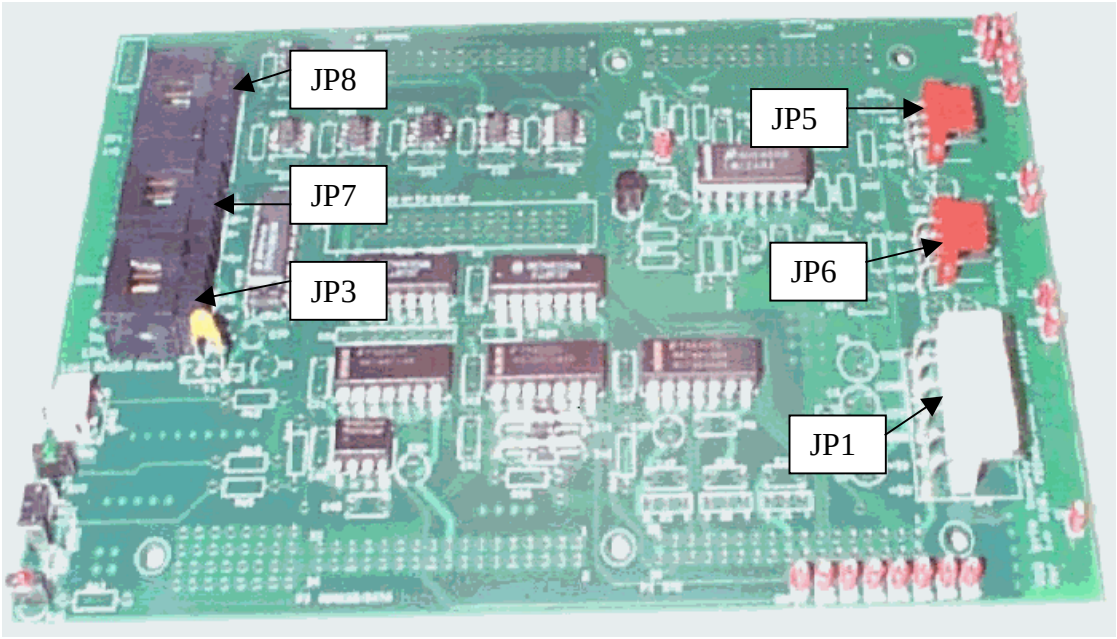

Figure 13

8. See Fig. 14 for step 8. Insert P1 through P4 on the backside of the board. These components should be soldered so that the face of each connector is one-half inch from the face of the board as shown in Fig. 14.

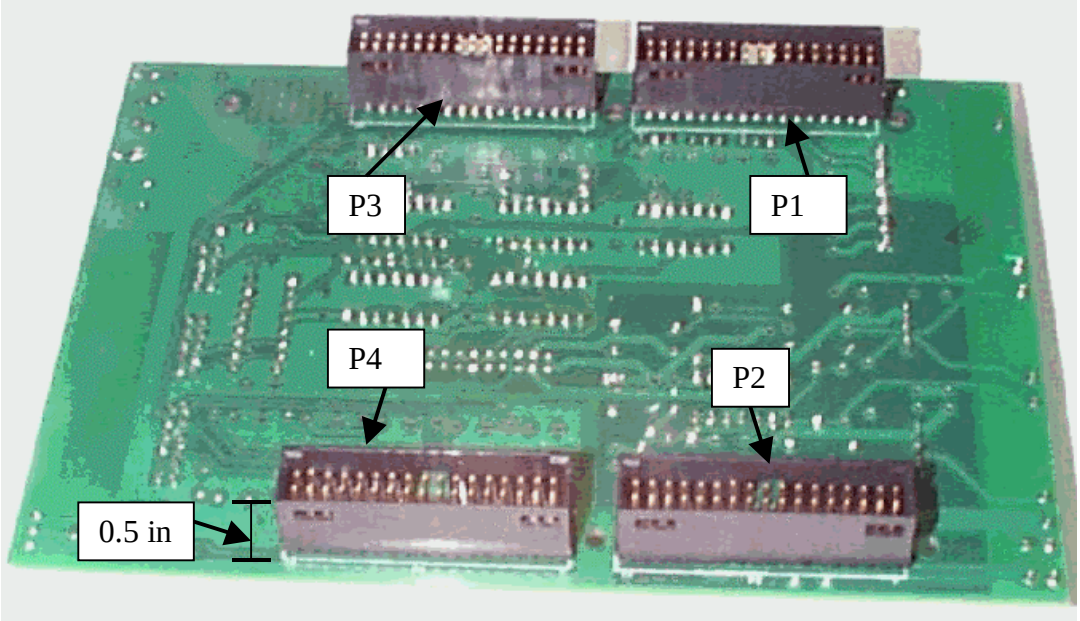

Figure 14

9. See Fig. 15 for steps 9 through 11. Insert test point, PREF. Insert connector JP4 (TSS-115-12-6-D). Insert J1, J2, and J3. Also insert R21 (20KΩ, 1/4 Watt) and R29 (10KΩ 1/4 Watt).

10. Insert R37, R43, R51, R52, and R55-58 (47KΩ, 1/4 Watt). Insert SIP 8 Resistor (R36, 20KΩ, 1/4 Watt).

11. Insert R42 (200 Ω, 1/4 Watt). Insert R46 (22 Ω, 1/4 Watt). Insert R47 (100KΩ, 1/4 Watt).

16. See Fig. 16 for steps 12 and 13. Insert R59, R60, R62, and R65 (33Ω,1/4 Watt). Also, insert R54, R64, and R66 (4.7KΩ 1/4 Watt).

17. Insert R63 and R67 (560 Ω 1/4 Watt). Also insert R3, R30, R31, R32, R33, and R34 (130Ω, 1/4 Watt). **Note**: Resistors are R35, R37, R40, and R50 are unnecessary.

18. See Fig. 17 for steps 14 through 17. Insert C11, C15, C18, C21, C22, C23, C30-35, C40, C42, C45, C47, C48 (0.1uF, 50V).

19. Insert C12, C17, C19, and C46 (100pF, 50wV). Also insert C8 and C29 (1uF, 16V).

20. Insert C6 and C3 (47uF, 25 V). In addition insert C1 (100uF, 16V). The capacitors in this step should lay on the board sideways because of their height.

21. Insert C25, C36, C37, C51, C52, C53 and C54 (1.5uF, 25V). Also insert C38 (1uF, 50V).

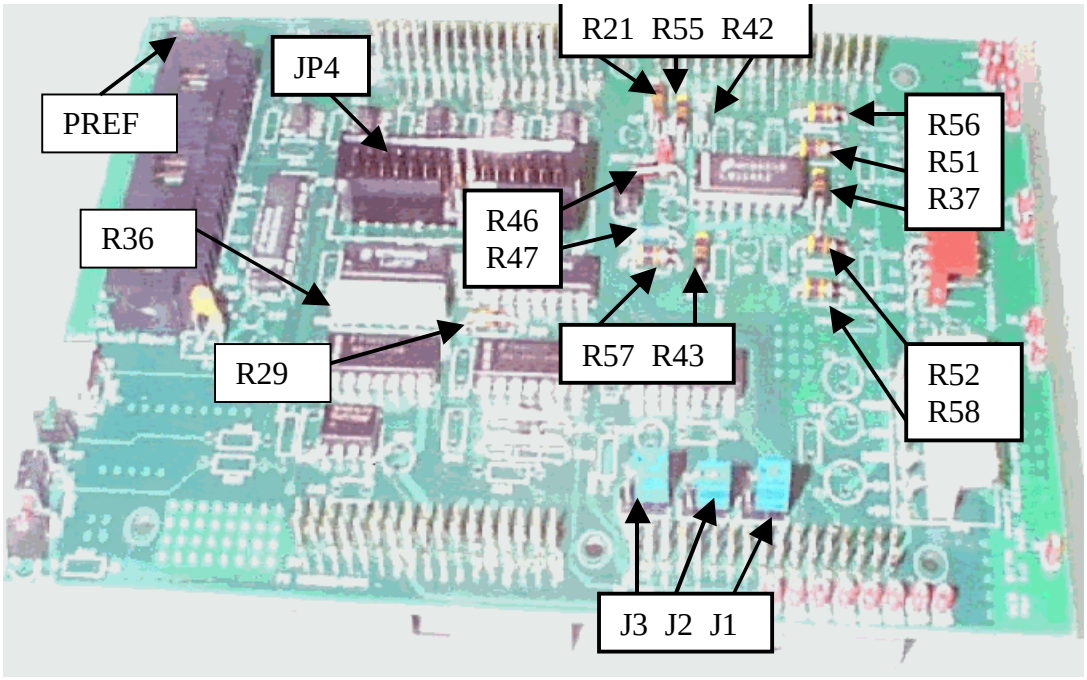

Figure 15

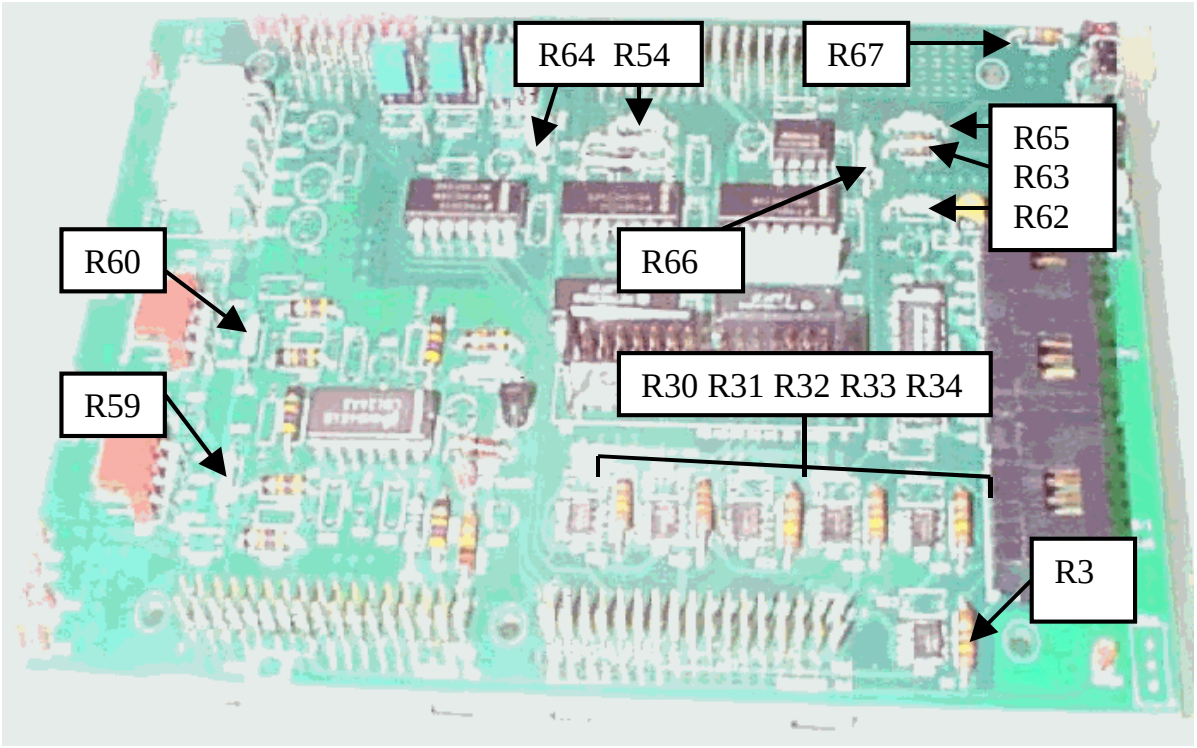

Figure 16

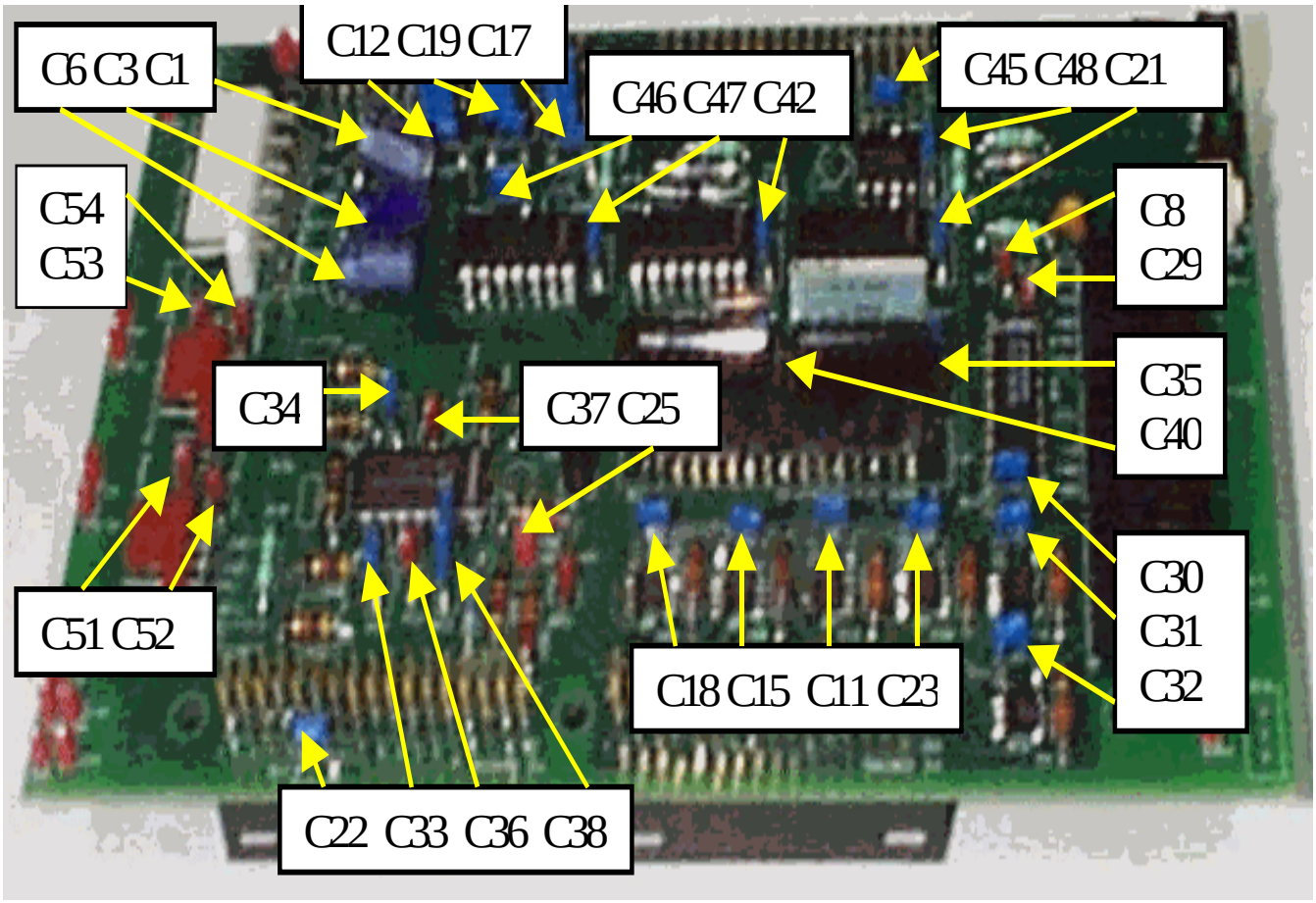

Figure 17

22. See Fig. 18 for steps 18 through 20. Insert C39 (10uF, 16 V). In addition insert C43 and C44 (0.01uF, 50 Volts).

23. Insert C49 and C50 (2.2uF, 50V). Also, insert C41 (1nF, 50 V).

24. Insert R16 and bypass capacitors as shown in Fig. 18.

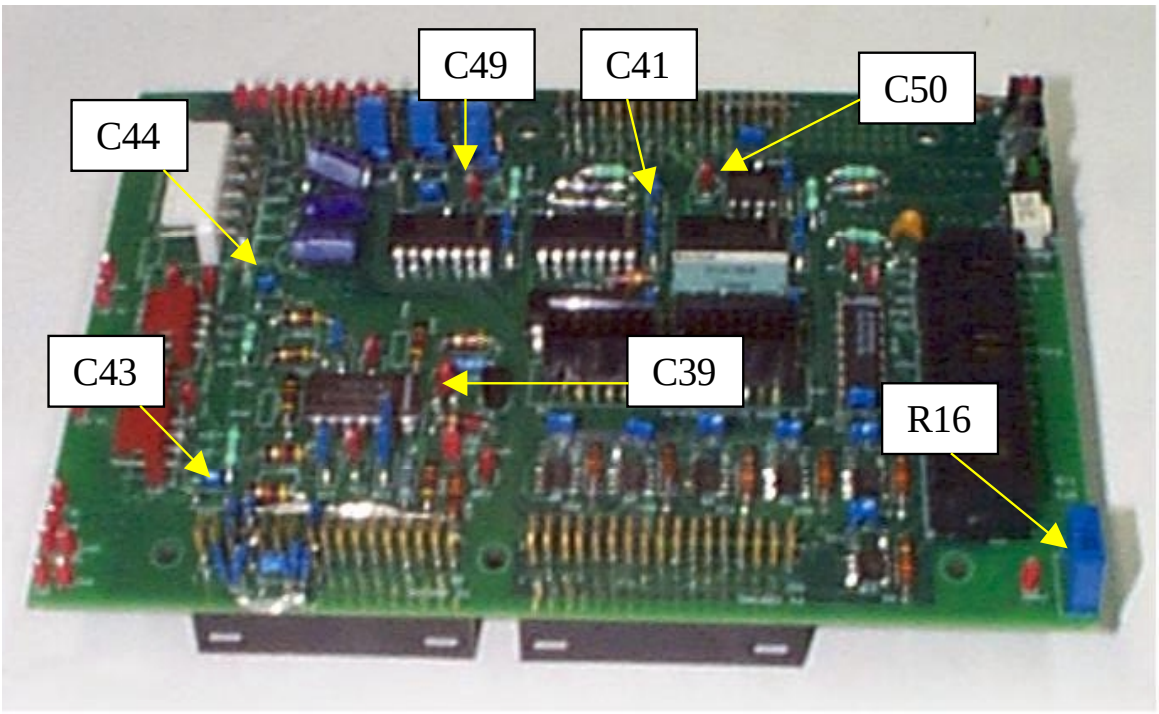

Figure 18

Appendix C.7

Schematic Circuit Diagrams

In thirteen (13) instances the silkscreen image of the diode is reversed on the PC board. These instances are noted on the schematics. during board assembly the direction of the diode must be reversed. This applies to D1 through D7, D8, D10, D11, D13, D14, and D16 on the Gate Drive Board.

In three (4) instances the schematic direction of the diode image is wrong, but reversal of the silk screen diode image restores the proper direction. During board assembly the direction of the diode must **NOT** be reversed. This applies to D9, D12, and D15 on the Gate Drive board and D11 on the Signal Conditioning board. The schematics in this report have been corrected.

In one (1) instance the polarity of the schematic and silkscreen image of a capacitor is wrong. During assembly the direction of the capacitor must be reversed. this applies to C64. The schematic in this report has been corrected.

Note that the silkscreen image of D17 is not reversed; consequently, it must NOT be reversed during board assembly.

Appendix C.7.1

Current Sensor Interface (Low-pass Filter and Level Shifting)

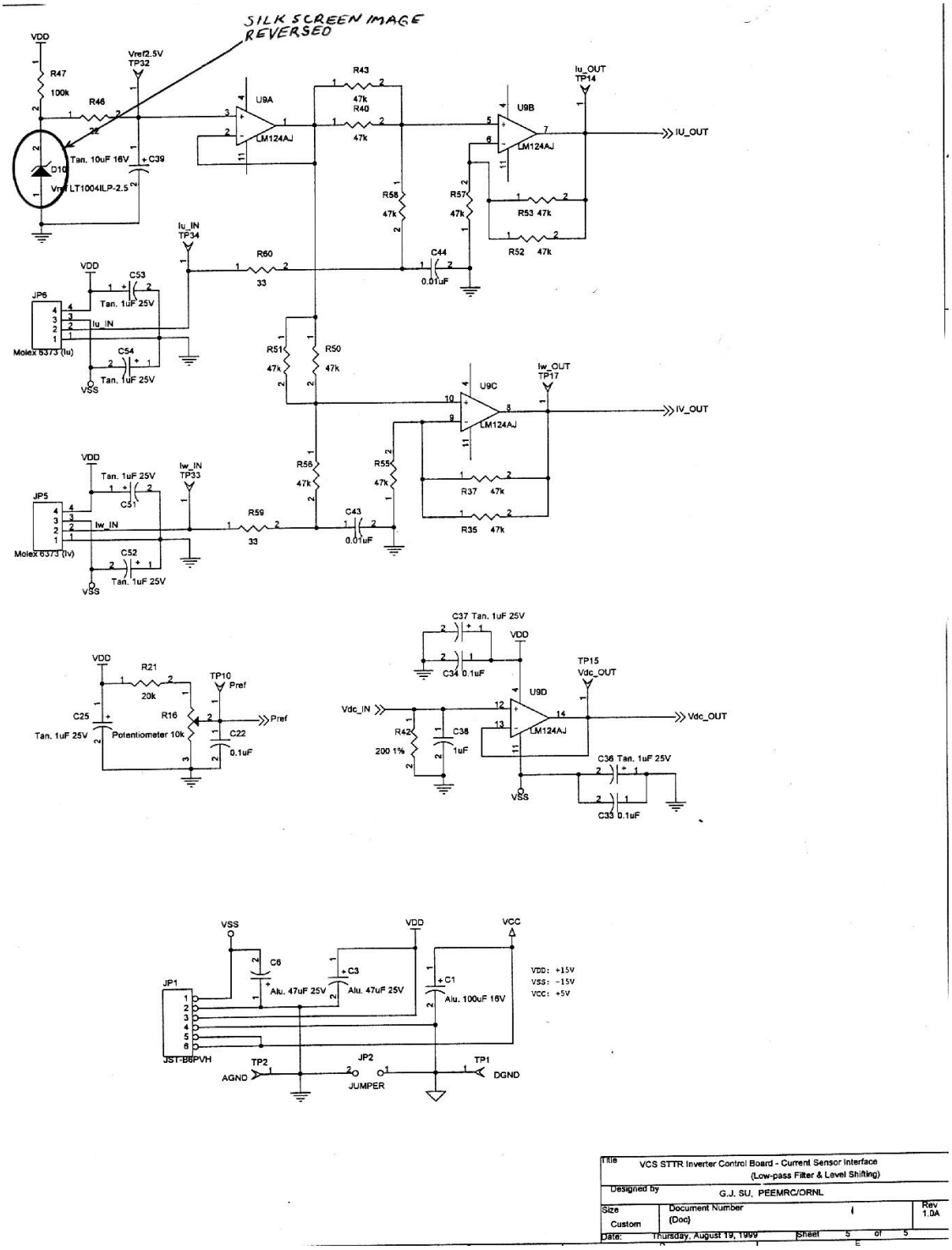

Appendix C.7.2

Limit Switches and Emergency Stop Inputs

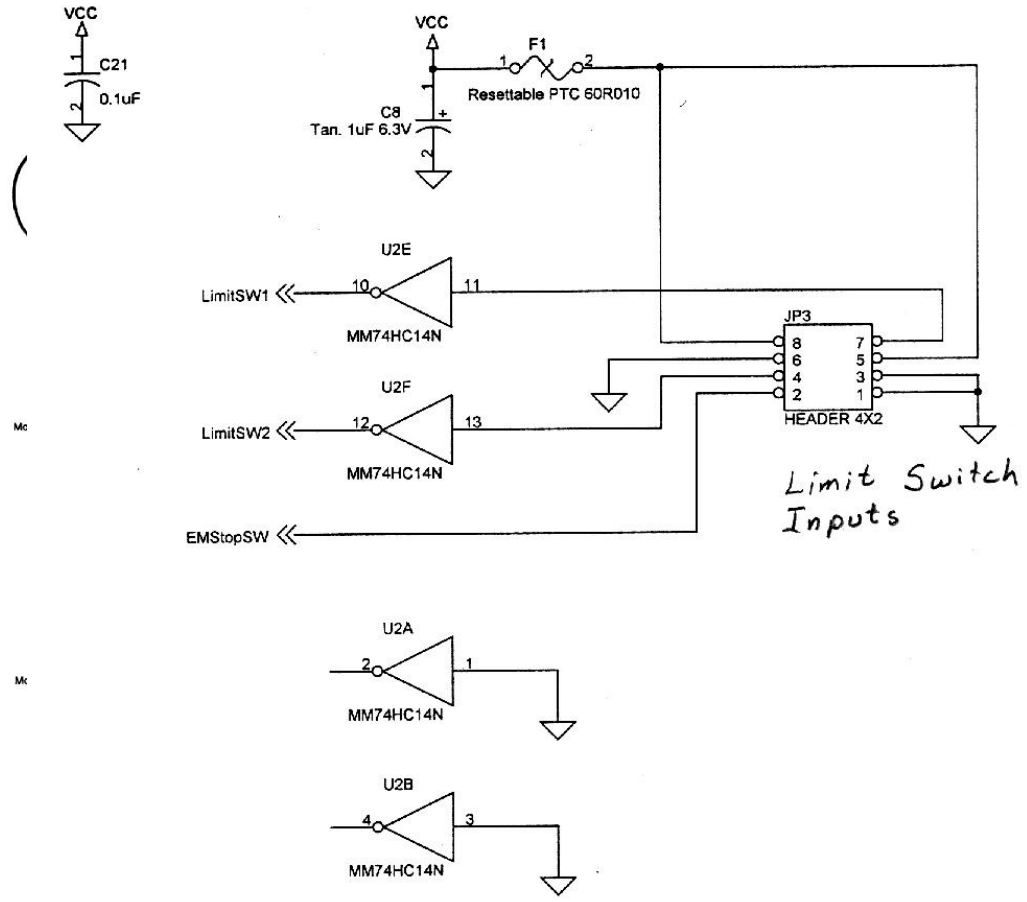

Title	VCS STTR Inverter Control Board - Limit Switches & Emergency Stopy Inputs	
Designed by	G.J. SU, PEEMRC/ORNL	
Size: Custom	Document Number: {Doc}	Rev: 1.0A
Date: Thursday, August 19, 1999	Sheet 5 of 5	

Appendix C.7.3

RS 485 Encoder Interface

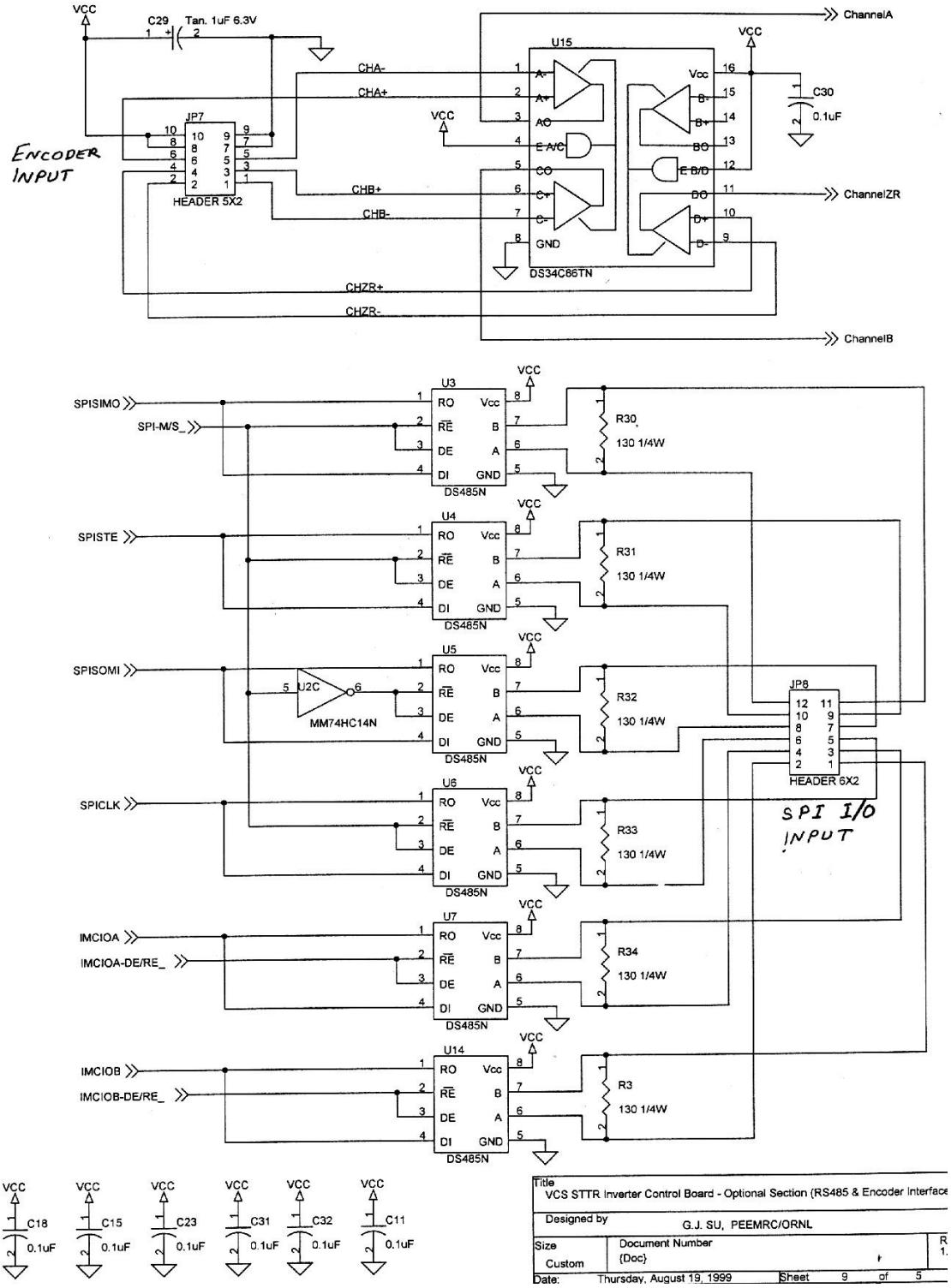

Appendix C.7.4

Gate Signal Generation and Protection Logic

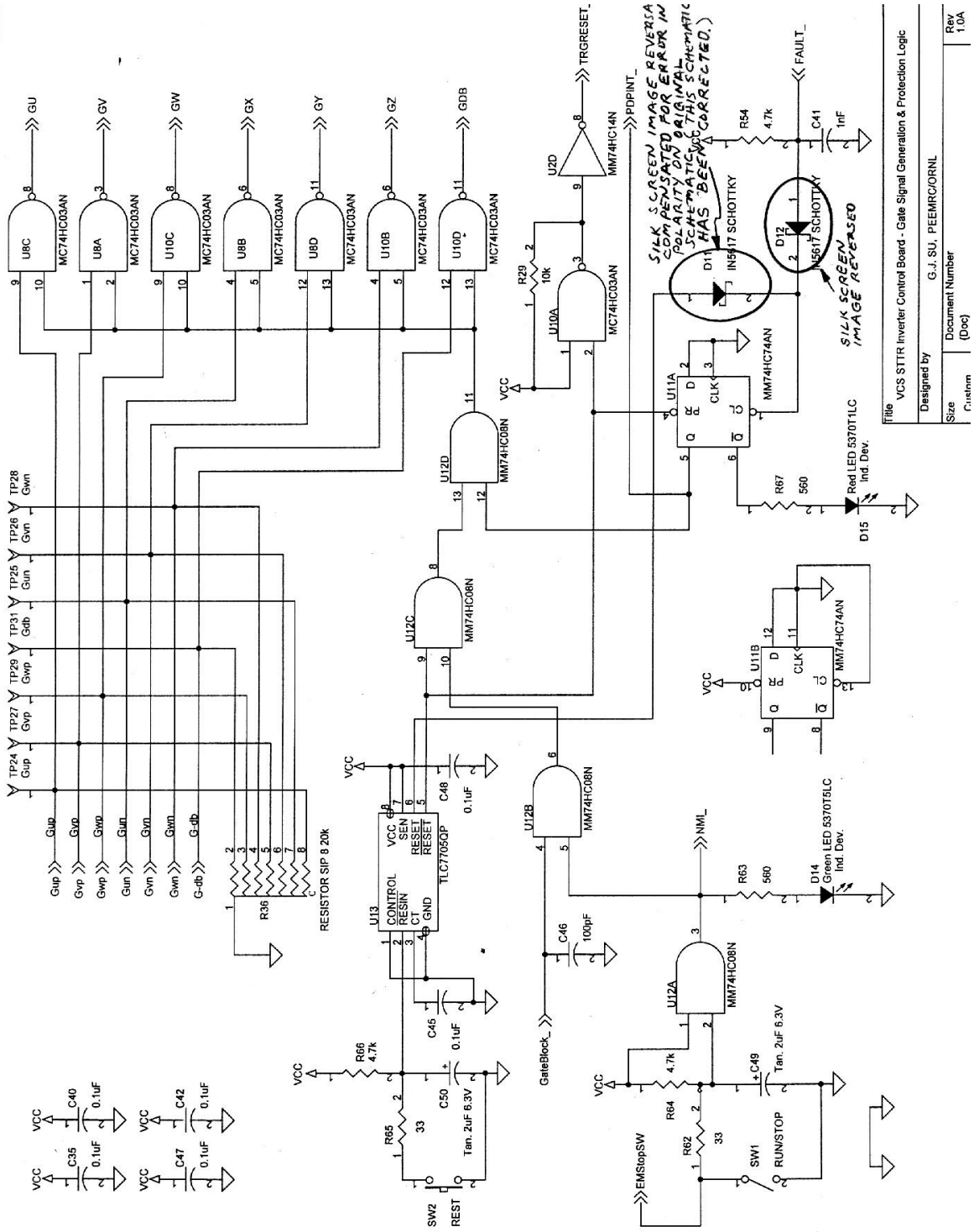

Appendix C.7.5

DSP Board Connectors

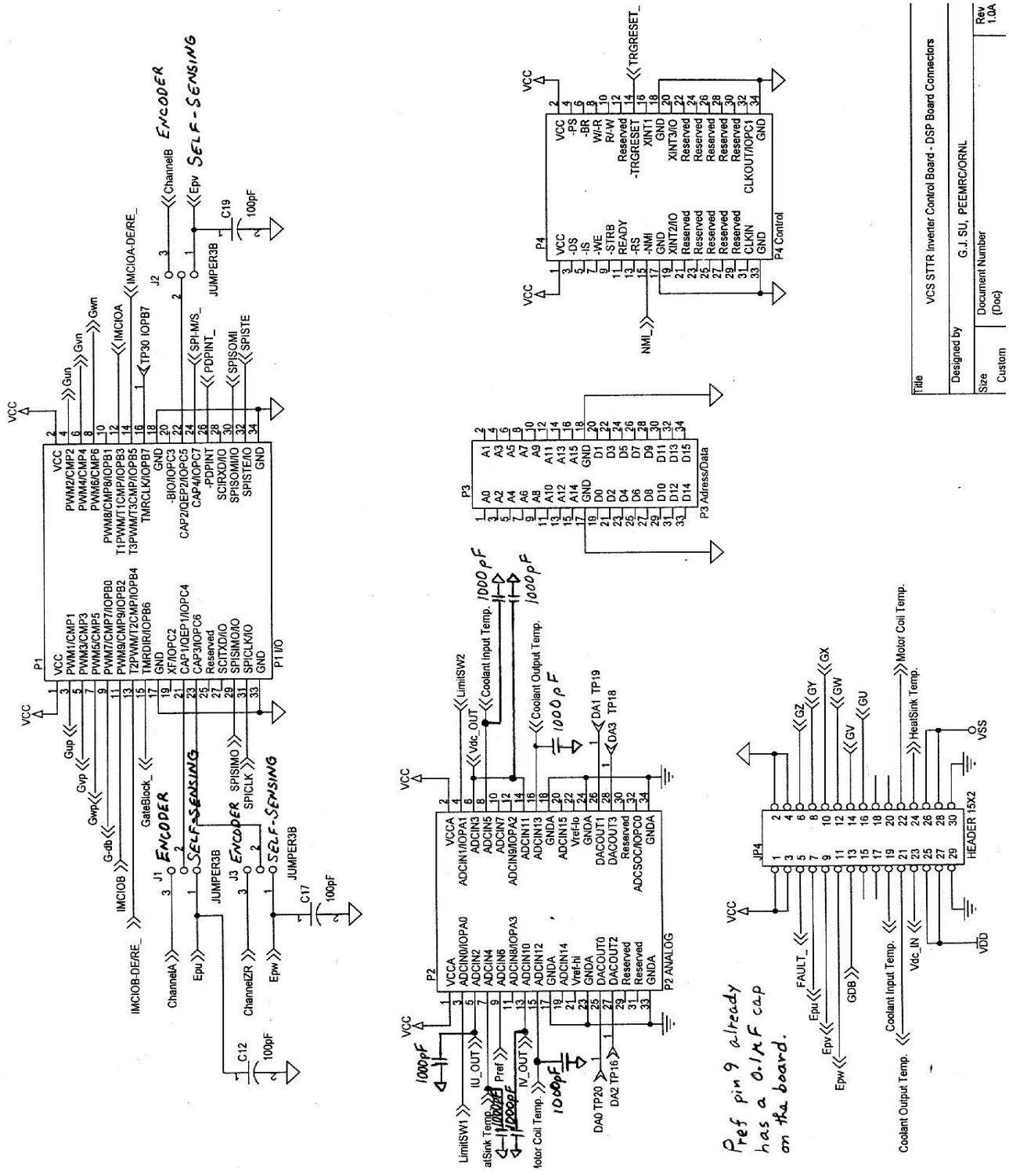

Appendix C.7.6

Back EMF and DC Voltage Detection

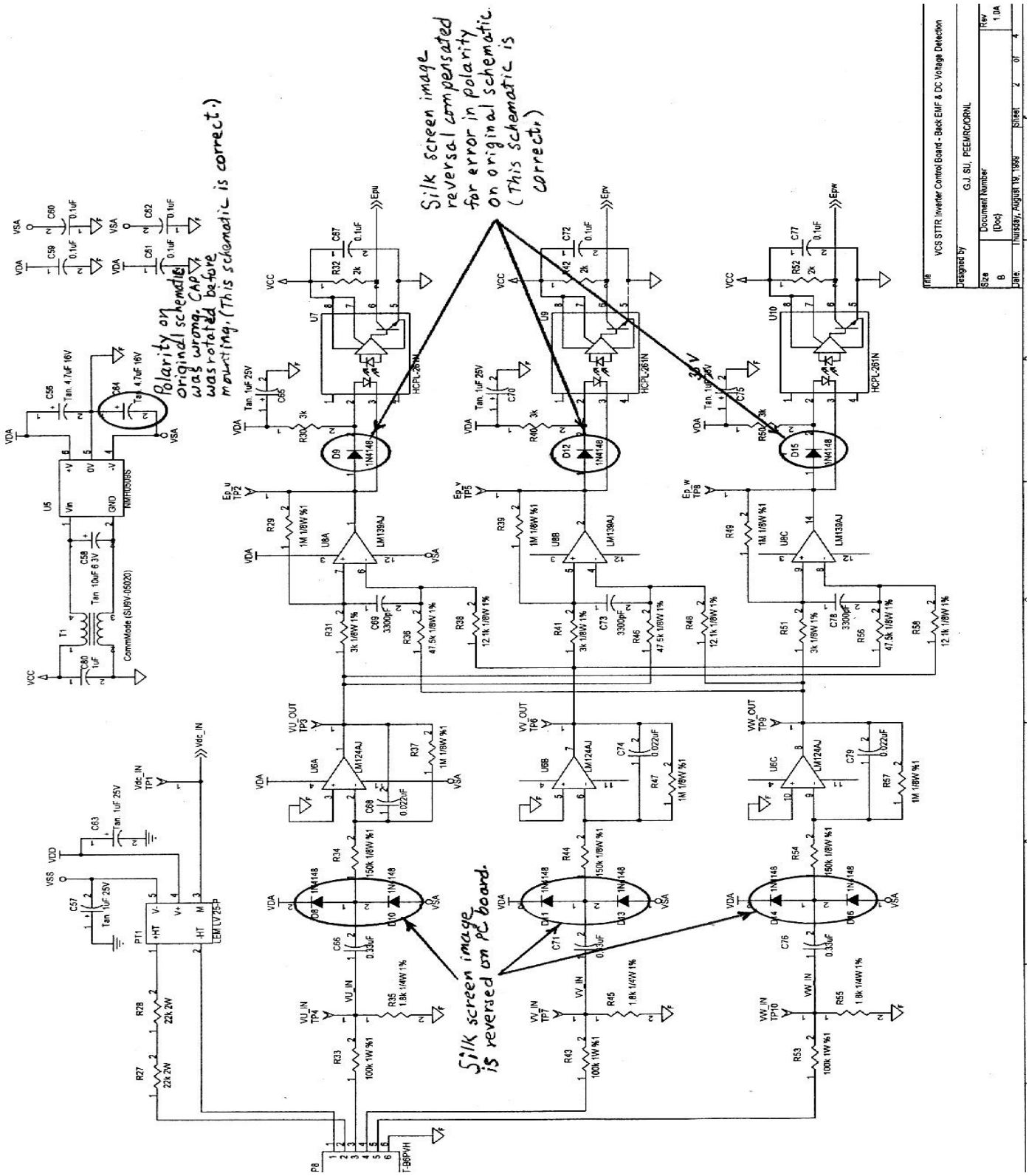

Appendix C.7.7

Thermocouple Interface

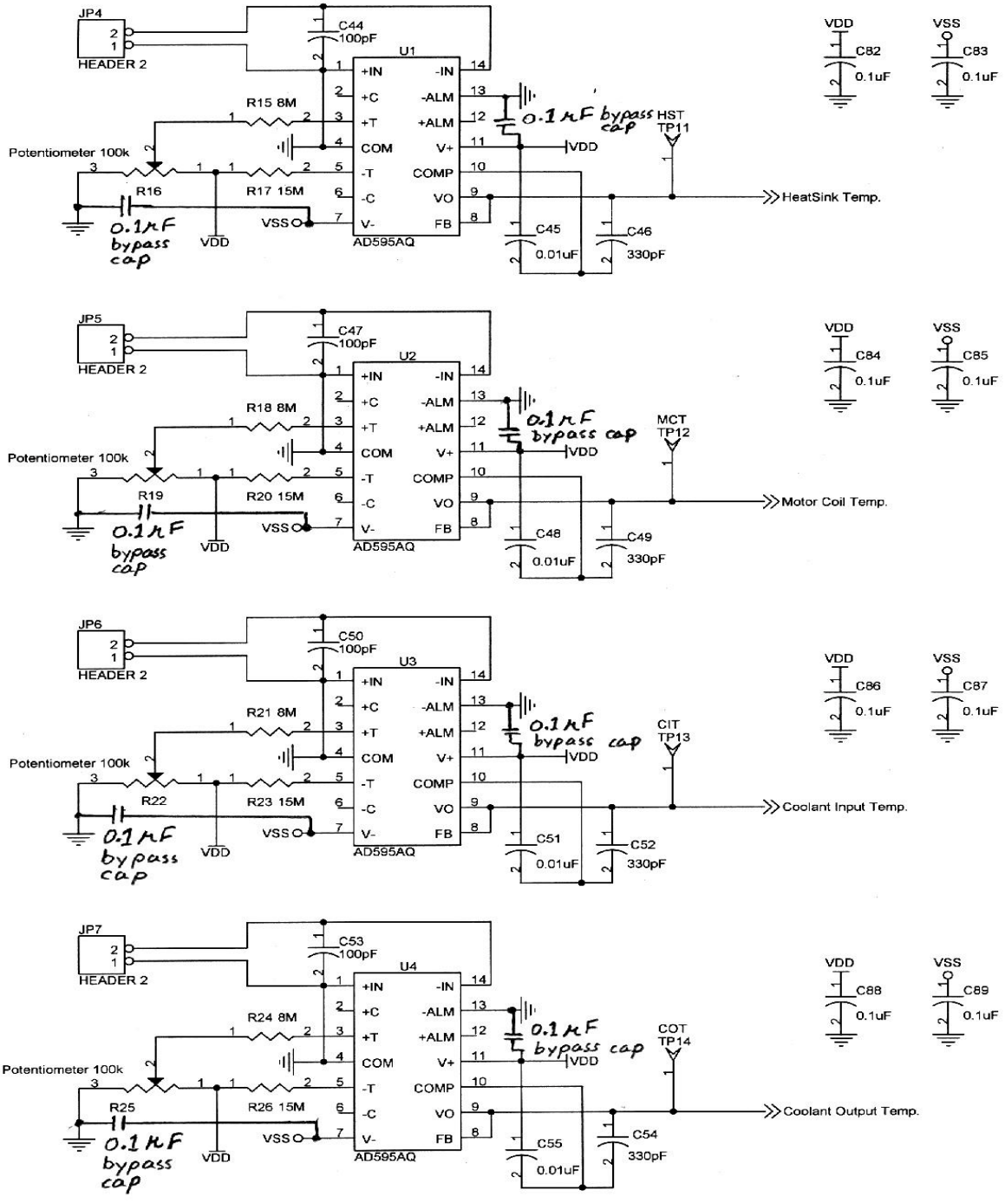

Title: VCS STTR Inverter Control Board - Optional Section (Thermocouple Interface)		
Designed by: G.J. SU, PEEMRC/ORNL		
Size: Custom	Document Number: {Doc}	Rev: 1.0A

Appendix C.7.8

Gate Drive Power Supply Section

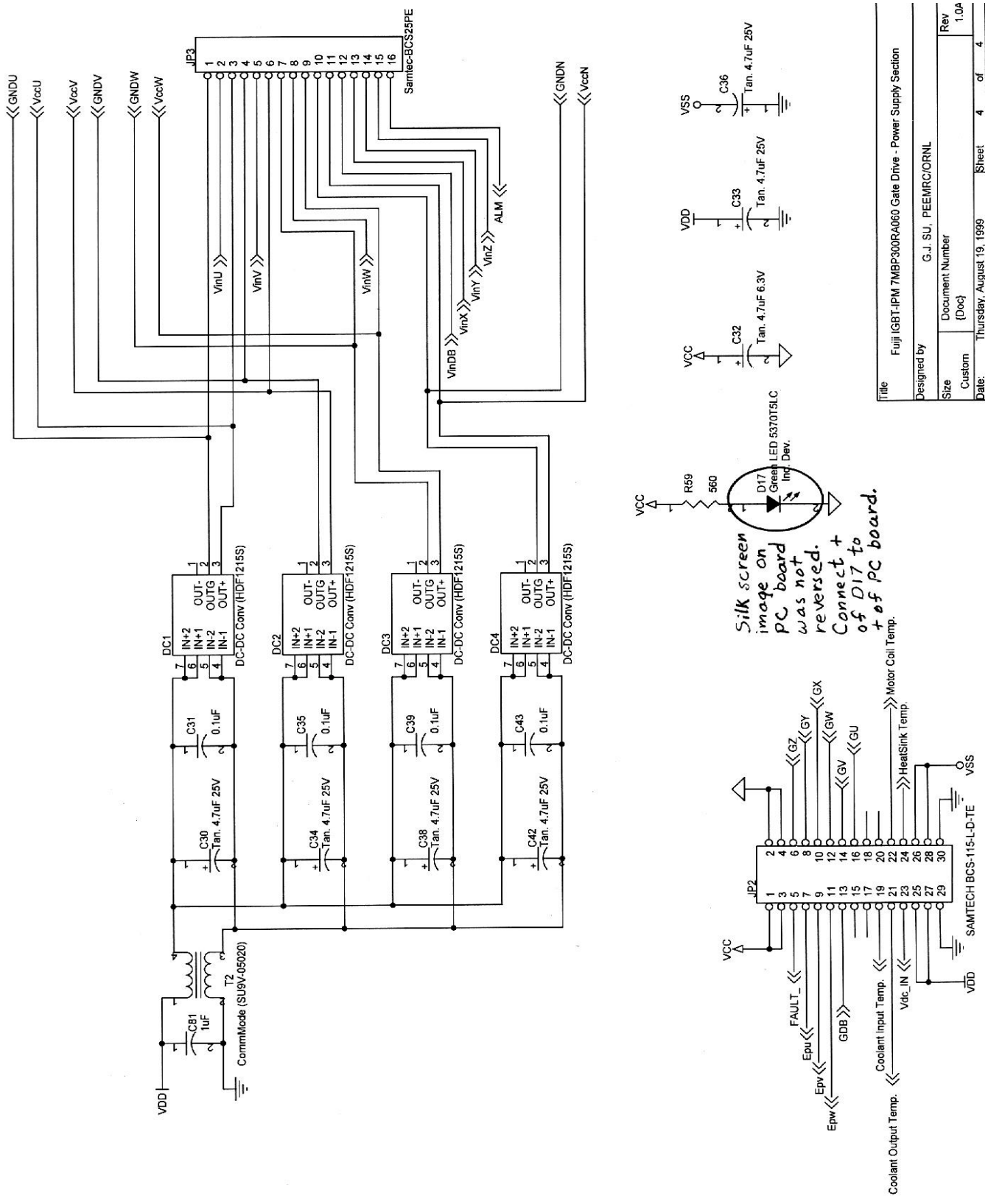

Appendix C.7.9

Predrive Section

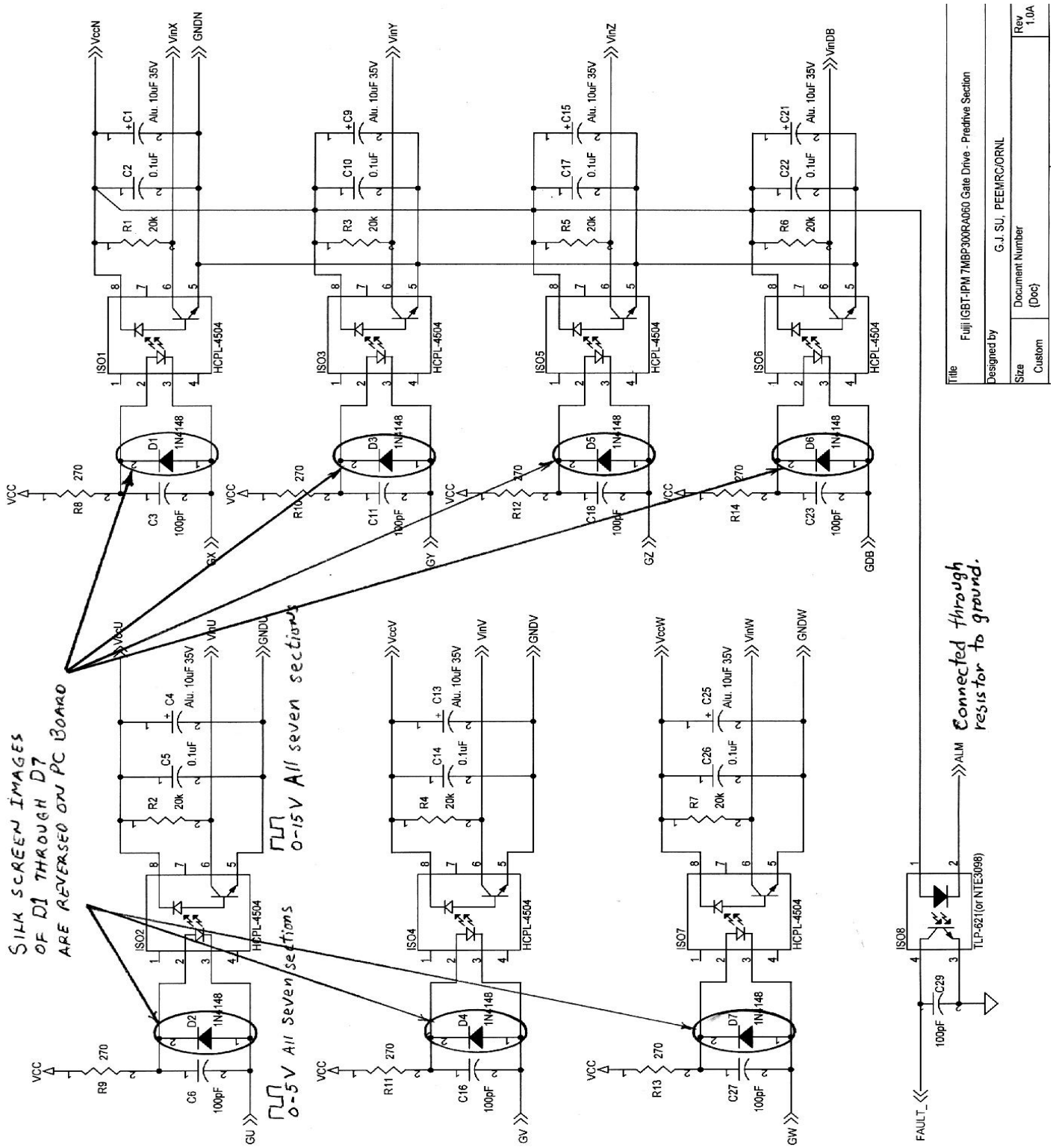

Appendix C.7.10

Copper Bus Bar Fabrication Procedure

(7/29/99 modified)

1. Make a two-dimensional layout on the copper sheet of the 3D object using dimensions from the Pro-Engineering drawings, Figs. C.7.1 and C.7.2.
2. Allow a dimensional increase of one copper thickness transverse to each fold line to account for fold length losses.
3. Fold the side tabs down on both the positive and negative bars at the fold line and fit them together. Mark the hole locations on the top piece and match drill a small center hole through each hole location.
4. Drill holes to proper diameter using the match-drilled holes. See Pro-Engineer drawings for the various hole sizes for each location.
5. After the holes are drilled, laminate the two pieces with insulating 0.015-in. thick teflon sheet, allowing the teflon to extend at least 1.8 in. beyond all edges. All screw holes through the teflon should be approximately the diameter of the screw to help keep the teflon aligned with the copper bars. Do not allow any cuts or slits in the edges of the teflon or around the screw hole. These precautions insure no shoot-through between the oppositely charged bus bars.
6. With the bars laminated and clamped or bolted together in proper alignment, fold the terminal tabs outward together to ensure uniform bolting and alignment of the copper bars to the IGBT. Use the Pro-Engineering drawings to determine exact elevation for the fold line. Remember to allow about one copper thickness of distance for each fold line.

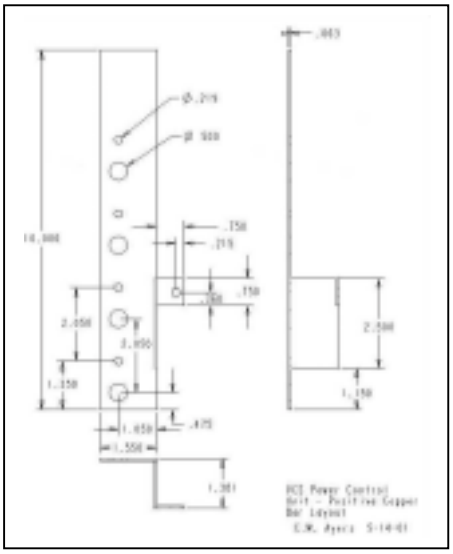

Fig. C.7.1.1. Plus copper bus bar.

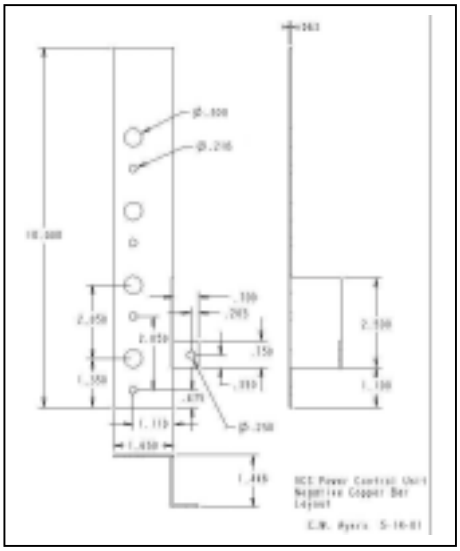

Fig. C.7.1.2. Minus copper bus bar.

Appendix C.7.11

General Purpose Rectifier Box Assembly

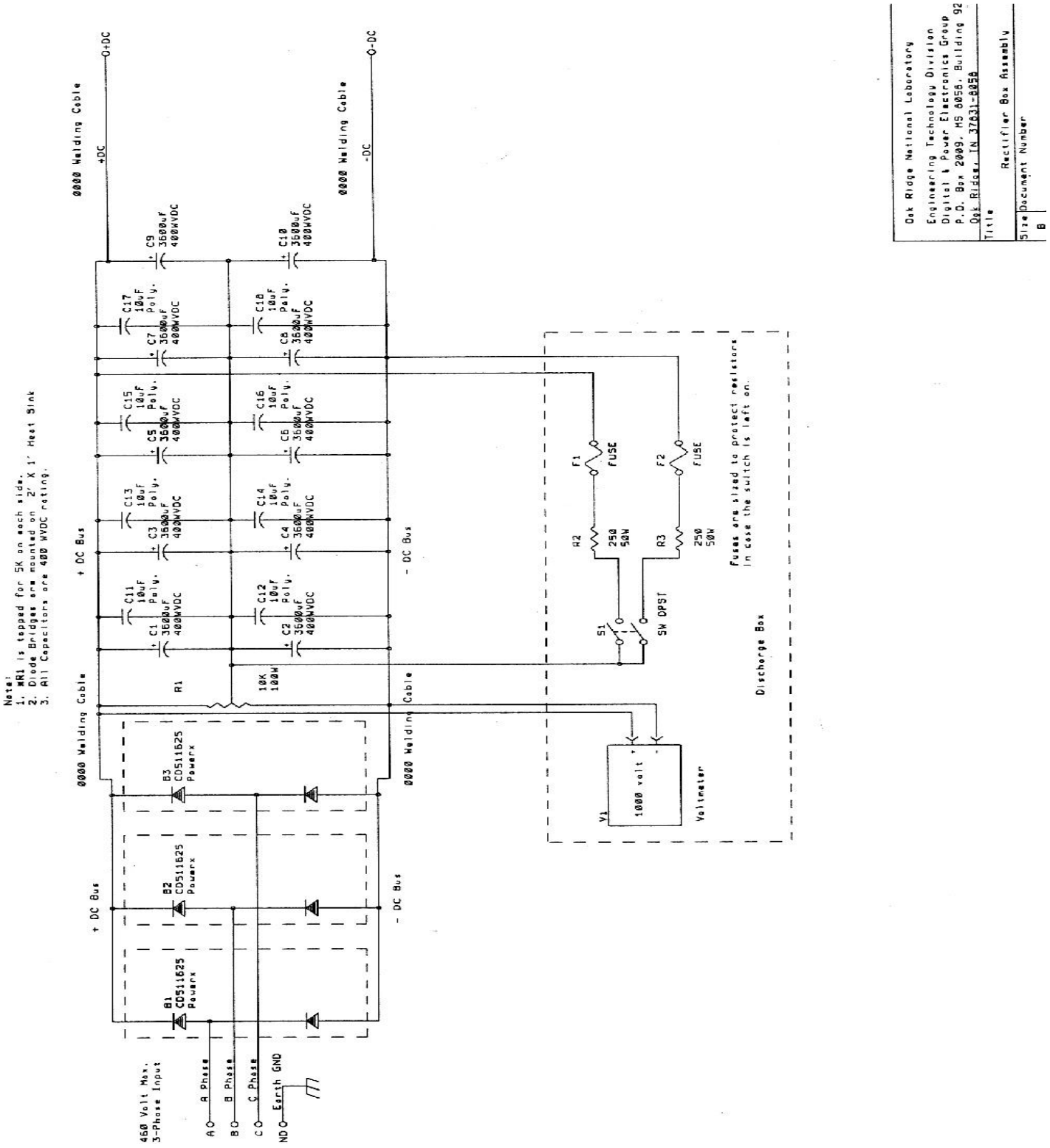

Appendix C.12

Assembly Notes from George Ott's Notebook 4/11/97 to 7/08/99

(Pages 146 through 149)

Resistance Check of VCS PC Boards (page 146)

Signal Conditioning Board

Resistors R35, R40, R50, and R53 were never mounted.
+5 V connection resistance is 606 Ω.
+15 V connection resistance is 29.98 kΩ.
-15 V connection resistance is 3.70 MΩ.
+15 V to –15 V connection resistance is 4.78 MΩ.

Gate Drive Board

Labeling of VCC and DG on the PC board is wrong. They should be interchanged. The analong graound , AGND, and digital ground, DGND, are not tied together on the PC board. They are connected through a tie pin on the signal conditioning board.

Connection Points		
+	-	
DG pin1	VCC pin 2	+5 V connection resistance is 250.5kΩ.
VDD pin 25	AG pin 29	+15 V connection resistance is 25.12 kΩ.
VSS pin 26	AG pin 30	-15 V connection resistance is 28.49 kΩ.
VDD pin 25	VSS pin 26	+15 V to –15 V connection resistance is 3.47 kΩ.

With Gate Drive and Signal Conditioning Boards Connected

+5 V connection resistance is 607 Ω.
+15 V connection resistance is 13.56 kΩ.
-15 V connection resistance is 16.89 kΩ.
+15 V to –15 V connection resistance is 3.48 kΩ.

VCS Power Supply Check (page 147)

Power Supply Output Voltages with No Load

+5 V voltage is 5.09 Vdc.
+15 V voltage is 14.84 Vdc.
-15 V voltage is –14.94 Vdc.

Power Supply Output Voltages Loaded with Signal Conditioning Board

+5 V voltage is 5.09 Vdc.
+15 V voltage is 14.91 Vdc.
-15 V voltage is –14.92 Vdc.

The LT1004ILP-2.5 V diode D10 image is reversed on the silk screen and was rotated 180° before mounting.

Changed out 2.5 V regulator.
Reversed flat side of package to properly position anode.

Vref=2.496 V after change out.
Test point 10 Pref voltage is 4.88 V max. Pot can make this 0.

20kΩ Resistor Network

R36 pin 1 is tied to ground. Gui-Jia said the drawing was wrong. Pin 1 should be tied to ground. (Schematic in this report has been corrected to show ground connection.)

VCS Board Check (page 148)

Power Supply Output Voltage Loaded with Signal Conditioning and Gate Drive Boards

+5 V voltage is 5.05 Vdc.
+15 V voltage is 14.89 Vdc.
-15 V voltage is –14.93 Vdc.

Gate Drive Board Problems

The polarity of C64 is incorrect on the schematic and on the PC board.

The silk screen images on the PC board for D8, D11, D10, D13, D14, and D16 are reversed.

Voltage Measurement of the Newport Technologies DC-DC Converter.

VDA the +9 V voltage is +9.25 Vdc
VSA the –9 V voltage is –9.26 Vdc.

Self Sensing versus Encoder Monitor Connections

Self sensing requires connecting pins 1 to 2 of J1, J2, and J3 on the Signal Conditioning Board.

The Encoder monitoring requires connecting pins 3 to 2 of J1, J2, and J3.

VCS CRADA Notes (page 149)

An AD595AQ thermocouple amplifier must be specified. VCS uses a Type K thermocouple on their motor. ORNL originally ordered an AD594AQ thermocouple amplifier, which is a Type J thermocouple.

If the thermocouple is electrically isolated, then according to page 3 of the application note, we must tie pin 1 to pin 4, the power supply common. The instrumentation amplifier needs a return path for its biasing currents. It must NOT be left floating.

The supplies connected to the thermocouple amplifiers require bypass capacitors. Use eight 0.1 μF, 50 V ceramic monolithic across UDD to ground and VSS to ground.

Appendix D

ORNL Test Plan for STTR Motor and Power Inverter

(December 30, 1998)

ORNL Power Electronics and Electric Machine Group will perform performance characterization and efficiency testing of a 10kw, 3-phase, ac motor designed to operate on a 320 V dc bus and draw 30 A continuous current from a PCU designed by ORNL. The test program is designed to determine selected motor terminal properties, thermal and electrical data under several load conditions, and the overall efficiency of the motor and PCU.

The motor will be anchored to the base-plate of a motor test stand and coupled to either a generator or a dynamometer. If a generator is used, an in-line torque cell will be used. Otherwise, the torque sensor, which is a part of the dynamometer, will be used. A precision coupling will align the shafts within 20-mils. Voltage, current, and resistance sensors are calibrated at least every two years. Torque and speed sensors are calibrated every month. Calibrations are performed with instruments and standards whose accuracy is traceable to NIST. Thermocouples embedded in the motor will be checked for accuracy. Redundant thermal measurement will be used where practical.

Motor Operating Restrictions (from VCS on May 10, 1999)

No Liquid Cooling – The motor was not equipped for liquid cooling when refurbished. Therefore DO NOT ATTEMPT TO LIQUID COOL THE MOTOR.

Due to a previous failure, VCS has established the operational and thermal limits for the Delta motor. Although the motor has been repaired, the root cause of the magnet departure has not been resolved. The restricted operational and thermal limits are intended to ensure the safe, reliable operation of the Delta motor. Limitations are as follows:

Motor Coil Temperature	NTE 80 C (as indicated by thermocouple #2, which is at the hottest coil location)
Continuous	
Speed	**1750 RPM**
Torque	**80 in-lb**
Peak	
Speed	**2000 RPM**
Torque	**150 in-lb**

Preliminary Testing

Three preliminary tests will be performed before actual motor operation.

1. DC resistance – The dc resistance of each of the phase-to-phase windings will be measured using a micro-ohmmeter. The three sets of windings will be differentiated and matched to the corresponding resistance measurements.

2. AC resistance – The impedance at 400 Hz of each set of windings will be measured and recorded in a similar fashion.

3. Thermocouple verification – A secondary device to sense temperature will be used to verify readings of ambient temperature obtained from the thermocouples embedded in the motor. Discrepancies will be resolved before motor operation begins.

Two additional tests will be performed as the motor is driven to speed with a second motor.

4. Back emf – Open-circuit voltage at the motor terminals will be measured using a voltage sensor at each phase-to-phase winding. Corresponding rotor speed data will be recorded from 0 to 4000 rpm.

5. Full current test – The three motor terminals will be connected to 10 ohm, 3kW resistors in a Y-configuration, and the current to the resistors will be measured. Load voltages and coil temperatures at measured points will also be recorded. These data will enable ORNL to derive the synchronous inductance of the motor.

Load Testing and Thermal Properties

The required equipment needed for each test will be an array of electrical, thermal, and mechanical sensors whose signals will be sent to a computer near the test stand, where it will be recorded and analyzed. The equipment list includes:

- Voltage sensors for the PCU and motor
- Current sensors for the PCU and motor
- ac wattmeter for redundancy
- dc wattmeter for redundancy
- Torque cell
- Speed sensor
- Flow meter for motor coolant line
- Thermocouples
- Digital thermometer
- Rotor shaft current sensor
- Motor loading device capable of stalling motor
- Pentium computer
- Data collection and analysis using LabView™ software

As testing begins for each of the three load conditions (i.e., stall torque, no load, and rated load), a one hour warm-up will take place before any electrical data are recorded for analysis. Thermal data will not be recorded for analysis until it is verified that temperature readings have stabilized to the point where there is no more than 1^{o} C rise in 30 minutes. Note: a temperature "rise" is determined by normalizing the motor temperatures to any change in ambient temperature that may have occurred in the same time period. Thus, if the motor temperature increased 2.5^{o} C and the ambient 2^{o} C, the motor temperature rise would be 0.5^{o} C.

Table D.1. Testing of STTR at stall conditions

Test	Measurements*	Derived Properties
Determination of stall torque	Electrical data - voltages for 3 motor phases - currents for 3 motor phases - power factors - dc voltage to PCU - dc current to PCU - total power data with redundant instrumentation Power out (rotor torque & speed) Motor coolant flow rate Temperature - coil (each element) - housing - magnet - coolant in/out	Motor heat generation under stall conditions **Overall motor thermal resistance** **Local motor thermal resistances** **Cooling scheme thermal resistance** **Torque constant**

- All data to be collected continuously as load is increased and until the time when the rotor stops rotating.

Table D.2. Testing of STTR at no-load

Test	Measurements	Derived Properties
No Load	Electrical data - voltages for 3 motor phases - currents for 3 motor phases - power factors - dc voltage to PCU - dc current to PCU - total power data with redundant instrumentation - rotor shaft voltage Power out (rotor torque & speed) Motor coolant flow rate Temperature - coil (each element) - housing - magnet - coolant in/out	_ Motor heat generation during no-load operation _ Overall motor thermal resistance _ Local motor thermal resistances _ Mechanical and eddy current losses

Table D.3. Testing of STTR at rated load

Test	Measurements	Derived Properties
Rated Load	Electrical data - voltages for 3 motor phases - currents for 3 motor phases - power factors - dc voltage to PCU - dc current to PCU - total power data with redundant instrumentation - rotor shaft voltage Power out (rotor torque & speed) Motor coolant flow rate Temperature - coil (each element) - housing - magnet - coolant in/out	_ Motor heat generation during normal full load operation _ Overall motor thermal resistance _ Local motor thermal resistances

Table D.4. Testing of STTR at overload

Test	Measurements	Derived Properties
Rated Load	Electrical data - voltages for 3 motor phases - currents for 3 motor phases - power factors - dc voltage to PCU - dc current to PCU - total power data with redundant instrumentation - rotor shaft voltage Power out (rotor torque & speed) Motor coolant flow rate Temperature - coil (each element) - housing - magnet - coolant in/out	_ Motor heat generation during overload _ Overall motor thermal resistance _ Local motor thermal resistances

Appendix E

Oak Ridge National Laboratory
Power Electronics and Electric Machines Research Center
And
Advanced Propulsion Laboratory

Testing and Demonstration of the Delta Motor

George W. Ott, Jr.

Initial No-load Testing

Friday, May 14, 1999

The initial test was conducted using the self-sensing feature of the signal conditioning board. The encoder, which was sent by VCS with the Delta Motor, was not used.

The Delta Motor was connected to the 10-hp dynamometer using a Trantorque coupling. The line-to-line voltage of the Advanced Propulsion Laboratory's variable transformer was set at 30 volts. The operator applied power to the 3-phase full-wave bridge and capacitor bank. The transformer was quickly adjusted to a line-to-line voltage of 211 volts, which corresponds to a dc bus voltage of 300 V. This technique was used to soft charge the capacitor bank, which prevented the destruction of some fast blow in-line fuses.

During the initial test the Delta Motor was operated at 1480 RPM with no load. Since the dynamometer rotation had to be counter-clockwise, the following information shows how the Delta Motor was wired to the power control unit. The maximum temperature of thermocouple, T2, during drive-up was 35^{o} C.

A ------ Phase 1 -------- Blue/White ------------------------- W
B ------ Phase 2 -------- Orange/White -- Black Shrink ---- V
C ------ Phase 3 -------- Orange/White ---------------------- U
D ------ Shield ---------- Grey ---------------------- No Connection
E ------ Center Tap ----- Green ------------------- No Connection
F ------ Red -- No Connection
G ------ Black --- No Connection

Testing with no load was repeated several times to address and solve software problems. No-limits were exceeded and the circuitry and motor performed as planed.

Initial Load Testing

The dc link voltage was raised to 300 V and the start sequence was initiated. The Delta motor accelerated to 1480 RPM after which the dynamometer applied a 40 in.-lb. torque load. The temperature of thermocouple, T2, reached a value of 41^{o} C after several minutes of operation. This test was repeated several times for short intervals to evaluate and correct

software problems. During these short tests the temperature did not exceed 41^{o} C. No thermal, load, or speed limits were exceeded. Operation of the system was as anticipated.

The Delta Motor and Power Control Unit Demonstration

Monday, May 17, 1999

At 10:00 a.m. a demonstration of ORNL's Power Control Unit driving the Delta Motor was given at the request of Milo Friesen, president of Lynx Motion Technologies, and Roy Kessinger, president of Visual Computing Systems Corporation. Those present for the demonstration included Miguel Lagunas also from Lynx Motion Technologies, Jonathon Kavaliunas and Clifford Lowrance from the Chattanooga Area Regional Transit Authority, Jose Herrera from the Electric Vehicle Research Institute, and Keith Buckner from Advanced Vehicle Systems.

To begin the demonstration the DC link voltage was raised to 300 V and the start sequence was initiated. The Delta Motor accelerated to 1480 RPM at which time the dynamometer was adjusted to apply a load torque of 20 in.-lb. The system was operated at this speed and torque for about an hour.

The motor temperature climbed slowly and steadily to 51^{o} C, during the demonstration. The battery of the thermocouple meter failed as the motor temperature reached 56^{o}C and the test was stopped as a precaution because the rising motor temperature could not be directly monitored. The steady rise in temperature was expected because the water cooling system had decommissioned by Lynx when the motor was repaired.

Demonstration during PEEMRC Lab Tour

Tuesday, May 18, 1999

After the demonstration, the Delta Motor and Power Control Unit were moved back to the Power Electronics and Electric Machines Laboratory. The system was then reconnected for the Power Electronics and Electric Machines Tour on the evening of May 18,1999. During the tour, which lasted from 7:30 PM to 10:00 PM, the motor was driven repeatedly to 1480 RPM with no load. The motor temperature never exceeded 36 ^{o} C.

Wednesday, May 19,1999

During the morning we drove the Delta Motor to 1480 RPM several times. The DC link was 300 V. The motor temperature was monitored with thermocouple, T2, and never exceeded 36^{o}C during operation with no load. This motor operation was done to test software modifications. In the afternoon the Delta Motor was disconnected from the mounting framework. Motor, cabling, Trantorque coupling, and encoder were packaged in the original box for return to Lynx Motion Technology.

Appendix F

00FCC-28

Development of a Sensor-less Speed Control Inverter for an Automotive Accessory Permanent Magnet Motor

Gui-Jia Su, George W. Ott, and John W. McKeever
Oak Ridge National Laboratory

Kelly S. Samons, Roy L. Kessinger
Visual Computing System

ABSTRACT*

Visual Computing Systems (VCS) and Oak Ridge National Laboratory (ORNL) are partnered in a research effort to design and build a power inverter for use with an automotive accessory permanent magnet (PM) motor provided by VCS. The inverter is designed so it can fit within the volume of the housing, which is integrated with the motor. Moreover, a modular design for both the inverter and motor is employed for easily expanding the power capability to other applications. A simple back electromotive force (EMF) based position detection scheme is implemented with a digital signal processor (DSP) to eliminate the need for position sensors. Issues related to position detection errors are addressed and correction methods are suggested and implemented in DSP software. Finally, since the motor has very low inductance because of its coreless stator structure, the influences of the low inductance on the motor current ripple are analyzed. This analysis is used to design a fast current control loop for the inverter to cope with the low inductance. Analytical and experimental results are included to verify the proposed schemes.

INTRODUCTION

PM motors have higher efficiency due to the elimination of magnetizing current and copper loss in the rotor. It is also easier to achieve high performance torque control with PM motors, in particular brushless DC (BLDC) motors. Owing to these advantages, PM motors have already been widely used in a variety of applications in industrial automation and consumer electric appliances [1]. Recent advancements in PM materials have made PM motors a great candidate for traction motors in electrical vehicle applications.

VCS and ORNL are partnered in a research effort to design and build a power inverter for use with an automotive accessory PM motor provided by VCS. To reduce the cost and space requirement of the drive system, great attention is placed in the layout design of the inverter so that it can fit within the volume of the housing, which is integrated with the motor. Although the motor has a rated shaft power of 8 kW with a maximum speed of 4000 rpm, a modular design approach for both the inverter and motor is employed for easily expanding the power capability to other application needs.

There are mainly two ways to excite a PM motor. One is to drive the motor in synchronous AC mode in which a three-phase sinusoidal current is delivered to a motor that has a sinusoidal back EMF. The other excitation scheme, which has been proved particularly attractive for high power drive systems and is thus the choice for the accessory motor drive, is for BLDC motors. It consists of a three-phase PM motor with a trapezoidal back EMF excited by quasi-square current waveforms. This excitation can be conveniently accomplished with a three-phase full-bridge voltage source inverter. An attractive feature of this approach is the resulting simplicity of inverter phase sequencing. The flat top of the trapezoidal back EMF waveform is well matched to the quasi-square wave current waveform that can be produced by a voltage source inverter, lending itself to a low cost drive system (refer to Fig. 1). One disadvantage of the trapezoidal back EMF waveform is the requirement for accurate stator current commutation control. The torque developed in a PM motor with a trapezoidal back EMF is very sensitive to the relative phase of the quasi-square wave currents imposed by the inverter with respect to the back EMFs. A small phase error in commutation can produce significant

* Prepared by the Oak Ridge National Laboratory, Oak Ridge, Tennessee 37831, managed by Lockheed Martin Energy Research Corporation for the U.S. Department of Energy under contract DE-AC05-96OR22464.

pulsating torques in such drives. Accurate phase information of the back EMF is thus required to properly commutate the stator currents with an inverter.

While the required phase information has conventionally been provided by using position sensors, such as a shaft mounted encoder or built-in hall sensors [2][3][4][5], sensor-less control is desired to reduce cost and to improve reliability. Furthermore, it is the only choice for some applications where those sensors can not function reliably [1][6][7]. Advantages of position sensor based control include: 1) availability of position information even at very low speed resulting in a wider speed control range; and 2) better dynamic speed control performance. The disadvantages are: 1) added components and cost; and 2) lower reliability due to more signal wiring.

A simple back EMF based position detection scheme is implemented with a DSP to eliminate the need for position sensors. The DSP also controls motor speed and current. Issues related to position detection errors are addressed and methods of error correction are suggested and implemented in DSP software. Advantages of the position sensor-less control are: 1) reduced cost by elimination of position sensors; and 2) improved reliability by using fewer components and less signal wiring. The disadvantages are: 1) back EMF signals that are difficult to detect at very low speeds resulting in a narrow speed control range; and 2) lower dynamic speed control performance due to the limited resolution of speed detection. For applications such as the automotive accessory motors where the motors are not intended to run at very low speeds, the back EMF based sensor-less control is able to meet the performance requirements for speed regulation.

Due to their large effective air gaps, PM motors tend to have low inductance. The use of a coreless stator in the VCS motor has further reduced the inductance (<100μH). While these types of very low inductance PM motors have fast current control response and a linear relationship between current and its developed torque, they demand stringent current regulation for the inverter to obtain acceptable current ripple. The problem becomes even more serious with high-speed motors. Such motors will be increasingly used due to their compact size [7][8]. An analysis of the influence of the low inductance on current ripple has been used to design a fast current control loop thereby enabling the inverter to cope with low inductance. Analytical and experimental results are included to verify the proposed schemes.

SENSOR-LESS CONTROL

BRUSHLESS DC MOTOR

Fig. 1 shows the excitation for a BLDC motor that consists of a PM motor with a trapezoidal back EMF excited by a three-phase current source. The source can be provided by a current controlled voltage source inverter. The PM motor is represented by an equivalent circuit consisting of a stator resistance, inductance, and back EMF connected in series for each of the three phases with the mechanical moving portion omitted. The figure also shows the desired stator currents that the current source should provide and their relationship with the back EMFs. The currents in each phase have a rectangular wave-shape and must be in phase with the back EMFs of the corresponding phase. In this way, the flat top of the trapezoidal back EMF waveform is well matched to the quasi-square wave current waveform that can be produced by a voltage source inverter, lending itself to a low cost drive system. Such currents will develop a constant power and thus torque delivered to the rotor. To be able to provide such currents, we need to know the rotor position information related to the angular phase of the back EMFs. The phase information of the six points per electrical cycle marked by arrows in the figure is sufficient to control a BLDC motor.

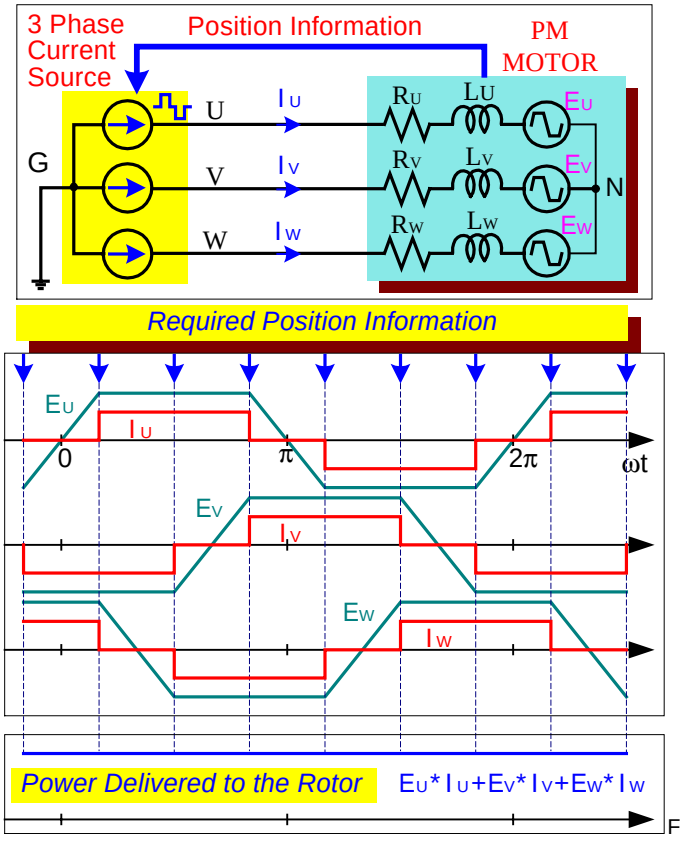

ig. 1 Excitation of Brushless DC motors.

POSITION DETECTION BASED ON INDIRECT MEASUREMENT OF BACK EMF

Fig. 2 illustrates the principle of position detection based on indirectly measuring the back EMFs. E_{U1}, E_{V1} and E_{W1} are the fundamental components of the back EMFs, E_U, E_V and E_W, respectively. Comparing the relationship between these waveforms reveals that the phase positions needed for commutation control correspond to the peak points of the fundamental waveforms. So all one needs to do is to extract the fundamental components and

detect their peak points. A functional block diagram of the suggested position detection is also shown in the figure. Because the back EMFs can be derived from the motor terminal voltages, motor terminal voltages are measured through a voltage divider of a resistor network and passed through a low-pass filter to obtain the fundamental components of back EMFs. Since zero-crossing detection is preferred to peak detection, an integrator is inserted to convert the peak points into zero-crossing points. The use of an integrator produces a signal of fixed amplitude that is dependent on the back EMF constant but independent of motor speed. Motor speed information can also be obtained by measuring the frequency of the detected signals.

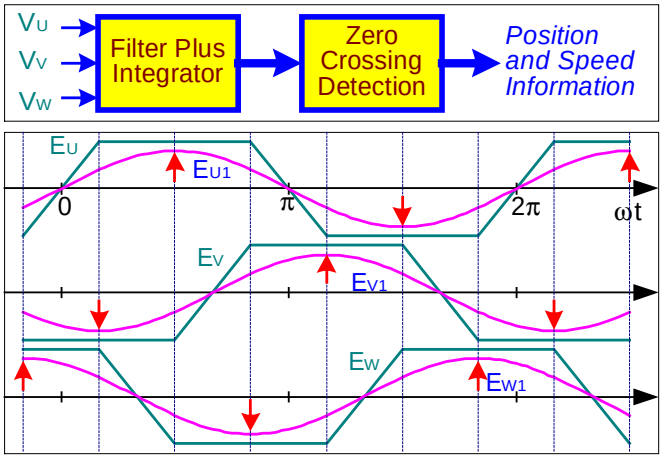

F

ig. 2 Principle of position detection.

ERROR CORRECTION IN POSITION DETECTION

Since low-pass filters are employed to extract the fundamental components of back EMF waveforms, they will inevitably introduce phase shifts into the measured fundamental components and in turn produce errors in the detected position information. Further, the phase-shift varies with the back EMF frequency, i.e. motor speed. The graph shown in Fig. 3 plots phase errors versus back EMF frequency for a typical filter design. Obviously the phase shift is too big to be ignored at low motor speed. To satisfactorily operate a motor at low speed we have devised a software method to correct the phase errors.

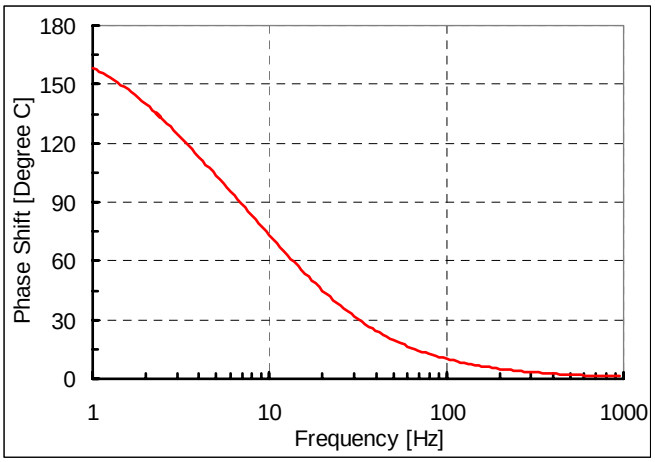

Fi

g. 3 Phase errors v.s. frequency for a typical filter design.

One disadvantage of the trapezoidal back EMF waveform is the need for accurate current commutation control. The developed torque in a PM motor with a trapezoidal back EMF is very sensitive to the relative phase of the quasi-square wave currents delivered by the inverter in response to the back EMF signals. A small phase error in commutation can produce significant pulsating torques in such drives. Fig. 4 gives an example where the currents are leading the back EMFs by 30 electrical degrees. For this condition the power and thus the torque delivered to the rotor is no longer constant but fluctuates to introduce a notch at every commutation.

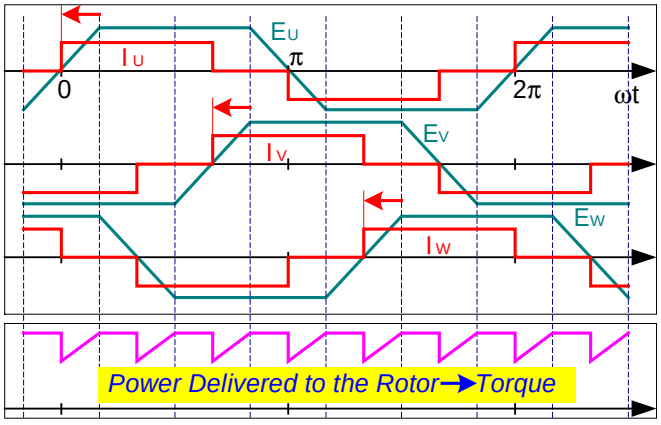

F

ig.4 Torque ripples due to current leading back EMF.

Fig. 5 shows a modified block diagram of position detection where a phase error correction block is added. The correction is determined by a look-up table since, once the filter is designed, the resulting phase shift information can be calculated. Another source of error is the voltage drop across the stator impedance, which also becomes significant at low speed. This error can be eliminated by measuring the currents and the stator impedance.

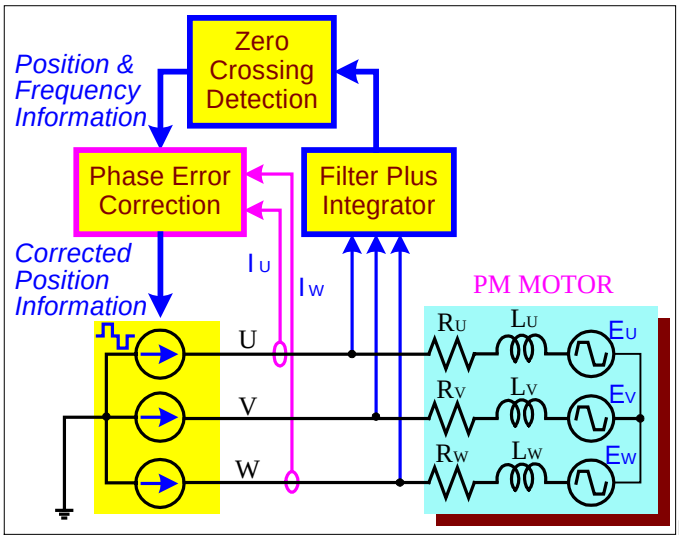

Fig. 5 Block diagram of modified position detection.

DSP BASED IMPLEMENTATION OF SENSOR-LESS CONTROL

Fig. 6(a) shows an implementation of the suggested position detection scheme using a DSP. A standard bridge inverter with a six-pack intelligent IGBT module is used to provide necessary current control for the motor. A voltage sensor is also used to monitor the DC bus voltage. Fig. 6(b) illustrates a PWM control scheme for stator current regulation. Only the upper three IGBT devices are performing PWM modulation to regulate the current of the motor. The lower switches conduct for a fixed period of 120 electrical degrees corresponding to the negative flat portion of each phase back EMF in each cycle. Because of the nonzero inductance of the state phase windings, the resulting actual phase currents will be unable to assume the desired quasi-square waveform. Instead, the currents are trapezoidal due to the finite rise and fall time, and contain ripples due to the limited switching frequency of the inverter. This affects the torque production and drive performance. While the low inductance of the VCS motor closely produces the desired rectangular current waveform, it also unfortunately generates larger current ripples for a given switching frequency of the inverter. The switching frequency and inductance dependency of the current ripple is discussed in detail later.

The DSP chip used in this development is TMS320F240 of Texas Instruments, which is specifically designed for motor control [10]. It contains all the hardware needed for motor control such as PWM modulators capable of the most commonly used carrier based or space vector PWM, capture/encoder input interface including necessary counters, and A/D converters of eight channels. The position signals from the detection block are fed to the DSP through the capture inputs. The DSP also provides a Master/Slave high-speed synchronous port, which may be used for RS-485 based communications between the modular inverters for expanding power capability. The use of the DSP and intelligent IGBT module, which include pre-drives and protection logic necessary for safe operating of the inverter, greatly reduces part count, and results in a compact inverter package with a volume of 10”×10”×3.5”.

Fig. 7 shows a block diagram of sensor-less speed control. A proportional-integral (PI) controller is used for speed regulation and a proportional control of gain K for current regulation. The use of proportional control for current loop provides a fast response, which is important for the low inductance motor. A feed-forward path with a gain equal to the back EMF constant K_{bemf} is also provided to improve the speed control response. Speed feedback is furnished with the position detection block that has a resolution of $6\times P$ pulses per revolution, where P is the pole pair number of the motor.

During the initial startup of the motor when no position information is available, a separate constant current reference is commanded to the current control loop and the frequency of the currents is increased in a linear manner from a low starting value. The motor is forced to rotate synchronized with the currents. Once the motor reaches the speed at which the back EMF can be detected the speed regulation loop takes control and the motor continues to accelerate to a desired speed. During this period the current is constant and equal to the maximum capability of the motor to ensure maximum motor acceleration.

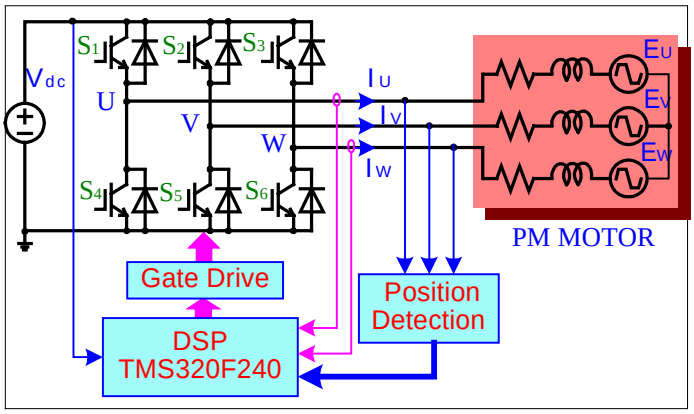

(a) Block diagram of DSP based position sensor-less control

Fig. 6 DSP implementation of position and speed sensor-less control.

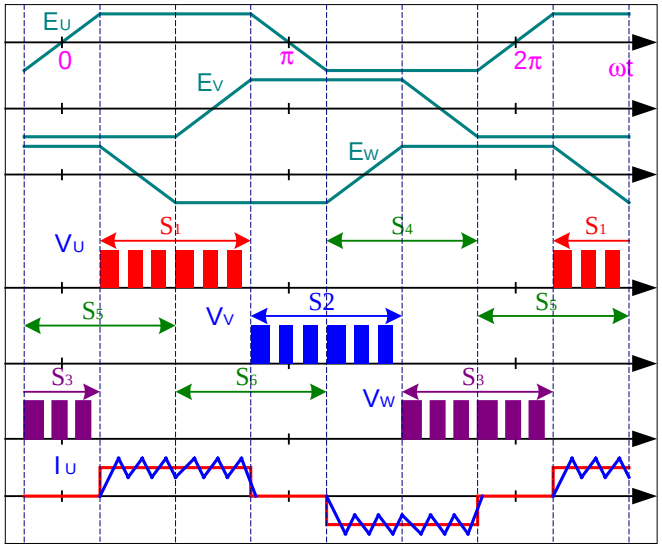

(b) Operationg waveforms.

Fig. 6 DSP implementation of position and speed sensor-less control.

CURRENT RIPPLE ANALYSIS

The influences of the low inductance on the current ripple can be analyzed based on an equivalent circuit for a BLDC motor with trapezoidal back EMF driven by a standard bridge inverter, as shown in Fig. 8. Notice that phase commutation is not considered in the equivalent circuit. Ignoring the state coil resistance, R_m, the peak value of stator current ripple at steady state in the continuous conduction mode can be determined by the following equation.

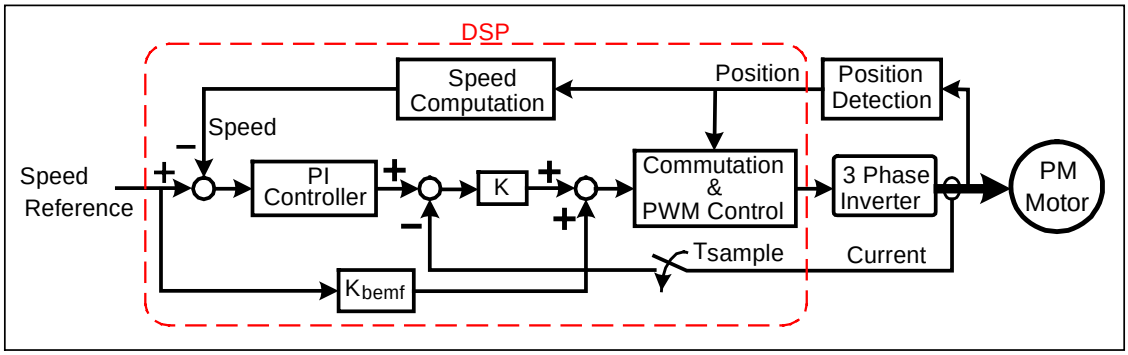

Fig. 7 Sensor-less speed control block diagram.

$$I_{mripple(Peak)} = \frac{1}{4L_m f_{SW}}(1-\frac{K_{emf}N}{V_{dc}})K_{emf}N$$

where

L_m is the phase leakage inductance, henries,
f_{SW} is the switching frequency, Hz,
V_{dc} is the inverter DC link voltage, volts,
K_{emf} is the back EMF constant, volts/RPM, and
N is the motor speed, RPM.

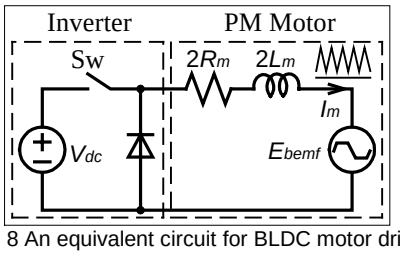

Fig. 8 An equivalent circuit for BLDC motor drive.

A plot of current ripple versus speed is given in Fig. 9 for the accessory motor at f_{SW}=20kHz, V_{dc}=320V. The motor has a rated shaft power of 8 kW and a measured phase inductance, L_m, of 65μH. As indicated in the graph, the current ripple is quite high over the speed range of 1000 rpm to 3500 rpm even at a switching frequency of 20 kHz, which is about the limit for IGBTs. This shows how challenging it is to regulate the current ripple for this type of low inductance motor. It is also interesting to notice that the maximum current ripple occurs at the speed where the

back EMF is equal to half the DC bus voltage, which is around the middle of the operating speed rage.

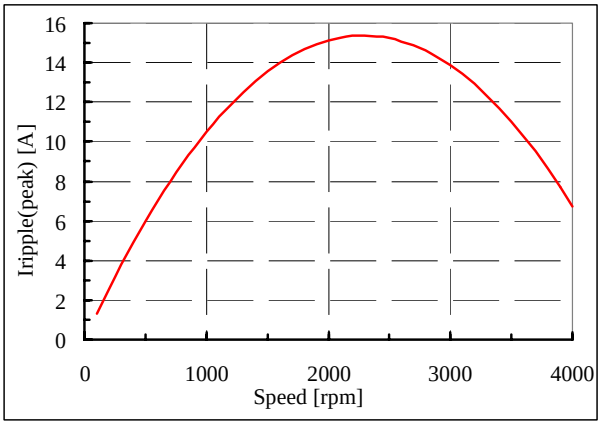

Fig. 9 Current ripple v.s. motor speed.

SIMULATION AND EXPERIMENTAL RESULTS

Fig. 10 shows a comparison of typical motor currents and the developed torque waveforms between a case where the currents are leading the corresponding phase back EMFs by 30 electrical degrees [Fig. 10(a)] and a case where the currents are in phase with the back EMFs [Fig. 10(b)]. These are generated by digital computer simulations, where the inverter switches at 20 kHz and the fundamental frequency of current is set for 250 Hz.

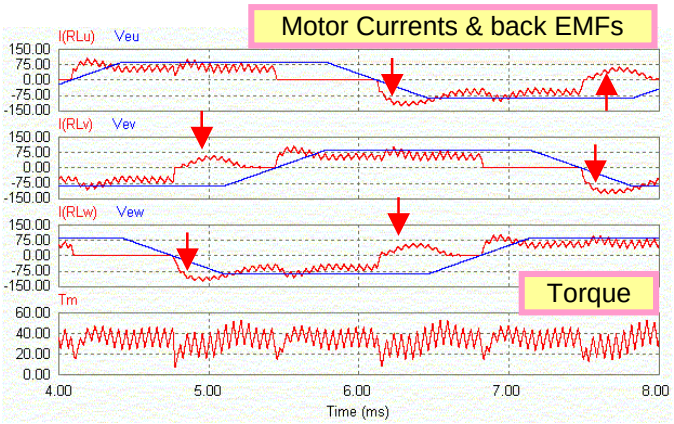

(a) Motor currents are leading the phase back EMFs by 30 degrees.

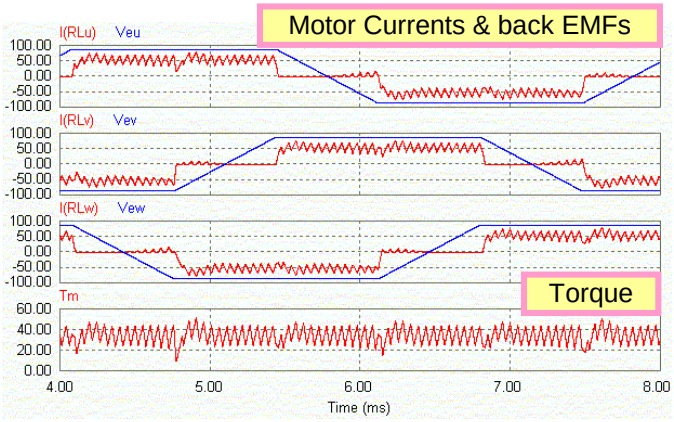

(b) Motor currents are in phase with the back EMFs.

Fig. 10 Comparison of motor currents and torque waveforms.

The differences between the two cases are that current bumps, marked by arrows, occur at the beginning of each half cycle when the currents are out of phase with the back EMFs. The current bumps result from the shorting of the corresponding two phase back EMFs through the conducting IGBT of the lower devices and the diode associated with the lower IGBT of the open leg. Take phase U for instance and refer to Figs. 4 and 6. At the beginning of each negative half cycle when the current is commutated from S_6 to S_4 while S_2 is conducting, the diode of S_6 is positively biased over the first period of 30 degrees during which back EMF, E_U, is greater than E_W. Therefore, the two phase back EMFs are shorted through the diode and S_4, and consequently a current bump is produced. Similarly at the beginning of each positive half cycle when the current is commutated from S_4 to S_5 while S_3 is conducting, the two phase back EMFs E_V and E_U are shorted through S_5 and the diode associated with S_4. The deteriorated current waveforms also produce large torque pulsations as is evident from the sizeable differences in the torque waveforms shown in Fig. 10(a).

Every time the stator current is commutated from one phase to another, a torque pulsation is also generated even when the phase currents are properly switched from one to another as can been seen in Fig. 10(b). Again the magnitude of the pulsation depends on the inductance and operating current, and a low inductance helps to reduce the magnitude. In addition to these pulsations, high frequency torque pulsations also occur due to the current ripples produced by the PWM switching. Although these are of sufficiently high frequency that they are effectively filtered out by the rotor inertia, the current ripples generate additional copper and iron losses.

Fig. 11 gives typical oscillograms of no-load current waveforms. Fig. 11(a) is recorded without the correction of position error resulting from the back EMF detection filters. For comparison, Fig. 11(b) shows the corresponding waveforms when the position error is corrected. Notice the differences in the current waveforms marked by arrows, which shows a clear reduction in the current bumps after the position detection error is corrected. The current bumps can not be eliminated because the back EMF of the motor does not have a perfect trapezoidal waveform.

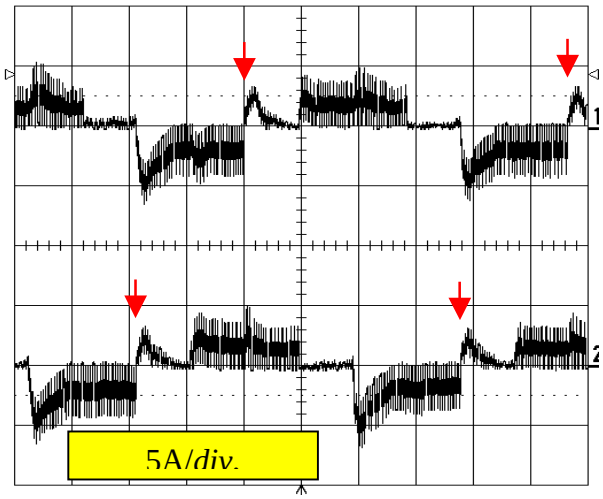

(a) No position error correction.

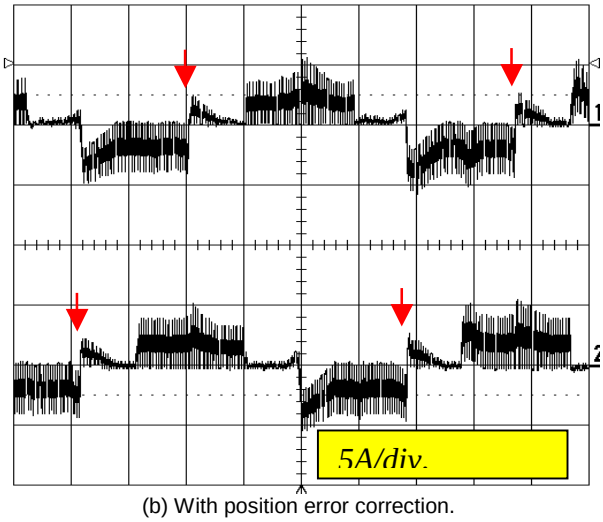

(b) With position error correction.

Fig. 11 Experimental current waveforms.

CONCLUSION

This paper presents a DSP implementation of an indirect back EMF detection based position and speed sensor-less control for an automotive accessory PM motor drive. Issues related to position detection error and current ripple due to the low inductance are addressed. The suggested sensor-less control coupled with the position error correction can

1. extend control into lower speed by eliminating the position detection errors, which are significant at low speeds, thus expanding speed control range; and
2. reduce torque ripple and improve motor efficiency by always maintaining the motor currents in phase with the back EMFs.

The use of the DSP and intelligent IGBT module greatly reduces the parts count, and results in a compact inverter package.

CONTACT

sugj@ornl.gov
http://www.ornl.gov/etd/peemrc

REFERENCES

1. D. M. Erdman, H. B. Harms, J. L. Oldenkamp, “Electronically Commutated DC Motors for the Appliance Industry,” *Conf. Rec. 1984 IEEE Ind. Applicat. Soc. Ann. Mtg.*, pp. 1339-1345.
2. M. Lajoie-Mazenc, C. Villanueva, J. Hector, “Study and Implementation of Hysteresis Controlled Inverter on a Permanent Magnet Synchronous Machine,” *Conf. Rec. 1984 IEEE Ind. Applicat. Soc. Ann. Mtg.*, pp. 426-430.
3. C. Bergmann, P. Goreau. J. P. Louis, “Direct Digital Control of a Self-Controlled Synchronous Motor with Permanent Magnet,” 1st European Conf. on Power Electronics and Applications, pp. 3.269-3.273, October 1985.
4. A. Kusko, S. M. Peeran, “Brushless DC Motors Using Unsymmetrical Field Magnetization,” *Conf. Rec. 1986 IEEE Ind. Applicat. Soc. Ann. Mtg.*, pp. 774-780.
5. B. V. Murty, “Fast Response Reversible Brushless DC Drive with Regenerative Breaking,” *Conf. Rec. 1984 IEEE Ind. Applicat. Soc. Ann. Mtg.*, pp. 445-450.
6. T. Endo, F. Tajima, H. Okuda, K. Iizuka, Y. Kawaguchi, H. Uzuhashi, Y. Okada, “Microcomputer-Controlled Brushless Motor without a Shaft-Mounted Position Sensor,” *IPEC-Tokyo'83 Conf. Record*, pp. 1477-1488, March 1983.
7. I. Takahashi, T. Koganezawa, G. J. Su, K. Ohyama, “A Super High Speed PM Motor Drive System by a Quasi-Current Source Inverter”, *IEEE trans. Ind. Applicat.*, Vol. 30, pp. 683-690, May/June 1994.
8. F. Caricchi, F. Crescimbini, O. Honorati, G. Lo Bianco, E. Santini, “Performance of Coreless-Winding Axial-Flux Permanent-Magnet Generator with Power Output at 400 Hz, 3000 r/min”, *IEEE trans. Ind. Applicat.*, Vol. 34, pp. 1263-1269, Nov./Dec. 1998.
9. “TMS320C24x DSP Controllers Reference Set,” Texas Instruments, 1997.

Appendix G

Fig. G.1. Block diagram of SEMA motor controller using Hall Probes.

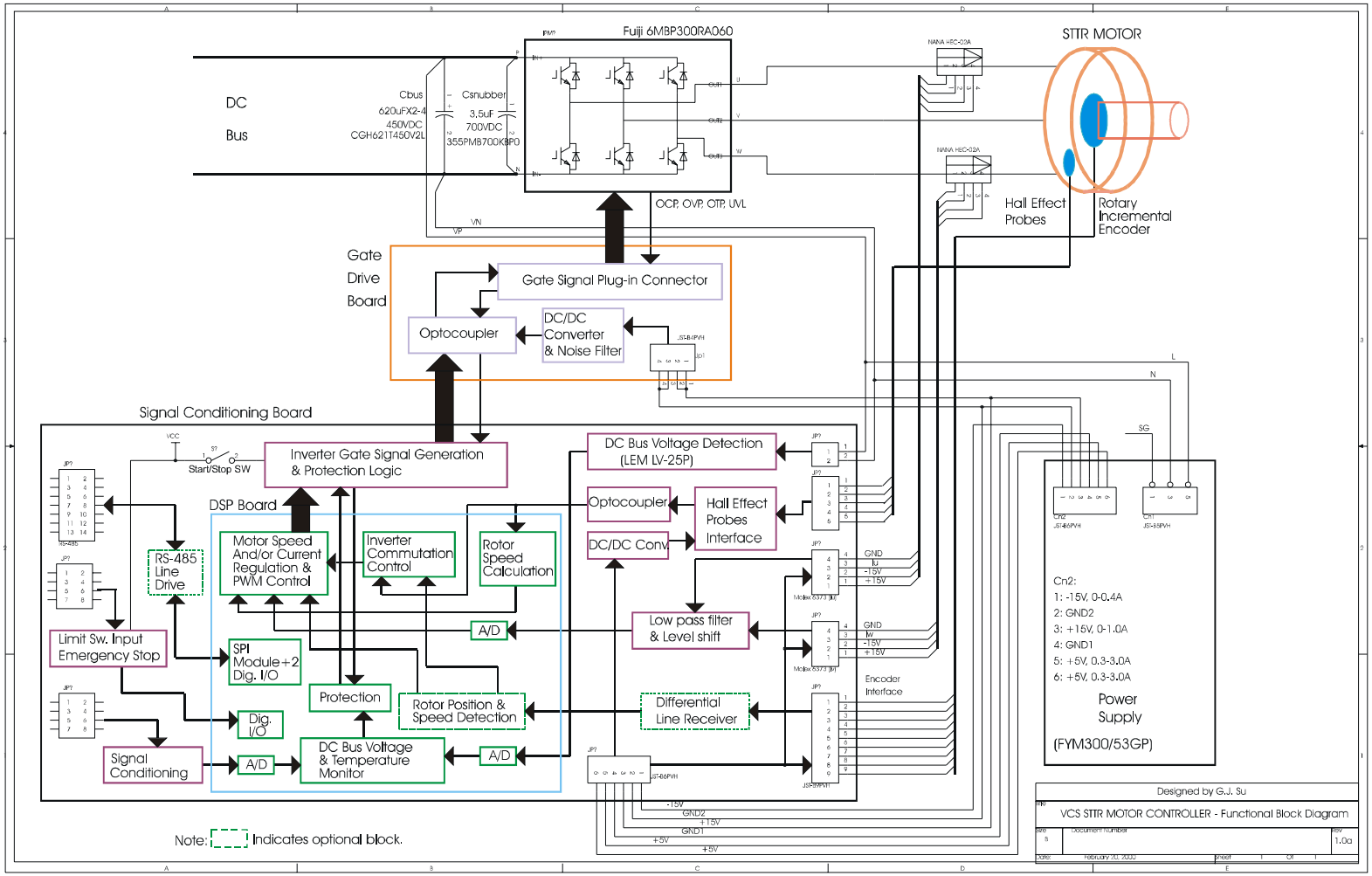

Appendix H

Design of a PM Brushless Motor Drive for Hybrid Electrical Vehicle Application

Gui-Jia Su and John W. McKeever
Oak Ridge National Laboratory
Oak Ridge, Tennessee
Phone: (865) 576-7917, Fax: (865) 241-6124
Email: sugj@ornl.gov

Kelly S. Samons
Visual Computing Systems
Greenville, Indiana
Phone: (812) 923-7474
Fax: (812) 923-8777

ABSTRACT*[*]

This paper describes a modular design of axial gap permanent magnet (PM) motor drives, in which identical PM motor modules are mounted on a common shaft and each motor module is powered separately by an inverter module. The advantages of the modular design approach for both inverter and motor include: 1) power rating scalability - one design meets different power requirements by simply increasing or decreasing the number of modules, thus avoiding redesigning and reducing the development cost, 2) increased fault tolerance, and 3) easy repairing. An automotive traction motor drive system was constructed by using two modular inverters and a PM motor with two sets of three-phase stator coils. Each inverter separately drives a set of stator coils. The PM motor is operated in brushless DC mode. The effect of different pulse-width-modulation strategies for both motoring and regenerative modes on current control is analyzed. Torque and regenerative control algorithms are implemented with a digital signal processor. The drive system is used to repower a hybrid electric vehicle converted from a Chevrolet Suburban to increase its fuel economy substantially. Analytical and initial testing results are included in the paper.

1. INTRODUCTION

Most adjustable speed AC drives (ASD) employ a single three-phase induction motor. With such a drive system, the drive has to be shut down if any phase fails. In order to improve reliability of ASD systems, six-phase induction motors fed by double current source inverters have been introduced [1] [2]. Further Jahns in [3] presents an extensive investigation of an induction motor drive system having multiple independent phases with each phase driven by an independent single-phase inverter. Such a drive requires a specially wound multiphase motor but enables the motor to continue to operate at failure of any single drive unit, although it does degrade motor performance.

Compared to induction motors, permanent magnet (PM) motors have higher efficiency due to the elimination of magnetizing current and copper loss in the rotor. It is also easier to achieve high-performance torque control with PM motors, in particular, brushless direct current (BLDC) motors. Owing to these advantages, PM motors have been widely used in a variety of applications in industrial automation and consumer electric appliances. Recent advancements in permanent magnetic materials and motor design have made the PM motor a great candidate for traction drives in electric and hybrid electric vehicle applications [4][5][6][7][8][9].

[*] * Research sponsored by Oak Ridge National Laboratory, managed by UT-Battelle, LLC, for the U.S. Dept. of Energy under contract DE-AC05-00OR22725.

This paper presents a true modular motor drive employing axial gap permanent magnet (PM) motors, in which identical PM motor modules are mounted on a common shaft and each motor module is powered separately by an inverter module, forming an independent drive unit. The advantages of the modular design approach for both inverter and motor include: 1) power rating scalability - one design meets different power requirements by simply increasing or decreasing the number of inverter and motor modules, thus avoiding redesigning and reducing the development cost, 2) increased fault tolerance – failure of any drive unit does not require drive system shutdown, and 3) easy repair by simply replacing the faulted module. An automotive traction motor drive system was constructed by using two modular inverters and a PM motor with two sets of three-phase stator coils. Each inverter separately drives a set of stator coils. The PM motor is operated in brushless DC mode. The effect of different pulse-width-modulation strategies for both motoring and regenerative modes on current control is analyzed. Torque and regenerative control algorithms are implemented with a digital signal processor. The drive system is used to repower a hybrid electric vehicle converted from a Chevrolet Suburban to increase its fuel economy substantially. Analytical and initial testing results are included in the paper.

2. MODULAR DRIVE SYSTEM CONFIGURATION

Although a modular motor drive can be constructed by using multiple sets of stator windings with a single rotor, a true modular design can be realized with axial gap PM motors. Each motor module has its own stator and rotor and all modules are mounted on a common shaft, as shown in Fig. 1. Each motor module is powered by a separate inverter module, forming an independent drive unit. The inverter modules can share a common DC power source to reduce cost or can have a separate DC source to increase the level of fault tolerance. Once the inverter and motor modules are developed, an adequate number of them can be stacked together to meet the power rating requirement of specific applications, thus leading to significant development cost savings compared to the approach that employs specific designs for specific applications. The drive system can continue to operate as long as not all of the drive units fail, albeit at reduced power. This may be important for certain applications that require a high level of fault tolerance as in EV/HEV applications. As is well known, rotor position information is required to properly control a PM motor and can be provided by position sensors such as an optical encoder or Hall effect probes. In certain situations where the inverter is not required to start the motor, position sensor-less schemes may be employed to eliminate the position sensors. Again, one can either employ one set of position sensors for all of the drive units to reduce cost or equip each drive unit with its own position sensor to increase the drive system reliability.

There are mainly two ways to excite a PM motor. One is to drive the motor in synchronous AC mode in which a three-phase sinusoidal current is delivered to a motor that has a sinusoidal back EMF. The other excitation scheme, which has been proved particularly attractive for high power drive systems and is thus the choice for the traction motor drive, is for BLDC motors. It consists of a three-phase PM motor with a trapezoidal back EMF excited by quasi-square current waveforms. This excitation can be conveniently accomplished with a three-phase full-bridge voltage source inverter. An attractive feature of this approach is the resulting simplicity of inverter phase commutation. The flat top of the trapezoidal back EMF waveform is well matched to the quasi-square wave current waveform that can be produced by a voltage source inverter, lending itself to a low cost drive system. One disadvantage of the trapezoidal back EMF waveform is the requirement for accurate stator current commutation control. The torque developed in a PM motor with a trapezoidal back EMF is very sensitive to the relative phase of the quasi-square wave currents imposed by the inverter with respect to the back EMFs. A small phase error in.commutation can produce significant pulsating torque in such drives. Accurate phase information of the back EMF is thus required to properly commutate the stator currents with an inverter.

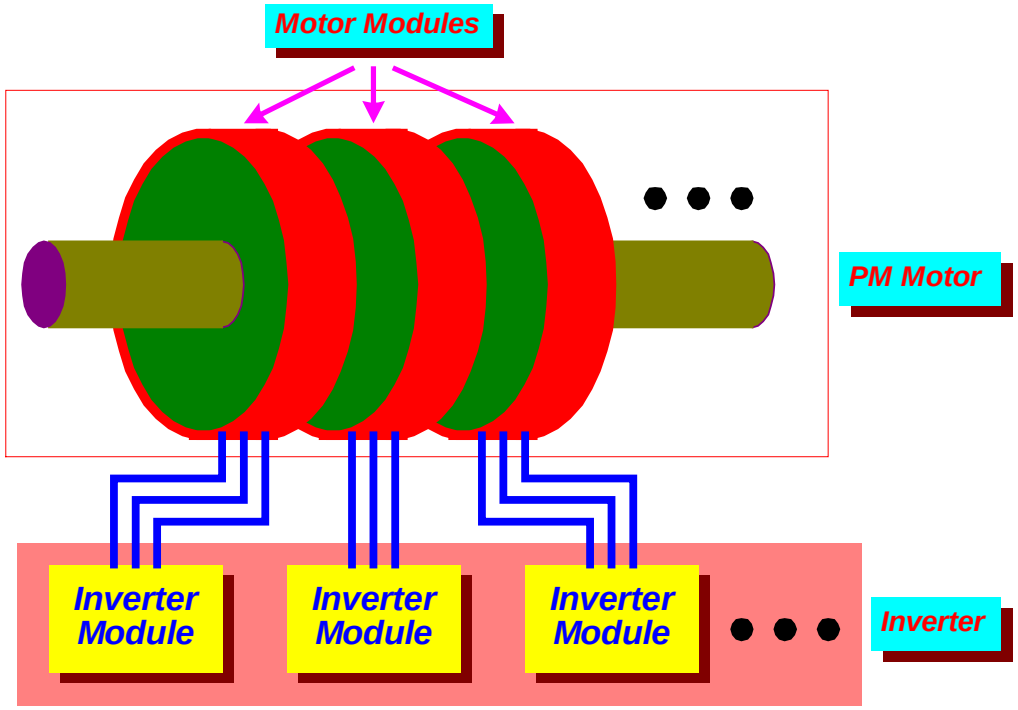

Fig. 1. Modular inverter and modular motor drive system configuration.

3. PULSE WIDTH MODULATION STRATEGIES

While both synchronous and brushless PM motors can be used for the modular motor drive, a brushless PM motor is adopted for its relative ease of control and low cost. The effect of different pulse-width-modulation (PWM) strategies for both motoring and regenerative modes on current control is analyzed. Fig. 2 shows two PWM strategies for current control with a three-phase full-bridge voltage source inverter in motoring mode. The PM motor is represented by an equivalent circuit consisting of a stator resistance, inductance and back EMF connected in series for each of the three phases with the mechanical moving portion omitted, where E_a, E_b and E_c are phase back EMFs. The figure also shows the ideal stator currents that the inverter should provide and their relationship with the back EMFs. The currents in each phase have a rectangular wave-shape and must be in phase with the back EMFs of the corresponding phase. In this way the flat top of the trapezoidal back EMF waveform is well matched to the quasi-square wave current waveform that can be produced by a voltage source inverter, lending itself to a low cost drive system. Such ideal currents will develop a constant power, and thus torque, delivered to the rotor. Because of the nonzero inductance of the state phase windings, the resulting actual phase currents will be unable to assume the desired quasi-square waveform. Instead, the currents are trapezoidal due to the finite rise and fall time, and contain ripples due to the limited switching frequency of the inverter. This affects the torque production and drive performance. While a low inductance motor produces a closer-to-desired rectangular current waveform, it also unfortunately generates larger current ripples for a given switching frequency of the inverter. To reduce the current ripple, a higher switching frequency is required, which in turn produces higher switching loss. To reach an optimum design, all factors must be evaluated, which include switching loss and extra loss generated from current ripple and.current control response. One added feature of the modular drive is that one can increase the frequency of torque ripple by introducing a phase shift into the PWM carriers of each drive unit.

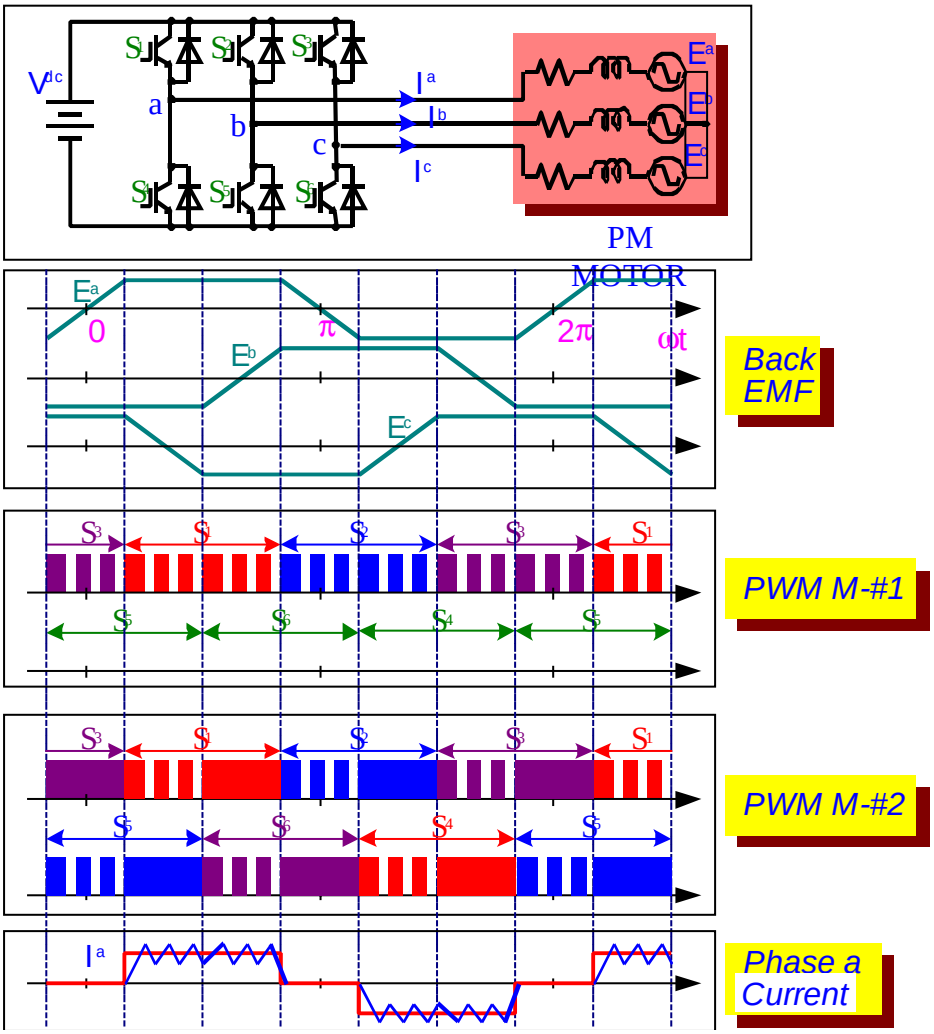

Fig. 2 PWM strategies for current control in motoring mode.

For PWM strategy M-#1, only the upper three switches of the inverter phase legs perform pulse-width-modulation to regulate the motor current, while the bottom switch of a given phase leg keeps conducting for 120 electrical degrees corresponding to the negative flat segment of the phase back EMF. Alternatively, one can implement this strategy by putting the lower three switches into PWM mode while keeping the upper switches conducting for their respective 120 degrees. In strategy M-#2, PWM operation is rotated among the six switches synchronized with the back EMFs. Each switch begins PWM for the first 60 electrical degrees and then keeps conducting for another 60 electrical degrees. Again, one can implement this strategy by letting each switch conduct for the first 60 degrees and then doing PWM for the rest of the 120 degrees. However, doing PWM for the second part of the 120 degrees has an adverse effect on the current waveforms as with the strategy M-#1. Another possible PWM scheme is to let both the upper and lower conducting switches do PWM simultaneously. This, however, produces higher current ripples.

Compared to PWM strategy M-#2, PWM strategy M-#1 is easy to implement but has the following disadvantages.

- The three devices performing PWM bear higher heat stress than the other three because of their switching loss,

- At the commutation between the lower switches the rising rate of the incoming phase current can not match the decaying rate of the outgoing phase current, producing an adverse effect on the motor current waveform, as will be shown in the simulation results.

Fig. 3 shows a comparison of typical simulation waveforms genergated by the two PWM strategies, where I(RLu), I(RLv) and I(RLw) are the three phase currents, and Veu, Vev and Vew represent the three phase back EMFs. It can be seen that strategy M-#1 produces an oscillation at the middle of the positive half cycles of current waveform, which is caused by the fact that the decaying rate of outgoing phase current is faster than the rising rate of incoming phase current at the commutation between the lower switches. This is not the case for the modulation strategy M-#2 and thus it produces smaller disturbances to the conducting phase current at the instants of switch commutation.

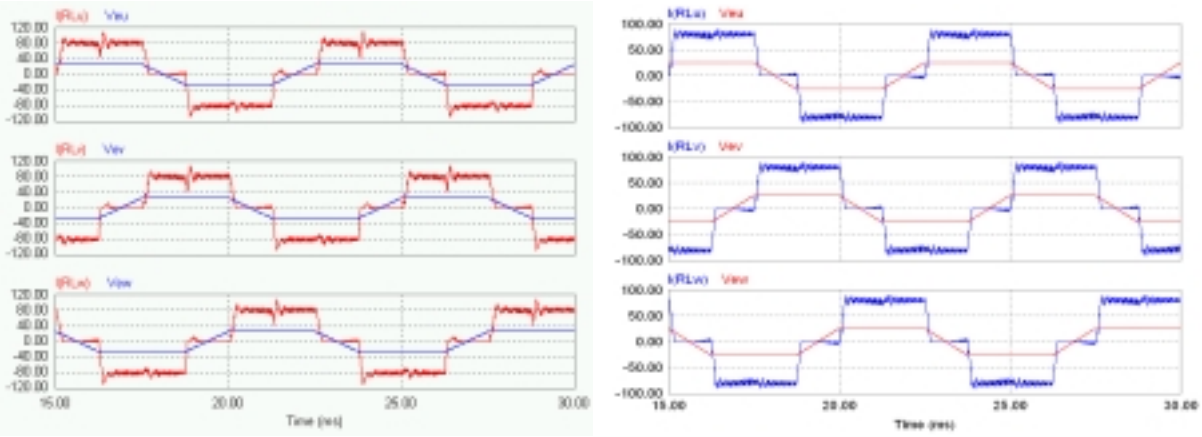

(a) for PWM M-#1. **(b) for PWM M-#2.**

Fig. 3 Simulation waveforms with different PWM strategies for motoring mode.

There are also several possible PWM strategies for regenerative power control. Two of them are illustrated in Fig. 4. For the PWM R-#1, the lower switch of each phase leg performs pulse width modulation during the time period corresponding to the positive 120 degree flat top of the phase back EMF. With strategy R-#2, the modulation period of each switch extends to 180 degrees. There is an overlap period of 60 degrees between two consecutive modulations, which is employed to improve the current waveform, as will be seen in the following simulation results. For both the PWM schemes, the bypass diodes allow all three upper switches to remain off. Two other possible strategies, for which all three switches perform PWM simultaneously or each switch does PWM during the entire positive half cycle of the corresponding phase back EMF, will produce essentially the same current waveform as PWM R-#2. It is also obvious that one can reverse the roles of the upper and lower switches by keeping the lower switches off but controlling the upper switches with PWM. Further, one can rotate the part doing PWM among the lower and upper switches to distribute the switching loss and the resultant heat among the switches.

Fig. 5 shows a comparison of typical simulation waveforms genergated by the two PWM strategies, where I(RLu), I(RLv) and I(RLw) are three phase currents, and Veu, Vev and Vew represent the three phase back EMFs. It can be seen that the strategy R-#1 produces an asymmetrical current waveform with a noticeable oscillation at commutation instants. In contrast, the strategy R-#2 yields a symmetrical current waveform without a noticeable oscillation at commutation instants. The following observations can be made. Although PWM strategy R-#1 produces less switching loss since only one switch does PWM at a time, it may generate larger di/dt noise due to the sharp change in the current waveform at commutation instants. In contrast, PWM strategy R-#2 produces larger switching loss because there is an overlap of 60 degrees when two switches perform PWM, but it generates lower di/dt noise due to the slow change in the current waveform, as shown in Fig. 5(b).

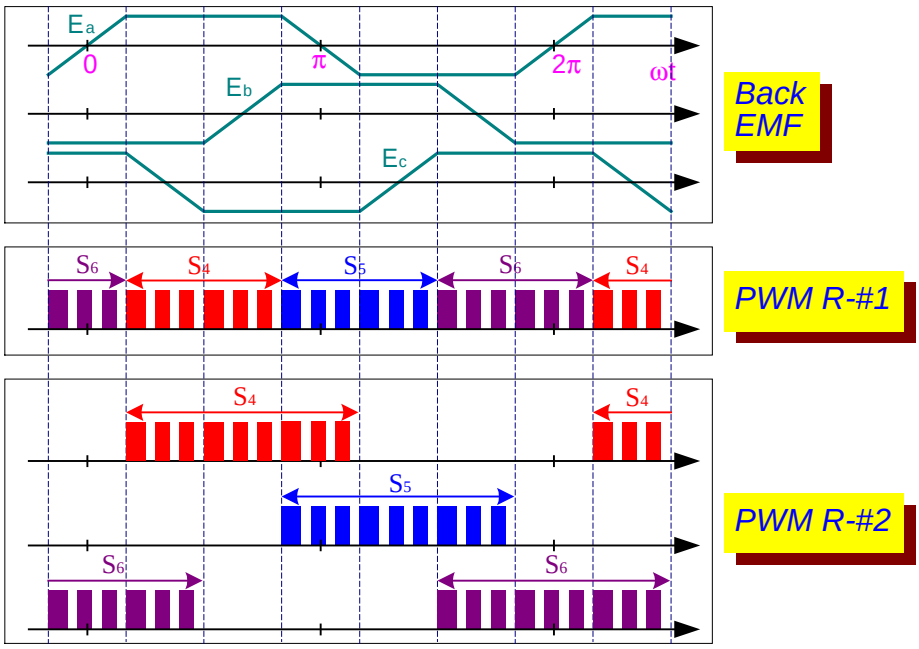

Fig. 4 PWM strategies for current control in regenerative mode.

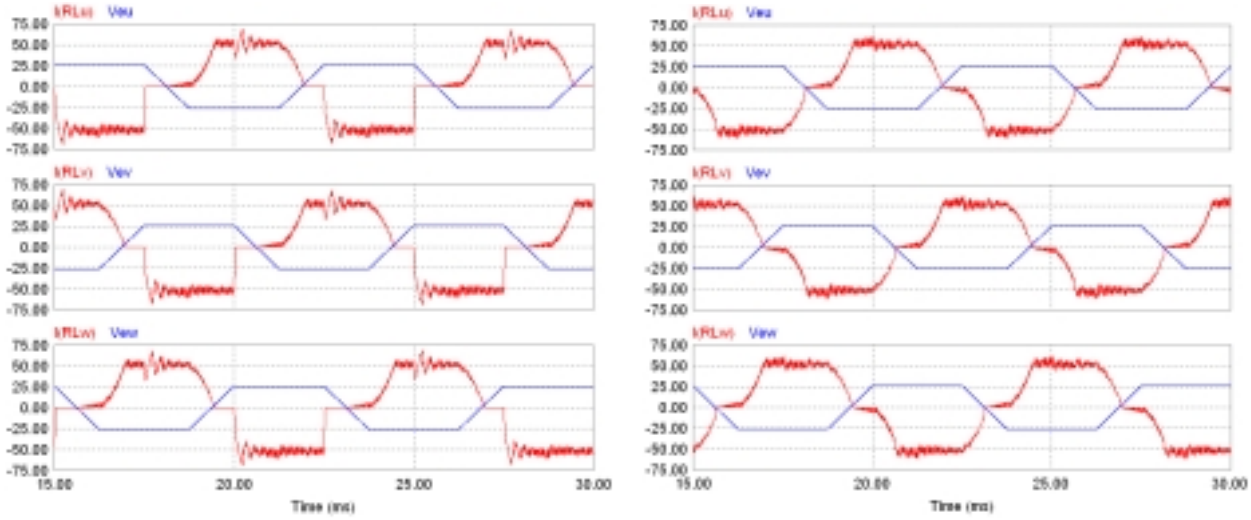

(a) for PWM R-#1. **(b) for PWM R-#2.**

Fig. 5 Simulation waveforms with different PWM strategies for regenerative mode..

4. EXPERIMENTAL RESULTS

A prototype traction drive system is built based on the modular design to repower a hybrid electric vehicle converted from a Chevrolet Suburban. Fig. 6 shows the traction drive system configuration, in which two modular inverters are employed to drive an axial gap PM motor with two sets of three-phase stator coils; each inverter separately powers one set of stator coils and the two inverter-modules share a common DC power source provided by a string of batteries. Each inverter module uses a standard bridge inverter power circuit provided by a six-pack intelligent IGBT module and is rated at 15 kW continuous power with a peak power of 45 kW for a short period of time. A voltage sensor is also used to monitor the DC bus battery voltage. The PWM strategies discussed above were tested.

The motor has a maximum speed of 4000 rpm and is operated in BLDC mode. Torque and regeneration control algorithms for HEV applications are implemented with a digital signal processor. The DSP chip used in this development is TMS320F240 of Texas Instruments, which is specifically designed for motor control [10]. It contains all the hardware needed for motor control such as PWM modulators capable of the most commonly used carrier based or space vector PWM, capture/encoder input interface including necessary counters, and A/D converters of eight channels. The position signals from a set of Hall effect probes are fed to both DSPs through their capture inputs. The DSP also provides a Master/Slave high-speed synchronous port, which may be used to implement a communication link between the inverter modules, if necessary. The use of the DSPs and an intelligent IGBT module, which includes pre-drives and protection logic necessary for safe inverter operation, greatly reduces part count, and results in a compact inverter package.

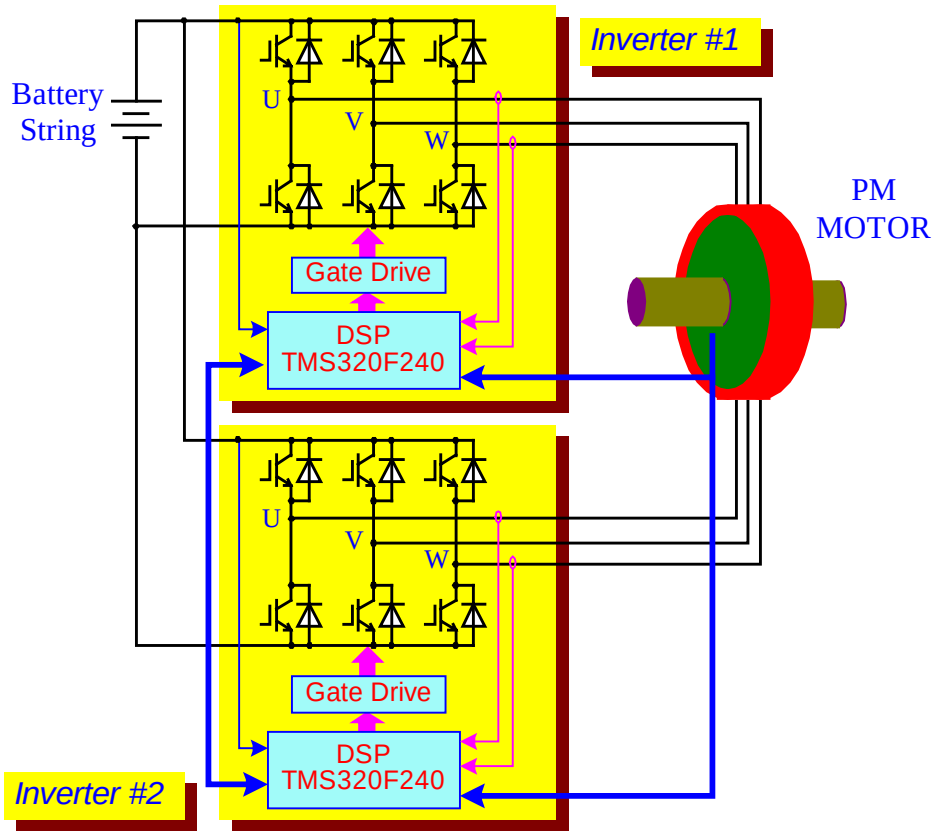

Fig. 6 A prototype of traction drive configuration based on the modular design.

The drive system was thoroughly tested for both motoring and regenerative modes with a dynamometer. Fig. 7 shows typical current and DC bus voltage waveforms of both inverters in steady states, where (a) is in the motoring mode and (b) is in the regeneration mode. It clearly indicates that the two inverters are operating in a perfectly synchronized manner.

Fig. 8 shows typical current and DC bus voltage waveforms of both inverters in transient states, where (a) shows a transition from motoring to regeneration and (b) a transition from regeneration back to motoring. Successful operation of mode transition can be observed by the increase in the DC bus voltage as the inverter is switched from motoring to regeneration and by the decrease in the DC bus voltage as the inverter is switched from regeneration back to motoring mode.

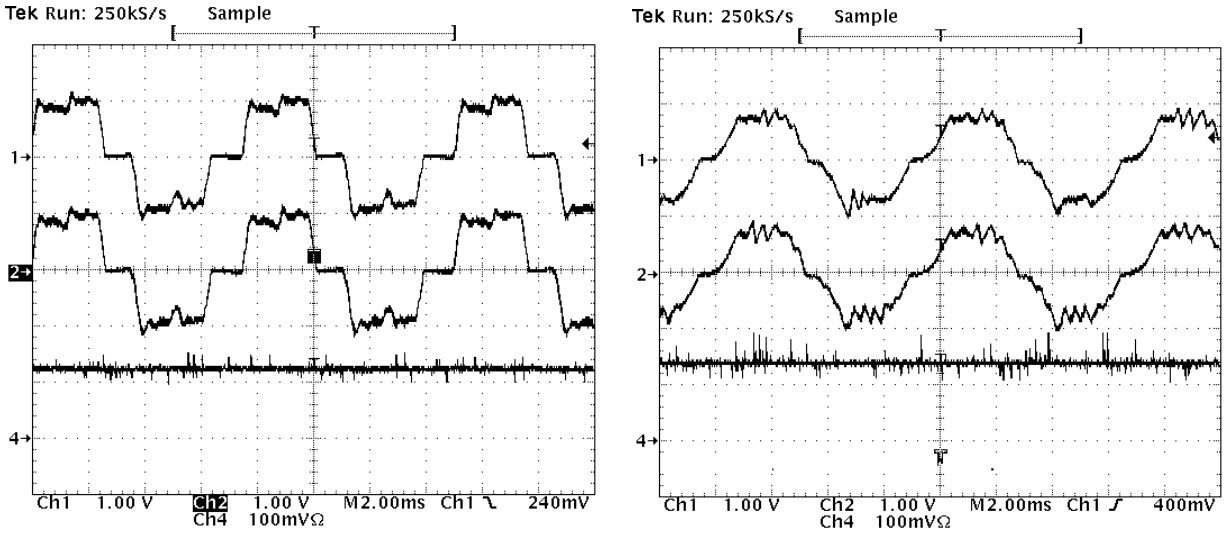

(a) Motoring **(b) Regeneration**

Fig. 7 Steady state waveforms at 1000 rpm. 1: Phase C current of inverter #1, 100 A/div; 2: Phase C current of inverter #2, 100 A/div; 4: DC bus voltage, 200 V/div; Time: 2 ms/div.

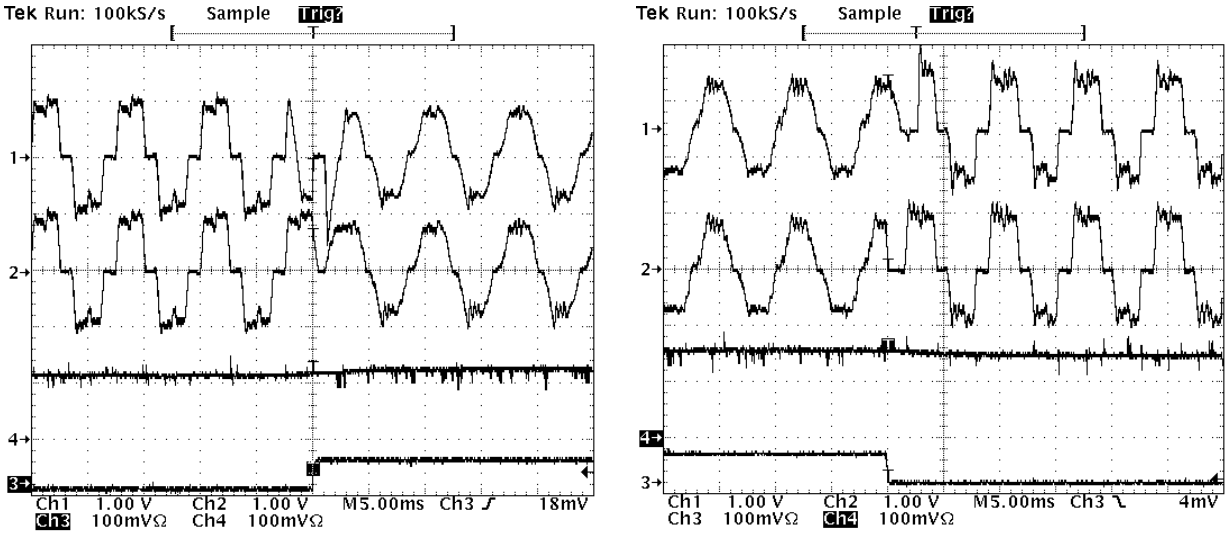

(a) Transition from motoring to regeneration **(b) Transition from regeneration to motoring**

Fig. 8 Transient state waveforms at 1000 rpm. 1: Phase C current of inverter #1, 100 A/div; 2: Phase C current of inverter #2, 100 A/div; 4: DC bus voltage, 200 V/div; 3: mode transition command; Time: 5 ms/div..

5. CONCLUSIONS

A modular design of both inverter and PM motor is described for adjustable speed drives. The modular approach can significantly reduce the development time and cost due to the power rating scalability and increase the level of fault tolerance. The effect of various PWM strategies on current control is analyzed. It is shown that PWM strategies M-#2 and R-#2 yield the best results for motoring and regenerative control, respectively.

Experimental results have demonstrated successful operation of a PM BLDC drive employing the modular design for hybrid electric vehicle applications.

ACKNOWLEDGEMENT

The authors are grateful to Craig Rutherford and Jiann-Long Wu for their assistance in the prototype assembly and testing.

REFERENCES

[1] E. A. Klingshirn, "High Phase Order Induction Motors, Part II – Experimental Results," IEEE Trans., Power App. Syst., vol. PAS-102, pp. 54-59, Jan. 1983.
[2] M. A. Abbas et al., "Six-Phase Voltage Source Inverter Driven Induction Motor," IEEE Trans. Ind. Applicat., vol. IA-20, pp. 1251-1259, Sep./Oct. 1984.
[3] T. M. Jahns, "Improved Reliability in Solid-state AC Drives by Means of Multiple Independent Phase Driven Units," IEEE Trans. Ind. Applicat., vol. IA-16, pp. 321-331, May/June 1980
[4] D. M. Erdman, H. B. Harms, J.L. Oldenkamp, "Electronically Commutated DC Motors for the Appliance Industry," *Conf. Rec. 1984 IEEE Ind. Applicat. Soc. Ann. Mtg.*, pp. 1339-1345.
[5] M. Lajoie-Mazenc, C. Villanueva, J. Hector, "Study and Implementation of Hysteresis Controlled Inverter on a Permanent Magnet Synchronous Machine," Conf. Rec. 1984 IEEE Ind. Applicat. Soc. Ann. Mtg., pp. 426-430.
[6] C. Bergmann, P. Goreau. J.P. Louis, "Direct Digital Control of a Self-Controlled Synchronous Motor with Permanent Magnet," 1st European Conf. on Power Electronics and Applications, pp. 3.269-3.273, Oct. 1985.
[7] A. Kusko, S. M. Peeran, "Brushless DC Motors Using Unsymmetrical Field Magnetization," Conf. Rec. 1986 IEEE Ind. Applicat. Soc. Ann. Mtg., pp. 774-780.
[8] B. V. Murty, "Fast Response Reversible Brushless DC Drive with Regenerative Breaking," Conf. Rec. 1984 IEEE Ind. Applicat. Soc. Ann. Mtg., pp. 445-450.
[9] G.J. Su, G. W. Ott, J. W. McKeever, K. S. Samons, R. L. Kessinger, "Development of a Sensor-less Speed Control Inverter for an Automotive Accessory Permanent Magnet Motor", 2000 Future Car Congress, April 2000.
[10] "TMS320C24x DSP Controllers Reference Set," Texas Instruments, 1997.